

AD-A206 159

FILE COPY



CHARACTERIZATION OF DELAMINATION IN
 ADVANCED COMPOSITE MATERIALS UNDER
 MODE III LOADING CONDITIONS

THESIS

Cynthia L. Lingg
 Captain, USAF

AFIT/GAE/AA/88D-21

DTIC
 ELECTE
 30 MAR 1989
 S E D

DEPARTMENT OF THE AIR FORCE
 AIR UNIVERSITY

AIR FORCE INSTITUTE OF TECHNOLOGY

Wright-Patterson Air Force Base, Ohio

This document has been approved
 for public release and sale its
 distribution is unlimited.

89 3 29 05

AFIT/GAE/AA/88D-21



CHARACTERIZATION OF DELAMINATION IN
ADVANCED COMPOSITE MATERIALS UNDER
MODE III LOADING CONDITIONS

THESIS

Cynthia L. Lingg
Captain, USAF

AFIT/GAE/AA/88D-21

DTIC
SELECTED
30 MAR 1989
S E

Approved for public release; distribution unlimited

CHARACTERIZATION OF DELAMINATION IN ADVANCED
COMPOSITE MATERIALS UNDER MODE III LOADING CONDITIONS

THESIS

Presented to the Faculty of the School of Engineering
of the Air Force Institute of Technology
Air University
In Partial Fulfillment of the
Requirements for the Degree of
Master of Science in Aeronautical Engineering

Cynthia L. Lingg, B.S.
Captain, USAF

December 1988

Accession For	
NTIS GRA&I	<input checked="" type="checkbox"/>
DTIC TAB	<input type="checkbox"/>
Unannounced	<input type="checkbox"/>
Justification	
By _____	
Distribution/	
Availability Codes	
Dist	Avail and/or Special
A-1	

Preface

Delamination is one of the most common failure mechanisms in composite materials. Three types of delamination often seen in a delaminated composite are the peeling mode (mode I), the forward shearing mode (mode II), and the tearing mode (mode III). While much attention has been focused in the study of mode I and mode II delamination, very little strain energy release rate data exists on mode III delamination. In this study, mode III critical strain energy release rate was obtained from unidirectional graphite epoxy composite laminates.

The purpose of this study was to investigate tearing mode delamination in graphite epoxy laminates by employing primarily the split cantilever beam test specimen. The specific tasks were to study the effect of thickness, crosshead rate sensitivity, temperature, and the addition of shim resulting in the addition and subtraction of different degrees of a peeling mode fracture component. As an alternate type of specimen, a few double split cantilever plate specimens were also tested.

I would like to thank my thesis advisor, Dr. Shankar Mall for all the advice and guidance received during the experimentation, analysis, and writing of this thesis. I also wish to thank my sponsor Mr. Steve Donaldson for helping me with developing the fixtures for the thickness testing, and for showing me the techniques for preparing

the specimens. Additionally, I wish to thank Mr. Joe Hofele of the Air Force Institute of Technology model fabrication shop for machining the fixtures and many aluminum and steel adherends. Further, I wish to thank Dr. Ran Kim of UDRI for his suggestions and for allowing me to use the MTS equipment. Most importantly, this work would not have been possible without Mr. Ron Esterline and Mr. John Camping who on many occasions alternated operating the MTS equipment. Lastly, I wish to thank my husband Tim and daughter Lisa for their understanding during the past eighteen months of study.

Cynthia L. Lingg

Table of Contents

	Page
Preface	ii
List of Figures	vi
List of Tables	x
Abstract	xi
I Introduction	1
Problem	1
Objective	2
Approach	3
II Background	4
III Theory	12
Balance of Energy	12
Constant Displacement	15
Constant Load	17
Beam Theory	20
Area Method	21
Compliance Method	21
IV Experimental Procedure	24
Specimen Preparation	24
Testing the Effect of Adherend Thickness	30
Testing the Effect of Loading Rate	35
Testing the Effect of End Opening	38
Testing the Effect of Temperature	40
Double Split Cantilever Plate Testing	41
V Data Reduction	43
VI Results and Discussion	52
Effect of Adherend Thickness	52
Effect of Loading Rate	62
Effect of End Opening	69
Effect of Temperature	80
Double Split Cantilever Plate Test	84

	Page
VII. Scanning Electron Microscopy and Surface Photography	89
VIII. Conclusions and Recommendations	99
Appendix: Computer Program	104
Bibliography	110
Vita	113

List of Figures

Figure	Page
1 Mode I Crack Propagation	5
2 Mode II Crack Propagation	5
3 Mode III Crack Propagation	5
4 Types of Mode III Test Specimens	7
5 Body with Single Crack	13
6 Load versus Displacement Crack Growth Plot with Constant Displacement	16
7 Load versus Displacement Crack Growth Plot with Constant Load	18
8 Load versus End Displacement During Crack Extension for the Split Cantilever Beam Specimen	22
9a Aluminum bar adherend	25
9b 24 ply unidirectional graphite/epoxy laminate with Kapton implant starter crack inserted to a depth of 50.8 mm	25
9c Duplicate aluminum adherend for opposite side	25
9d The bonded specimen	25
10 Split Cantilever Beam Specimen under Load	26
11 Top view of a Split Cantilever Plate Specimen	31
12 Split Cantilever Beam Specimen and Load Fixture	32
13 MTS 24.5 kN Load Frame	34
14 Displacement versus Load plot	36
15 MTS 24.5 kN Load Frame with Indented Fixtures and Loaded Specimen	39
16 Split Cantilever Beam Specimen and its Loading Test Fixtures on an Instron Machine	42

	Page
17a Cantilever Beam	45
17b Mode III Split Cantilever Beam	45
18a Mode I End Opening Diagram	48
18b Mode I Boundary Condition Diagram	48
18c Beam Free Body Diagram	49
18d Beam Segment Free Body Diagram	49
19 Compliance versus Crack Length from Thickness Testing	53
20 G_{IIIIC} versus Crack Length (19.05 mm thickness - specimen #1)	54
21 G_{IIIIC} versus Crack Length (19.05 mm thickness - specimen #2)	55
22 G_{IIIIC} versus Crack Length (12.7 mm thickness - specimen #1)	56
23 G_{IIIIC} versus Crack Length (12.7 mm thickness - specimen #2)	57
24 G_{IIIIC} versus Crack Length (12.7 mm thickness - specimen #3)	58
25 G_{IIIIC} versus Crack Length (8.128 mm thickness - specimen #1)	59
26 G_{IIIIC} versus Thickness	61
27 Compliance Versus Crack Length from Crosshead Rate Testing.	63
28 G_{IIIIC} versus Crosshead Rate	64
29 G_{IIIIC} versus Strain Rate	66
30 G_{IIIIC} versus Inverse of Fracture Initiation Time	67

	Page
31. Compliance versus Crack Length from End Opening Testing	70
32. G _C versus Crack Length from 1.729 mm End Opening	71
33. G _C versus Crack Length from 2.416 mm End Opening	72
34. G _C versus Crack Length from 2.991 mm End Opening	73
35. G _C versus Crack Length from 0.772 mm Compression	74
36. G _C versus Crack Length from 0.890 mm Compression	75
37. G _C versus End Opening	76
38. G _{IC} and G _{IIIC} versus Crack Length 1.729 mm End Opening	77
39. G _{IC} and G _{IIIC} versus Crack Length 2.416 mm End Opening	78
40. G _{IC} and G _{IIIC} versus Crack Length 2.991 mm End Opening	79
41. G _{IIIC} versus Temperature	83
42. Double Split Cantilever Plate Compliance Calibration	87
43. G _{IIIC} versus Crack Length from Double Split Cantilever Plate Specimen	88
44. SEM from high mode I component specimen	90
45. SEM from high mode I component specimen	90
46. SEM from high mode I component specimen	92
47. SEM from high compression specimen	92

	Page
48 SEM from high compression specimen	93
49 SEM from high compression specimen	93
50 SEM from high compression specimen	95
51 SEM from high crosshead rate specimen	95
52 SEM from high crosshead rate specimen	96
53 SEM from high crosshead rate specimen	96
54 Split Cantilever Beam Specimen Fracture Surface	98

List of Tables

Table		Page
I	Effect of Adherend Thickness	62
II	Split Cantilever Beam Effect of Crosshead Rate Results	68
III	Results from the Effect of End Opening	80
IV	Results from the Effect of Temperature	82
V	Double Split Cantilever Plate Specimen Results	85

Abstract

Delamination is the weakest and major failure mode in laminated fiber reinforced composite materials. Delamination is also a fundamental issue in the evaluation of laminated composite structures for durability and damage tolerance. This study involved the characterization of mode III delamination primarily using the mode III split cantilever beam specimen. The effects of altering four test parameters on the critical strain energy release rate of the split cantilever beam test specimen were studied, resulting in a critical evaluation of this mode III test specimen. This evaluation involved the investigation of altering aluminum adherend thickness on the mode III critical strain energy release value, investigation of altering crosshead rate on the mode III critical strain energy release rate, the effect of temperature on the mode III critical strain energy release rate, and the addition and subtraction of a mode I component on the critical strain energy release rate. For comparison, a few double split cantilever plate specimens were also tested

Results obtained from the compliance method, area method, and beam theory showed that altering adherend thickness produced no effect on mode III critical strain

energy release rate. Results obtained from the compliance method showed that higher crosshead rates produced lower mode III critical strain energy release rates. Results obtained from compliance method and area method showed that increasing end opening decreased critical strain energy release rate. Above room temperature G_{IIIc} decreased with increasing temperature

I. Introduction

Problem

The weakest and major failure mode in laminated fiber reinforced composite materials is delamination. Delamination is thus the most common life-limiting crack growth mode in composite structures. When considering damage tolerance and durability of laminated composite structures, delamination is one of the major issues. To date, most researchers have focused their attention on the delamination characterization in advanced composites under the opening or tensile mode I and in the in-plane shear mode II. Delamination, which is the separation between two plies in composites, is constrained to grow between two plies due to the presence of continuous fibers. This constraint in laminated composites introduces all three delamination modes under an arbitrary external load. Thus, investigation of the mode III delamination mechanism is needed.

Recently, Donaldson (1) proposed a split cantilever beam (SCB) test specimen to study mode III delamination in laminated composites. The SCB specimen consists of a composite laminate bonded with an adhesive between two metal adherends. Donaldson's study (1) was the first attempt at studying mode III delamination using the split cantilever

beam specimen. In Donaldson's study, two test parameters were investigated to determine their effect on the measurement of critical strain energy release rate, G_{IIIc} . These parameters were the depth of specimen and the laminate thickness. Laminate thicknesses of 8, 16, and 24 plies were tested (1).

Objective

The objective of the present study was to investigate the mode III delamination behavior of composite materials. A critical evaluation of the SCB test specimen was made. The effect of altering the thickness of the aluminum adherends on the measurement of mode III critical strain energy release rate of the composite was determined. Also the effect of crosshead speed or strain rate on mode III critical strain energy release rate was evaluated. Further, the effect of the presence of a small amount of mode I component with the addition of shim while maintaining mode III loading was examined. This mode I component may be present during testing of the SCB specimen due to several factors. Two factors are the distance between the splice plates and the total width of the specimen. Next, the effect of temperature on the mode III critical strain energy release rate G_{IIIc} was evaluated. Finally, as an alternative specimen type, a few double split cantilever plate specimens were examined in the investigation of mode III delamination.

Approach

To accommodate the change in thickness of the aluminum adherends in order to study the adherend thickness effect on GIIIC, new loading fixtures had to be developed. Bonding of the split cantilever beam adherends to the laminate was necessary before the testing could be accomplished on the MTS 24.5 kN load frame with appropriate loading fixtures. The composite used was 24 ply unidirectional Hercules AS4/3502, a typical brittle graphite/epoxy system and the adhesive used was Hysol EA 9309.3 NA. For testing the effect of the crosshead rate and for testing the effect of adding and subtracting a mode I component, the same material and adhesive was used but the thickness of the specimen was returned to 25.4 mm. In testing the effect of temperature on critical strain energy release rate, Hysol EA 9394, a high temperature paste epoxy replaced Hysol 9309.3 NA as the bonding adhesive. The double split cantilever plate material was also 24 ply unidirectional Hercules AS4/3502. To compute crack growth on these specimens a precracking and measurement marking system was developed.

II. Background

The properties of high strength and stiffness, and low density make advanced continuous-fiber reinforced composites acceptable for use as structural materials. Proper selection of laminating sequence makes it possible to design changes of strength and stiffness into a laminate. This ability is a direct consequence of the anisotropic nature of continuous-fiber reinforced composites. Transverse impact may result due to out of plane loading creating local matrix damage prior to any fiber dominated failure. Delamination often occurs as a result of matrix damage. The laminate then tolerates a decreased load as compared to its previously undamaged state. Figures 1 through 3 show the three modes of crack growth. All three modes may be present even when the composite is only subjected to membrane forces (2). The Griffith strain energy release rate is a quantifying method for crack driving mechanisms (3:123). The Griffith strain energy release rate is the amount of elastic energy required to increase a crack length a to an additional size of da . Previous tests on composites have measured mode I toughness (4), mode II toughness (5-6), and the interaction of modes I and II (7). Tearing mode (mode III) strain energy release rates can be a few orders of magnitude greater than the peeling (mode I) or forward shearing mode (mode II).

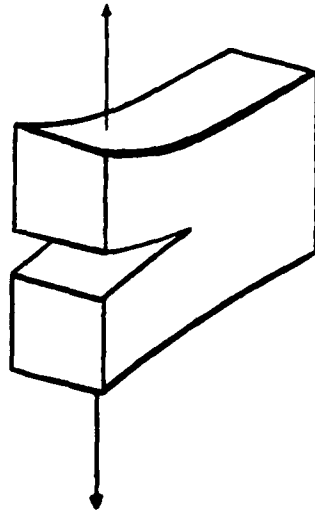


Figure 1. Mode I Crack Propagation
Broek (3:8)

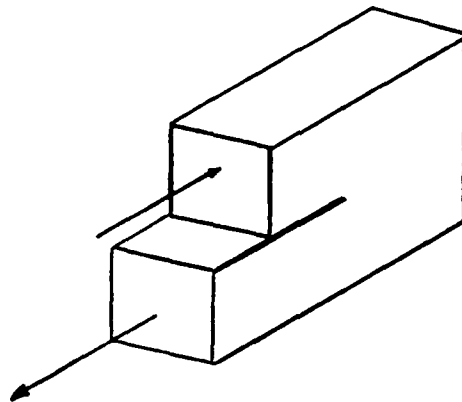


Figure 2. Mode II Crack Propagation
Broek (3:8)

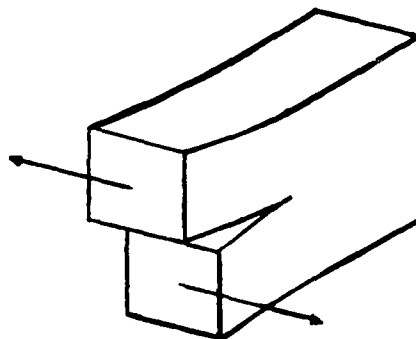


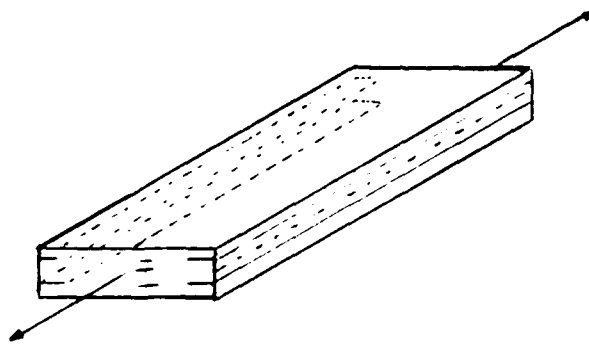
Figure 3. Mode III Crack Propagation
Broek (3:8)

Only a small amount of tearing mode (mode III) data has been obtained. Figure 4 shows possible mode III test specimens.

Previously conducted tests have used similar test specimens as those shown in Figure 4. An edge delamination specimen based on analysis of Wang (8) and finite element technique of Kim and Hong (9) is shown in Figure 4a. For a balanced angle ply layup with edge delamination between positive and negative ply interfaces, the crack propagated in a nearly uniform mode III condition when the angle ply was in the range 10 to 30 degrees. Blikstad (10) studied mixed mode I and III with modifications to this test.

Figure 4b illustrates a torsion mode III specimen. Anderson, Bennett, and DeVries (11:80-82) used a similar technique in a 90 degree cone test with adhesive bonds. Difficulties that arise in adapting this specimen are machining a circular specimen from a composite laminate, using an implant starter crack in the shape of a ring, calculating the torsional modulus as a function of angular position, and reducing the strain energy release data using a varying torsional modulus.

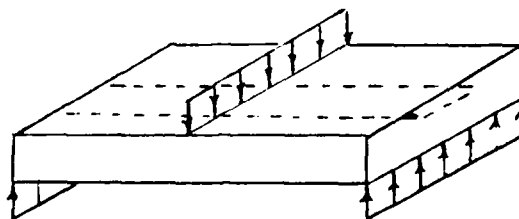
Chatterjee, Dick, and Pipes (12) analyzed beam bending which was modified and proposed by Donaldson (1) as a possible test method. Their elliptic delamination analysis showed that perpendicular to the longitudinal axis of the beam mode II conditions prevailed and along the beam length the delamination edges were predominantly Mode III. Figure



(a)

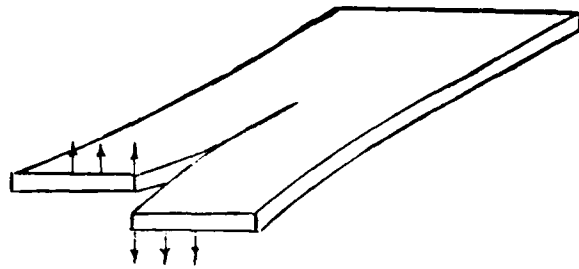


(b)

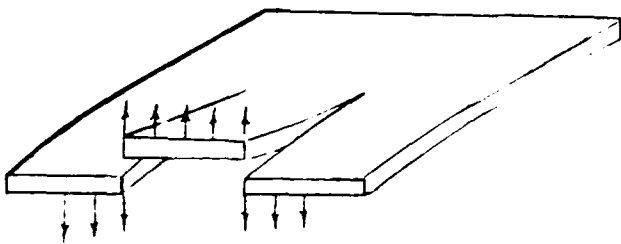


(c)

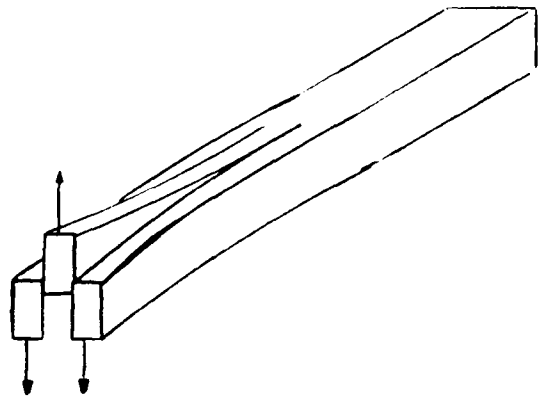
Figure 4 Types of Mode III Test Specimens
Donaldson (1)



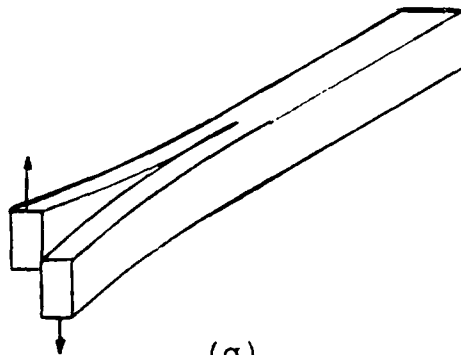
(d)



(e)



(f)



(g)

Figure 4 (cont). Types of Mode III Test Specimens
Donaldson (1)

4c illustrates the delamination extended throughout the length of the specimen showing the proposed beam bending test.

Notched plate arrangements on short fiber laminates were tested by Agarwal and Giare (13). This specimen is shown in Figure 4d.

Figure 4e illustrates a split plate type specimen used by Sidey and Bradshaw (14). Loading and unloading hysteresis resulted from fiber bridging in the unidirectional material of the test specimens used. In the Sidey and Bradshaw study the cracks became mode I cracks as they grew longer and twisting also occurred.

A double cantilever arrangement was used by Ripling, Santer, and Crosley (15). They changed the amount of mode III on a mode I specimen. Testing on the specimen in Figure 4f was accomplished using adhesively bonded composites. The double crack specimen has an advantage of beginning the test with symmetrical geometry, but a disadvantage is that it requires one to measure two cracks while the testing is in progress. The symmetry disappears if the cracks do not grow evenly (15).

A split cantilever beam configuration made of wood with only a single crack was tested by DeBaise (16) and is shown in Figure 4g. Modifications to this specimen and its testing procedure resulted in the majority of the data and analysis given in this work.

The effect of loading rates on the strain energy release rates of composite materials have been studied primarily in mode I and mode II. Smiley and Pipes found that mode I toughness decreased in graphite/PEEK (APC-2) and graphite/epoxy (AS4/3501-6) for crosshead speeds increasing from $4.2E-6$ to $6.7E-1$ m/s (17). Miller et al. showed that graphite/epoxy and toughened graphite/epoxy were not affected by changes in crack growth rate at crosshead speeds of 0.025 to 50 mm/min (18). Aliyu and Daniel saw increases of mode I strain energy release rate in unidirectional AS4/3501-6 with increases in strain rate (19). Smiley found that AS4/3501-6 and APC-2 had decreases in fracture toughness with increasing crosshead speed (20). Hunston and Bascom showed that fracture energy decreased as loading rates increased (21). Gillespie et al. found subcritical crack growth increased as the strain rate increased resulting in negligible changes in GIC with crosshead rates ranging from 0.25 mm/min to 250 mm/min on AS4-3501-6 and APC-2 material (22). Smiley and Pipes found that in crosshead speeds ranging from $4.2E-6$ to $9.2E-2$ m/s under mode II end notched flexure conditions decreases of strain energy release rate occurred as the crosshead speed was increased on both graphite/epoxy and graphite/PEEK. Additionally, they found that in APC-2 at high crosshead speeds and AS4-3501-6 at all crosshead

speeds no subcritical crack growth, a lack of ductile crack growth behavior, and brittle microscopic deformation (23)

III. Theory

In order to develop a database of critical mode III strain energy release rate, methods were required to convert raw data into strain energy release data. The theoretical background for these data reduction techniques is similar to those used for analyzing mode I double cantilever beam specimen tests. Necessary data include load, displacement, and crack length measured at discrete intervals during the testing of a specimen. The three techniques used were beam theory, area method, and compliance method. Discussions also center on the basis for these theories. Energy balances provide a basis for these theories. Energy balance for constant displacement and constant load are discussed as well as beam theory, area method, and compliance method. The following sections are based on the discussions presented by Donaldson (1) and Broek (3:123-125).

Balance of Energy

Fracture mechanics provides a basis for the resulting data reduction techniques that are presented in this work. A body which contains a single crack with a thickness of b and is loaded at pins A and B is shown in Figure 5. The crack extends in the original crack plane and its original length is denoted by a . The relative displacement between points A and B is denoted by v . The applied arbitrary load

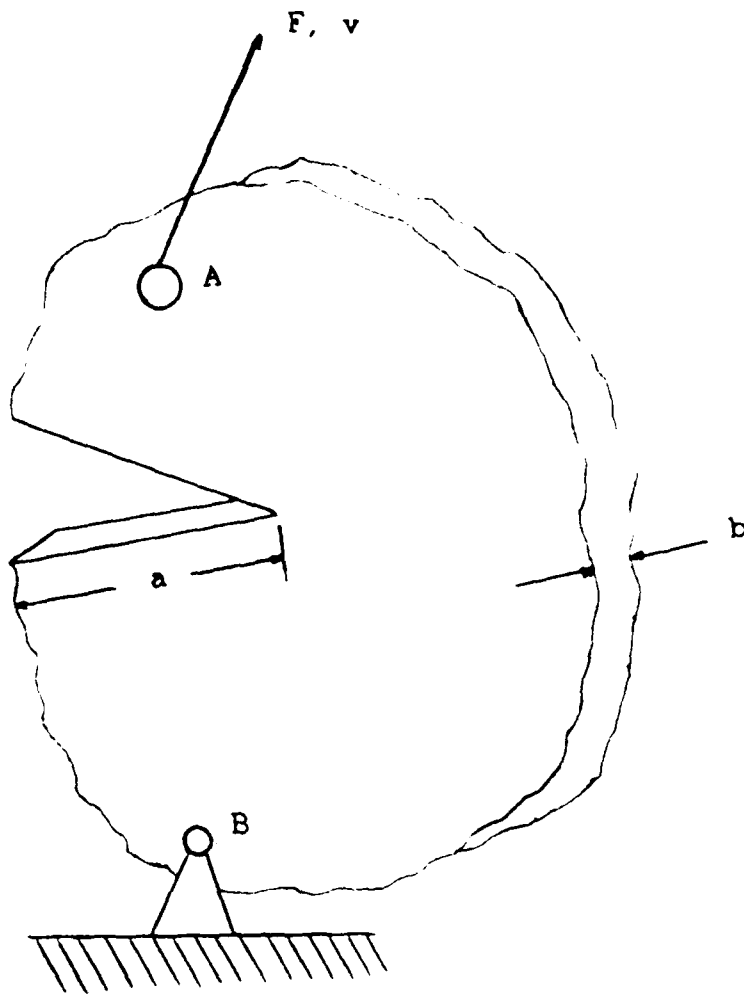


Figure 5. Body with Single Crack
Broek (3:124)

is given by F . The body is then said to have a compliance C , given as

$$C = v/F \quad (1)$$

$$v = CF \quad (2)$$

$$F = v/C \quad (3)$$

The incremental energy balance requires

$$\delta U = \delta P - \delta W \quad (4)$$

or

$$\delta W = \delta P - \delta U \quad (5)$$

where

U = elastic strain energy in the body

W = energy required for crack formation

P = work done by the applied load F on the body

The Griffith strain energy release rate is given by

$$G = dW/dA \quad (6)$$

$$A = ba \quad (7)$$

where

G = strain energy release rate

A = the total crack surface area

a = the crack length

b = the thickness of the body

When Equations 6 and 7 are substituted into Equation 5

and allowing b to be constant we obtain

$$G = (1/b) (dP/da - dU/da) \quad (8)$$

Constant Displacement

The crack growth load-displacement curve under constant displacement conditions is shown in Figure 6. In the constant displacement condition

$$\partial P / \partial a = 0 \quad (9)$$

Substitution into Equation 8 gives

$$G = -(1/b) (dU/da) \quad (10)$$

The work done by the applied load on the body is

$$P = \int_0^v F dx \quad (11)$$

where x is the dummy variable of the displacement of point A. Since point A does not move during crack growth, P is zero for all values of a . Thus

$$dP/da = 0 \quad (12)$$

Using Figure 6, the change in elastic energy is

$$dU = Fv/2 - (F - dF)v/2 \quad (13)$$

$$dU = v(dF/2) \quad (14)$$

The value of dF is positive for a decrease in load consistent with Figure 6. Applying the chain rule and differentiating results in

$$dU/da = v[(\partial F/\partial v) (\partial v/\partial a) + (\partial F/\partial C) (\partial C/\partial a)]/2 \quad (15)$$

Now substitute

$$v = CF \quad (1)$$

$$F = v/C \quad (3)$$

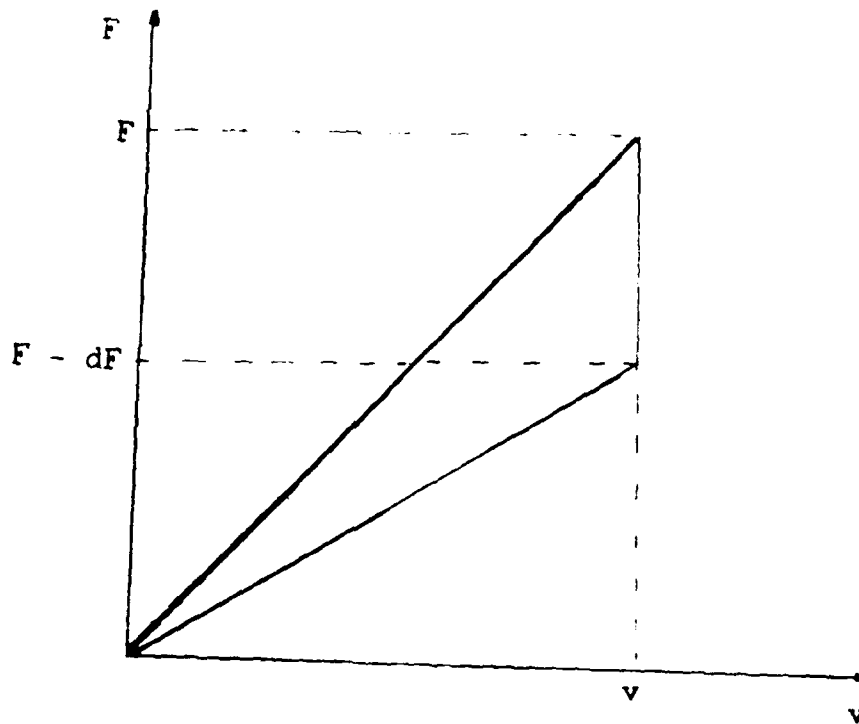


Figure 6. Load versus Displacement Crack Growth Plot with Constant Displacement Donaldson (1)

$$\text{or } \partial F / \partial C = -v / C^2$$

$$\text{and } \partial v / \partial a = 0 \quad (9)$$

into Equation 15 to obtain

$$dU/da = (CF/2) (-v/C^2) (\partial C/\partial a) \quad (16)$$

$$= -(CF/2) (CF/C^2) (\partial C/\partial a) \quad (17)$$

$$dU/da = (-F^2/2) (\partial C/\partial a) \quad (18)$$

Substituting into equation 10 gives

$$G = (F^2/2b) (\partial C/\partial a) \quad (19)$$

Constant Load

The crack growth load versus displacement curve under constant load conditions is shown in Figure 7. Linear elastic behavior will be the focus of this section. The displacement at point A increases as the body stiffness decreases. The applied load is constant while the crack is growing, therefore

$$\partial F / \partial a = 0 \quad (20)$$

The work done by the load is given by Equation 11

$$P = \int_0^v F dx \quad (11)$$

where x is again a dummy variable of displacement of point A on the body.

Since F is independent of x

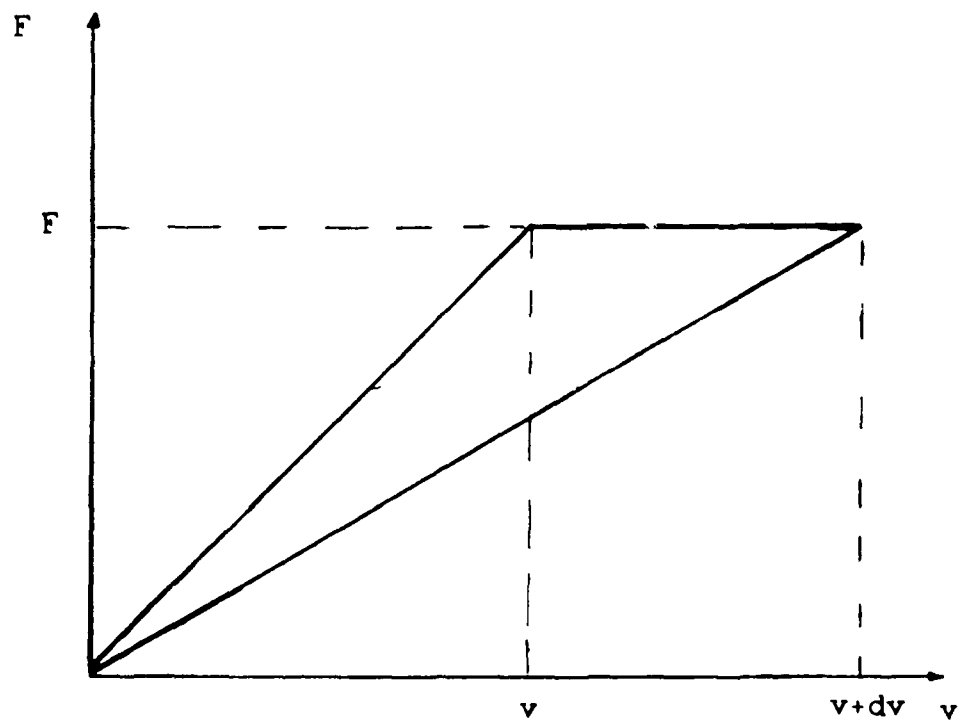


Figure 7. Load versus Displacement Crack Growth Plot with Constant Load Donaldson (1)

$$P = Fv \quad (21)$$

Taking a derivative with respect to crack length

$$dP/da = F dv/da \quad (22)$$

Using the chain rule

$$dP/da = F [(\partial v/\partial C) (\partial C/\partial a) + (\partial v/\partial F) (\partial F/\partial a)] \quad (23)$$

and substituting

$$v = CF \quad (2)$$

$$\text{or } \partial v/\partial C = F$$

$$\partial F/\partial a = 0 \quad (20)$$

results in

$$\partial P/\partial a = F^2 \partial C/\partial a \quad (24)$$

Addition and subtraction of areas in Figure 7 shows the change in elastic energy

$$\begin{aligned} dU &= Fv/2 + F dv - F(v + dv)/2 \\ &= (F dv)/2 \end{aligned} \quad (25)$$

Taking the derivative with respect to crack length

$$dU/da = (dF/da) (dv/2) + (F/2) (dv/da) \quad (26)$$

Now using Equation 20, Equation 26 simplifies as follows

$$dU/da = (F/2) (dv/da) \quad (27)$$

Differentiate Equation 2 with respect to a and substitute into Equation 27

$$dU/da = (F^2/2) (\partial C/\partial a) \quad (28)$$

Now combine equations 8, 24, and 28

$$G = 1/b (dP/da - dU/da) \quad (8)$$

$$dP/da = F^2 (\partial C/\partial a) \quad (24)$$

$$dU/da = (F^2/2) (\partial C/\partial a) \quad (28)$$

to obtain

$$G = (F^2/2b) (\partial C/\partial a) \quad (29)$$

This equation is identical to Equation 19 for constant or fixed displacement. Thus, using a constant load condition or a constant displacement condition results in the same equation for the strain energy release rate G.

Beam Theory

In beam theory, a beam freely rotates at the loaded end and is fixed on the opposite end. Beam length is assumed to equal the length of the crack. Thus, the end displacement shown in Figure 8e, is related to crack length via

$$v = 2(Fa^3)/3E^f I \quad (30)$$

$$\text{or } v = KFa^3 \quad (31)$$

$$\text{and } K = 2/3E^f I \quad (32)$$

where E^f is the beam flexural modulus and I is the beam area moment of inertia. Substituting Equation 1 into Equation 31 results in

$$C = Ka^3 \quad (33)$$

Now differentiate with respect to a and substitute into Equation 19 or 29 yielding

$$G_{IIIo,j} = 3v_j F_j / (2ba_j) \quad (34)$$

where the subscript j refers to the j^{th} data point, F_j is the load at the j^{th} extension of the crack, v_j is the total end displacement for the j^{th} extension of the crack, b is the beam depth and a_j is the j^{th} extension of the crack. No bending stiffness or moment of inertia are present in the form of Equation 34.

Area Method

The area method states that the change in area of the F - v curve is the energy lost during the process of crack growth. A portion of a load displacement curve from a test is shown in Figure 8. The change in area or dA is

$$\begin{aligned} dA &= Fv/2 + F dv + (dv dF)/2 - (F + dF) (v + dv)/2 \\ &= (F dv - v dF)/2 \end{aligned} \quad (35)$$

Energy lost from crack growth extension is then

$$dA = -dU \quad (36)$$

Applying Equations 35 and 36 to Equation 10 yields

$$G_{IIIo,j} = [F_j (dv/da)_j - v_j(dF/da)_j] / 2b \quad (37)$$

where the subscript j refers to the j^{th} data point and dF , dv , and da are the load, displacement, and crack extension increments respectively of the $j+1$ data.

Compliance Method

The compliance method is an empirical approach method often used in data reduction (24). Thus Equation 31 becomes

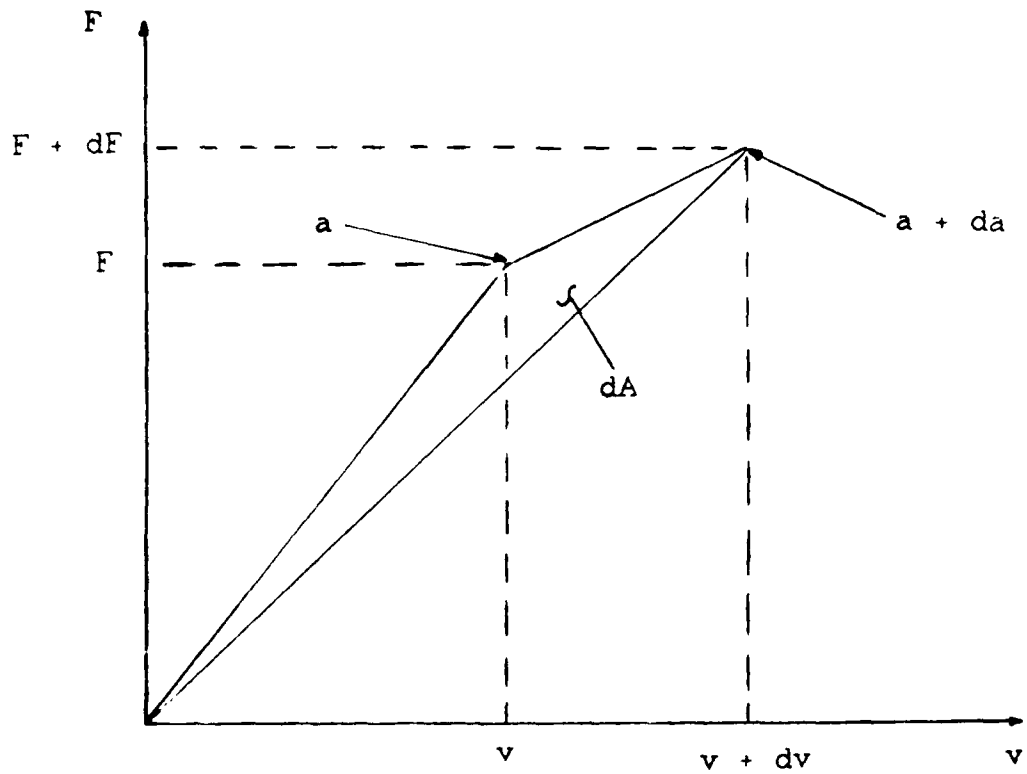


Figure 8 Load versus End Displacement During Crack Extension for the Split Cantilever Beam Specimen Donaldson (1)

$$v/F = K_2 a^n \quad (38)$$

where n is an empirical constant. Now taking the log of Equation 38 we obtain

$$\log(v/f) = \log(K_2) + n\log(a) \quad (39)$$

Using the same procedure used to derive beam theory strain energy release rates and applying this to Equation 39 above

$$G_{IIIo} = nv_j F_j / 2ba_j \quad (40)$$

The beam theory result of Equation 34 is recovered when $n = 3$. In actual experimentation, since the load is distributed over the entire splice plate, a small amount of shearing may have taken place. Thus, the exponent n can be expected to fall between and including the values of two and three (24). The exponent n can be computed by plotting the logarithm of the compliance (v/F) versus the logarithm of the crack length (a) of Equation 39.

IV Experimental Procedure

The split cantilever beam specimen is composed of a laminated composite bonded between two metal adherends. The double split cantilever plate specimen is composed of a composite laminate only. In this section, specimen preparation of the aluminum and steel adherends and double split cantilever plate specimens, as well as testing procedures for the effects of aluminum bar adherend thickness, crosshead rate, end opening, and temperature on GIIIIC. The procedures for the testing of the double split cantilever plate specimen are also presented. The specimen preparation of the aluminum bar adherends and the testing procedure used in the present study to investigate the effect of the aluminum adherend thickness is almost identical to the procedure used by Donaldson for the preparation and the testing of 25.4 mm thickness specimens (1) of 25.4 mm thickness.

Specimen Preparation

Figures 9a and c are top views of the aluminum adherends used in the assembly of the split cantilever beam specimen. Figure 9b is a top view of the 24 ply laminate used in between the two aluminum adherends. Figure 9d is a top view of the completed specimen. Figure 10 shows the specimen under mode III loading (1).

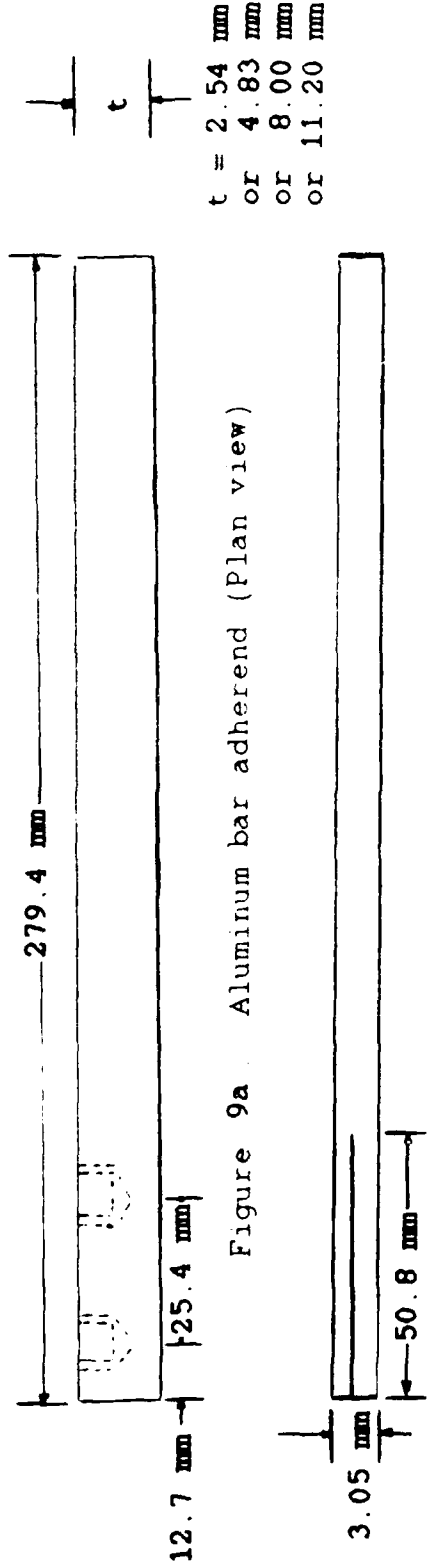


Figure 9a Aluminum bar adherend (Plan view)

Figure 9b 24 ply unidirectional graphite/epoxy laminate with Kapton implant starter crack inserted to a depth of 50.8 mm



Figure 9c Duplicate aluminum adherend for opposite side (Plan view)

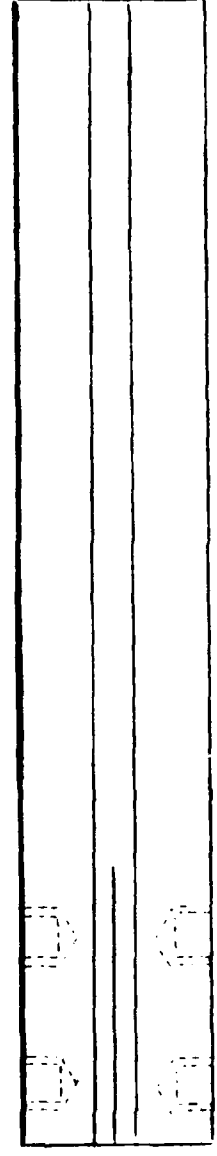


Figure 9d The bonded specimen (Plan view)

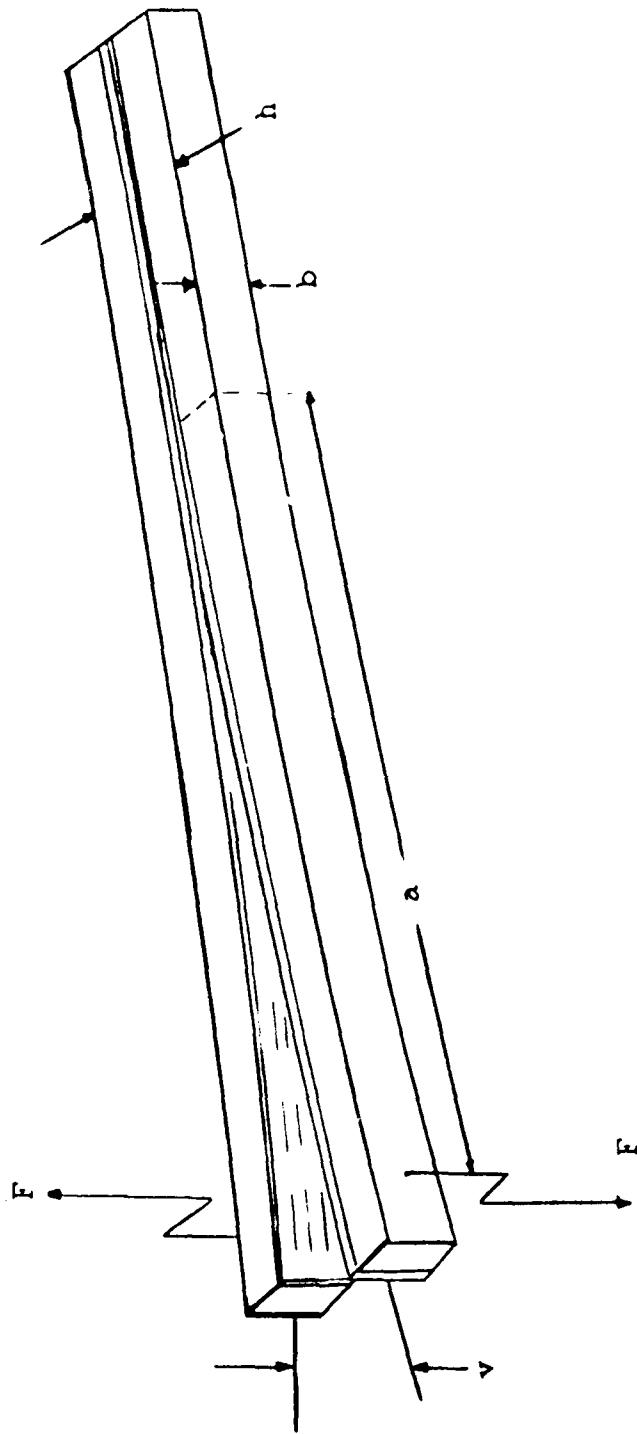


Figure 10. Split Cantilever Beam Specimen under Load Donaldson (1)

As shown in Figures 9a and 9c, the two aluminum bars were machined so that the surfaces along the major dimension were parallel. Two holes of 6.35 mm (1/4") diameter were drilled and tapped at 12.7 mm (1/2") and 38.1 mm (1 1/2") from the end of the beam. The adherends used in this study were made of 6061 T6 aluminum. The aluminum adherends were next sanded with coarse sandpaper on the inward faces. These inward faces eventually are bonded to the laminate. The sanding roughens the aluminum adherend thereby improving its ability to bond with the Hysol adhesive. Ivory dishwashing liquid and distilled water were used in conjunction with a scouring pad to clean the bars. The bars were then rinsed with methyl-ethyl-ketone (MEK). Next, a sodium bichromate and sulfuric acid solution was heated on a hot plate in a rectangular pyrex baking dish to 65.6 C and the aluminum bars were placed with their sanded sides down into the solution. Once the temperature returned to 65.6 C, the bars remained in the solution for 12 - 15 minutes as recommended for acid etch by the Forest Products Laboratory (FPL). This FPL acid etch procedure further improves the surface adhesion. When the allocated etching time had elapsed, the bars were rinsed with distilled water and were allowed to dry on tongue depressors aided with a heat gun. Throughout the process care was taken not to contaminate the bonding surface.

The 3502 resin preimpregnated AS4 fiber unidirectional tape was layed up and then cured in an autoclave per the manufacturer's directions. The panels were subsequently stored in a dessicator until needed to prevent the possibility of moisture absorption. The strip widths were equal to the aluminum adherend beam depth b in Figure 10 plus an additional 0.254 mm (0.01 inches). The additional 0.254 mm (0.01 inches) facilitated removal of excess Hysol adhesive from the laminate edges. The AS4/3502 laminate strips are naturally rough due to the texture of the peel ply and therefore were only rinsed with MEK and allowed to dry prior to bonding.

Next the two part Hysol EA 9309.3 NA was mixed and the laminate was bonded between the aluminum adherends using three C-clamps. Steel bars cut to the dimensions of 12.7 mm x 25.4 mm x 305 mm (1/2" x 1" x 12") surrounded the aluminum adherends, thereby evenly distributing the pressure of the C-clamps. Excess adhesive was continually removed with Kimwipes throughout the bonding process. A proper bondline thickness and maximum toughness was ensured due to the presence of 0.127 mm (0.005 inch) diameter glass beads in the Hysol adhesive. The adhesive was allowed to dry at room temperature for seven days. After the C-clamps and pressure distribution bars were removed, the laminate of the specimen were sanded to remove a thin coating of Hysol that could not be removed when in a liquid state. The sanding ensures that

crack propagation is not inhibited by any toughened material along the edges. Water base typewriter correction fluid was applied to the upper and lower composite edges. Two paper strips were cut from graph paper containing 1 mm divisions and rubber cemented to the upper and lower surface of the aluminum portion of the specimen, flush with the composite laminate edges. Prior to cementing, the paper strips were sequentially numbered at the centimeter divisions. The paper strips provided a scale for reference and the correction fluid improved crack length visibility.

As previously mentioned, each specimen contained a two inch Kapton implant starter crack between the twelfth and thirteenth plies of the layup. The scaled and painted specimen was finally given an extended natural mode I starter crack. By clamping the specimen at the opposite end and driving the razor wedge down the inserted crack, the crack was gradually extended from an implant of 5 cm to a natural crack of approximately 6 to 7.5 cm.

For temperature testing, steel as well as aluminum adherends were used with either a laminate of layup [9011/01]_s or a laminate of layup [024]_T. The [9011/01]_s layup was selected to match the coefficient of thermal expansion of the steel than the [024]_T. Debonding due to a mismatch of thermal expansion coefficients is less likely to occur when using the [9011/01]_s layup with steel adherends than when using the [024]_T layup with aluminum adherends. The steel

adherend preparation procedures were the same as for aluminum, including the acid etch; however, a two part high temperature paste epoxy, Hysol EA 9394, was used in place of the Hysol EA 9309.

The double split cantilever plate specimens were prepared from 24 ply AS4/3502 graphite/epoxy tape which was layed-up and autoclave cured into a panel following manufacturer's instructions. The plates were machine cut with through the thickness starter cracks of varying length having crack width of 0.254 mm (10 thousandths of an inch). Figure 11 shows the top view of a 24 ply thick split plate specimen. After machining, the split cantilever plate specimens were precracked from the machined crack. Water base correction fluid was applied to the non-precracked portion of the plate and lines were drawn with a fine point indelible marker transverse to the longitudinal axis of the specimen.

Testing the Effect of Adherend Thickness

Figure 12 is a drawing of the split cantilever beam specimen and its load fixture. The aluminum adherends were loaded in opposite directions. Dimension h in Figure 10 was 19.05 mm and 12.7 mm (0.75 in and 0.5 in) representing two of the three aluminum adherend thicknesses examined. The third thickness, $h=8.13$ mm (0.32 in) in Figure 10e was obtained by decreasing the dimension on the upper

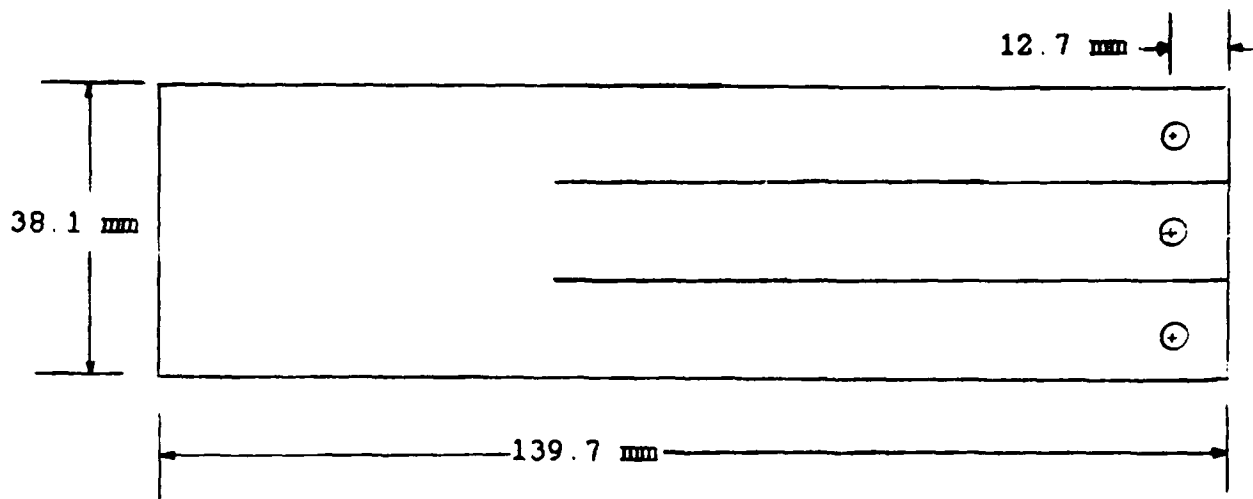


Figure 11. Top view of a Split Cantilever Plate Specimen

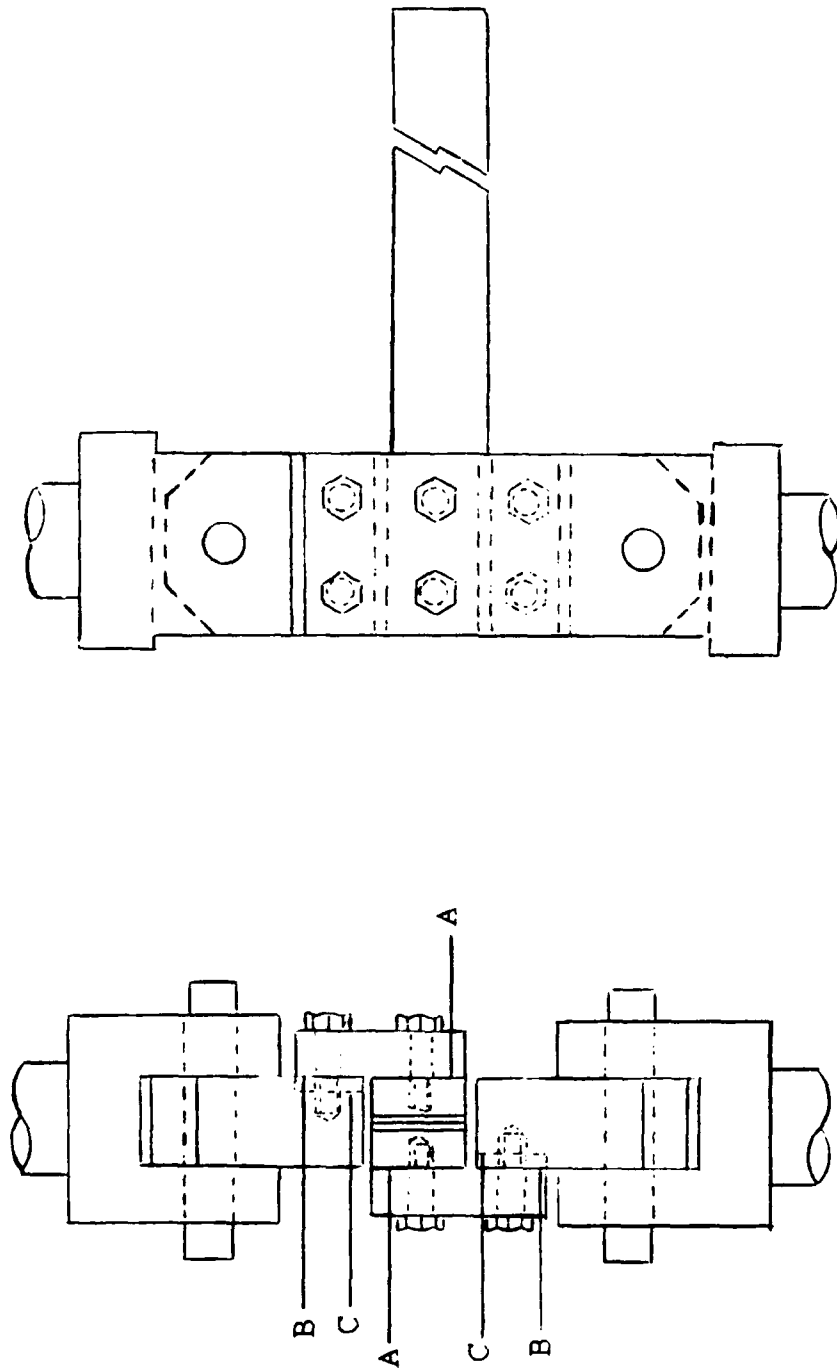


Figure 12. Split Cantilever Beam Specimen and Load Fixture Donaldson (1)

right side of the adherend for a length of 241.3 mm (9.5 in) in Figure 9a. This allowed the same fixtures as those used for the 12.7 mm bars. A separate load fixture was used for the 19.05 mm adherend thickness. Separate load fixtures were necessary since the adherend thickness changed while the laminate thickness remained the same. Refer to position C in Figure 12. Figure 13 shows the MTS 24.5 kN capacity load frame used to test the specimens.

As the crack length increased, the growth rate decreased when held at a constant crosshead speed. To promote an even specimen crack growth rate, three crosshead speeds were used. The crosshead speed used during testing from the initial precrack to approximately 12 cm was 0.254 mm/min (0.01 in/min). At approximately 12 cm, the crosshead speed was increased to 0.508 mm/min (0.02 in/min). At approximately 21 cm the crosshead speed was increased to 1.524 mm/min (0.06 in/min). Crack lengths were measured visually at intervals of approximately every centimeter during testing. Testing was accomplished at room temperature. The MTS data recording system monitored the applied load and the beam end displacement. The compliance of the fixture produced no appreciable errors in the measured displacement. Actual beam displacement was within 0.0254 mm (0.001 inch) of the crosshead displacement. An explanation for this phenomenon is that the range of the applied loads was 222.41 to 667.2 N

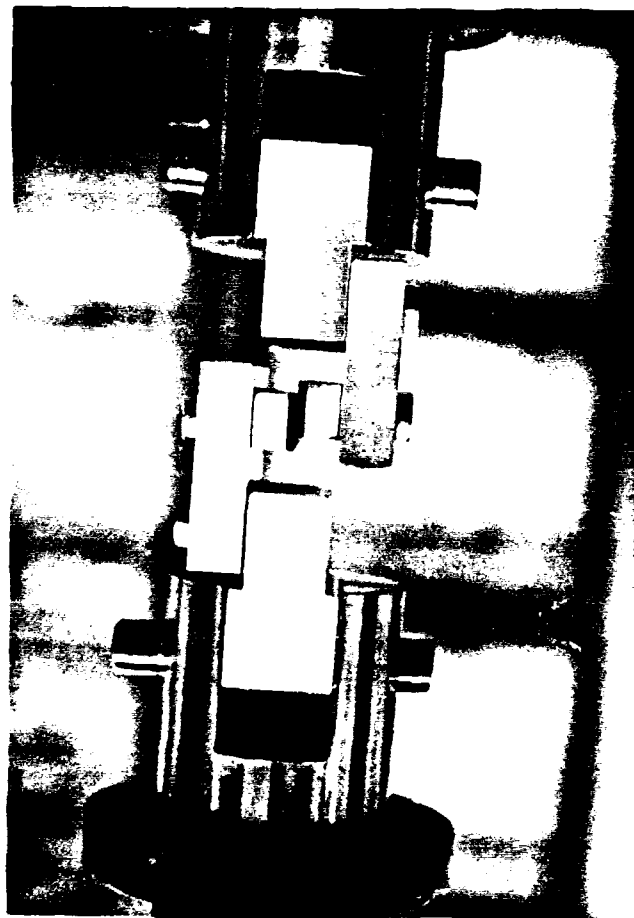


Figure 13. MTS 24.5 kN Load Frame

(50 to 150 pounds), relatively low in comparison to the stiffness of the fixtures used

The best method for monitoring crack length was to use a small battery operated flashlight to light the side of the crack and visually observe the crack growth with a 10x inch square magnifier as was done by Donaldson (1). The tip of the crack was most apparent from this method. The crack lengths measured from the attached graph paper grids were immediately recorded on an XY plotter with a displacement versus load curve. A typical displacement versus load plot with measured crack lengths is shown in Figure 14. For each specimen an average number of readings taken was 19, close to the average number of 18 taken by Donaldson (1). Similar to Donaldson's observations, it was seen that extension of the crack occurred at a relatively steady rate and that the upper and lower surface crack lengths were nearly equal at each reading. Twisting of the specimen ends was minimal. After the test was completed, the specimens were unloaded and returned to their original unloaded shape indicating a lack of plastic deformation of the aluminum adherends (1).

Testing the Effect of Loading Rate

In studying the effect of the crosshead speed or strain rate, procedures similar to testing the effect of thickness were used. Again refer to Figure 12 for the drawing of the specimen and its load fixture. Similar to the line of action taken during testing the effect

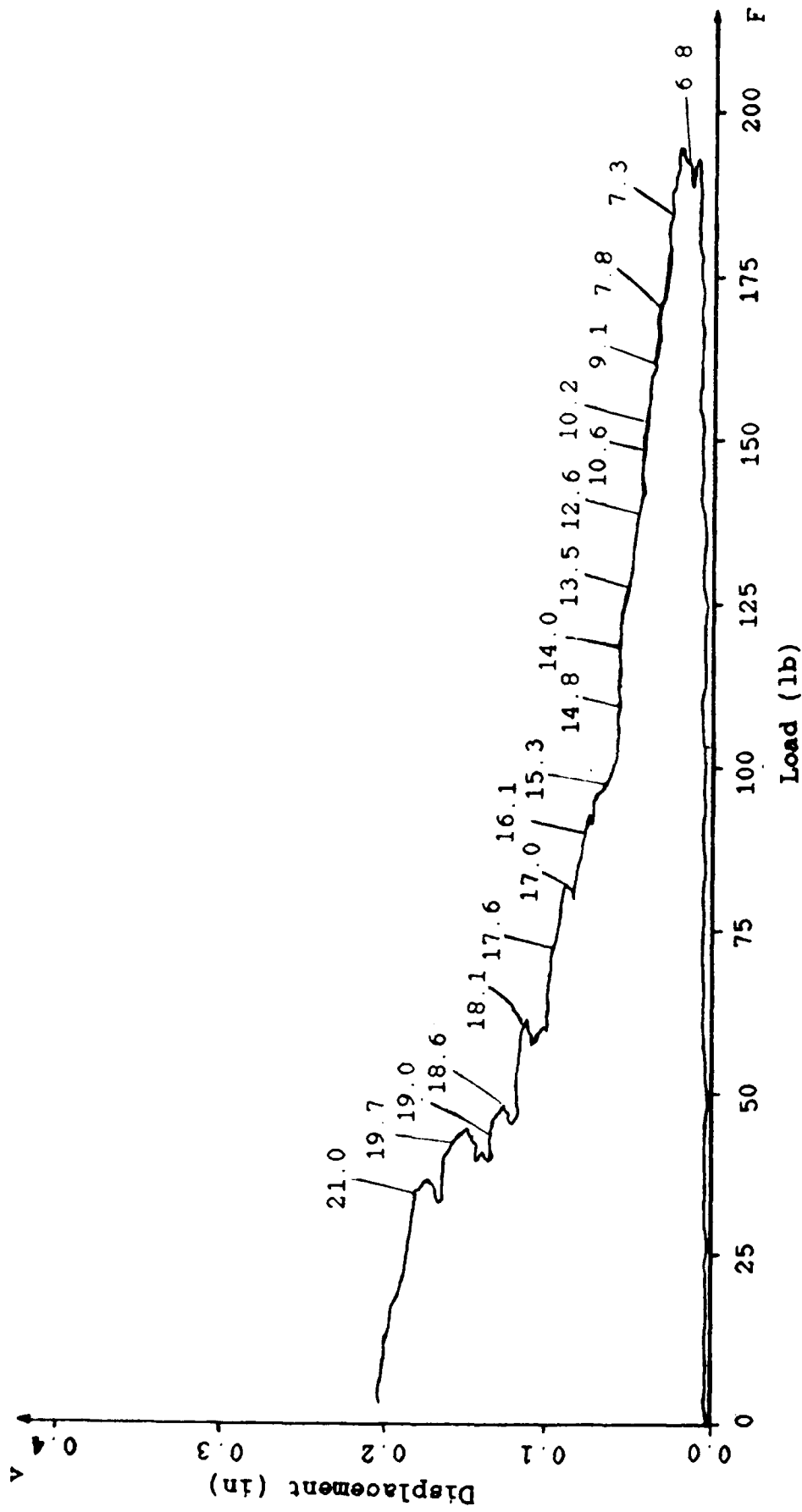


Figure 14. Displacement versus Load plot
 Vertical axis 0.1 inch per increment
 Horizontal axis 25 pounds per increment
 Crack Lengths a in centimeters are the numbers shown

of the aluminum adherend beam support thickness, the aluminum adherends were loaded in opposite directions. Dimension h in Figure 10 was 25.4 mm (1.00 inches). Again pins permitted free rotation of the specimen. Rather than testing a specimen to failure at one crosshead speed, rapid crosshead rates were chosen for initial short crack lengths. The procedure involved allowing the crack to grow an amount corresponding to a set relative vertical displacement and then the specimen was unloaded. This was repeated for nearly half the specimen. Next, the crosshead rate was decreased by a decade and the specimen was loaded to allow a set amount of vertical displacement at the new crosshead speed. Again the specimen was unloaded. Loading was repeated at the new crosshead rate or speed until the specimen completely failed. A new specimen was then mounted on the MTS equipment and the crosshead rate was decreased another decade. The process was then repeated, decreasing crosshead rate only after the crack had grown to half the length of the specimen. Testing was accomplished at room temperature. Again the MTS data recording system monitored the applied load and the beam end displacement. Critical strain energy release rates from the resulting compliances were computed using the compliance method. Upper and lower crack surfaces extended to near equal levels. No twisting nor plastic deformation occurred.

Testing the Effect of End Opening

Figure 12 shows a drawing of the split cantilever beam and its load fixture. Again the aluminum adherends were loaded in opposite directions. Dimension h in Figure 10 was 25.4 mm (1.00 in) as in the rate testing. Thus the same loading fixtures could be used. The addition of washers at position A between the splice plate and the specimen in Figure 12 resulted in an increase in compression which resulted in negative mode I component superimposed on mode III. Addition of washers at B between the center block and the splice plate in Figure 12 caused an increase in mode I which resulted in positive mode I component superimposed on mode III. The mode I component may increase or decrease slightly from machined inconsistencies in the adherends. If the dimension t in Figure 9a is smaller than the appropriate dimension the mode I component will increase. If t is larger than the appropriate dimension mode I component will decrease. During testing the end opening was measured with feeler gauges. At the loaded ends rotation of the pinned center blocks and specimen was permitted. Crosshead speeds were increased slightly as the crack length extended as was done in testing the effect of altering the thickness of the aluminum adherends. Figure 15 illustrates the step tapered center block fixtures and loaded specimen on the MTS 24.5 kN load frame. Crack lengths were measured visually approximately every centimeter during testing.



Figure 15. MTS 24.5 kN Load Frame with Indented
Fixtures and Loaded Specimen

Testing was accomplished at room temperature. The MTS data recording system monitored the applied load and the beam end displacement. A flashlight and a 10x magnifier were used to visually observe the crack growth. As with the effect of thickness and crosshead rate, the crack lengths were immediately recorded on an XY plotter displacement versus load plot. Figure 14 shows a typical plot. Crack extension occurred at a relatively steady rate. Upper and lower surface crack lengths were nearly equal at each reading. Twisting of the specimen ends was minimal. When the specimens were unloaded, they returned to their original unloaded shape. Thus, there was no plastic deformation of the aluminum adherends.

Testing the Effect of Temperature

Procedures followed in testing the effect of temperature on the strain energy release rate of the split cantilever beam specimen are the same as those followed in testing the effect of the aluminum adherend thickness except that the testing took place in a sealed environmental temperature chamber. The specimen and the appropriate loading fixtures were placed in the chamber at room temperature. The chamber was then heated electrically or cooled with liquid nitrogen to the desired temperature and allowed to stabilize at the desired temperature for 5 minutes prior to loading. Procedures for loading and measuring the crack length were the same as in the Testing the Effect of

Adherend Thickness section with the exception that the environmental test chamber had to be opened momentarily to obtain the crack length measurements.

Double Split Cantilever Plate Testing

The double split cantilever plate specimens were tested on an Instron 200 pound load frame. Prior to testing, the Instron 200 pound load frame was calibrated according to the manufacturer's instructions. Then the load fixture was attached to the Instron machine with pin connectors. After the crosshead distance was adequately adjusted, the split cantilever plate specimen was attached to the load fixture with screw fasteners.

Figure 16 is a photograph of the double split cantilever plate specimen in its load fixture on the Instron load frame used. The two outer pieces were loaded upward and the inner one was loaded downward. Crosshead speed was held at a constant 0.508 mm/min (0.02 in/min) during the entire test. Chart speed was 25.4 mm/min (1.00 in/min). At the initiation of the test the 88.96 N (20 pounds) full scale setting was used and increased to 222.4 N (50 pounds) full scale as necessary. Load versus displacement was measured continuously with an XY plotter. The displacement versus load chart was marked immediately at each half centimeter of crack growth until complete failure occurred.

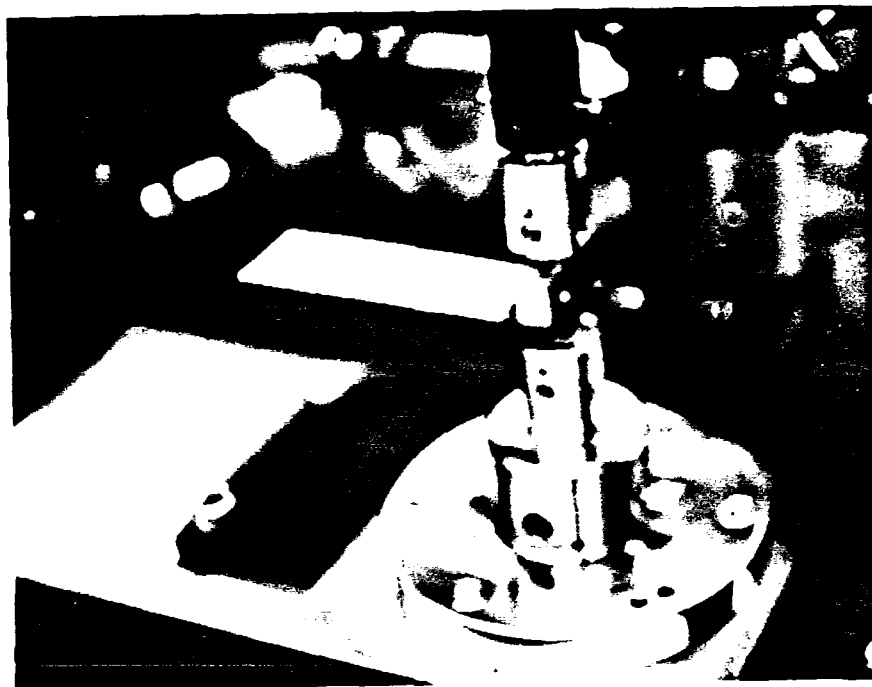


Figure 16. Split Cantilever Plate Specimen and its Loading Test Fixtures on an Instron machine

V Data Reduction

Data reduction performed to investigate the effect of thickness on the measurement of G_{IIIC} from split cantilever beam specimens involved the compliance method, beam theory, and the area method. The computer program listed in the Appendix was used for these computations. Input values for the computer program are load, displacement, and crack length. The computer program computes the critical strain energy release rate using the compliance method from Equation 40. The G_{IIIC} from beam theory was computed using Equation 34. The area method G_{IIIC} was computed from Equation 37. The program listed in the Appendix prints values for the compliance method, beam theory, and the area method as well as their averages for comparison.

Reduction of the rate test data was performed using only the compliance method which involved first using the relationship

$$C = B^* a^n \quad (41)$$

where

C = measured compliance

a = measured crack length

B^* = antilogarithm of the y intercept of the logarithm of C versus the logarithm of a relation

n = slope of the logarithm of C versus the logarithm of a relation

Differentiation gives

$$\partial C / \partial a = B^* n a^{n-1} \quad (42)$$

and substitution into Equation 29 gives

$$G_{IIIC} = (F^2 B^* n a^{n-1}) / (2 b) \quad (43)$$

where

F = maximum load at which crack growth begins

Data reduction for the measurement of rate testing concerning G_{IIIC} versus strain rate was accomplished in terms of the nominal strain rate which can be derived as follows beginning with the cantilever beam shown in Figure 17a:

$$EI (d^2 y / dx^2) = M \quad (44)$$

Thus

$$dy/dx = \int_0^x (M/EI) dx \quad (45)$$

The bending moment is $F(1-x)$ and thus

$$dy/dx = F/EI \int_0^x (1-x) dx \quad (46)$$

Upon integration

$$dy/dx = F/EI (1x - x^2/2) + A_1 \quad (47)$$

At $x = 0$ the slope dy/dx is zero and thus $A_1 = 0$

Now integrating a second time and allowing the second constant of integration to equal zero gives

$$y = F/EI (1x^2/2 - x^3/6) \quad (48)$$

For the mode III split cantilever beam shown in Figure 17b, this distance y is one half the total relative vertical

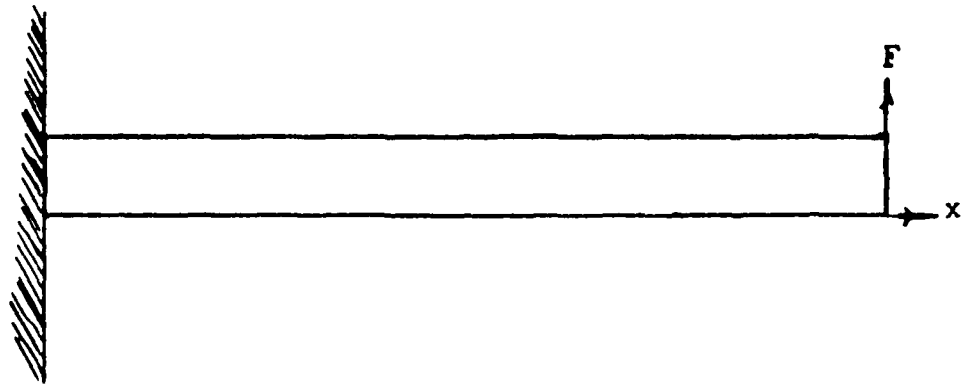


Figure 17a. Cantilever Beam

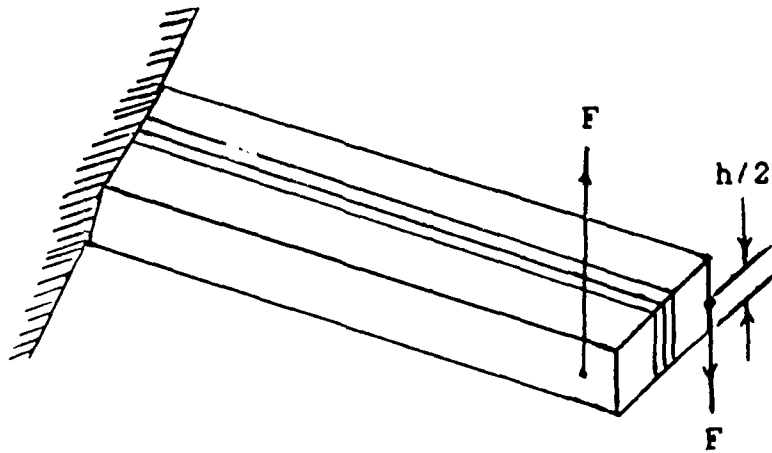


Figure 17b. Mode III Split Cantilever Beam

displacement v minus a constant overlap factor $h/2$ Thus

$$v/2 = F/EI(lx^2/2 - x^3/6) - h/2 \quad (49)$$

At the end of the cantilever beam $x = l$ and the above equation simplifies to

$$v = 2Fl^3/3EI - h \quad (50)$$

solving for E gives

$$E = 2Fl^3/(v + h)3I \quad (51)$$

Let the strain be equal to e . Then the stress is Ee and is equivalent to My/I or $Fa(h/2)/I$ where $M = Fa$ and a is the crack length in Figure 17b. Setting the stresses equal to each other gives

$$2Fl^3e/3I(v + h) = Fa(h/2)/I \quad (52)$$

Note that the effective moment of inertia I and the load F disappear from both sides upon simplifying. Now solving for the strain e

$$e = (3(v + h) a (h/2))/(2l^3) \quad (53)$$

Now realizing that $l = a$ in the split cantilever beam gives

$$e = 3h(v + h)/4a^2 \quad (54)$$

Then differentiating with respect to time results in v being replaced with \dot{v} , the derivative of the relative displacement with respect to time

Thus the nominal strain rate \dot{e} is

$$\dot{e} = 3h(\dot{v})/(4a^2) \quad (55)$$

where

$\dot{\epsilon}$ = nominal strain rate
 \dot{v} = crosshead rate

The data reduction technique used in quantifying G_{IIIC} versus inverse of fracture initiation time was also obtained from crosshead rate in the following way

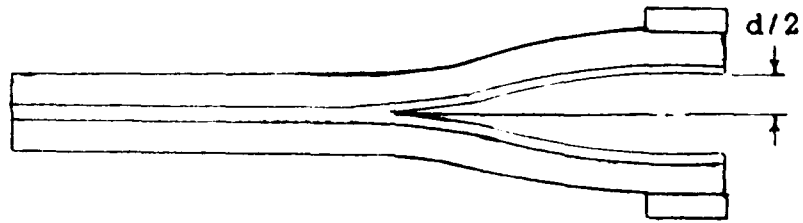
$$t_f = \dot{v}/v \quad (56)$$

where

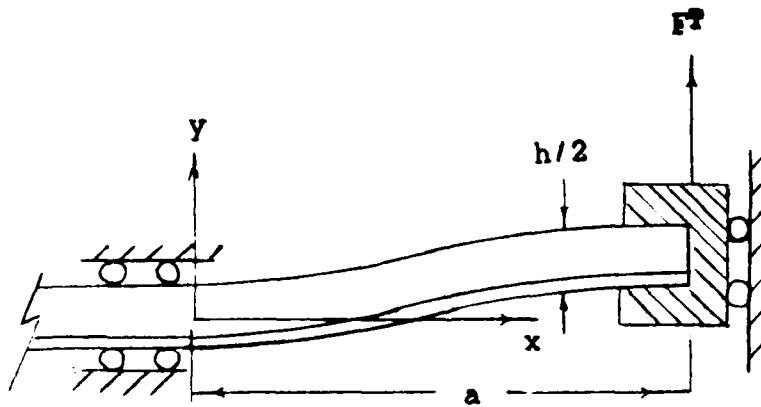
t_f = inverse of fracture initiation time
 v = relative displacement at the end of the specimen
 \dot{v} = crosshead rate

Data reduction performed to investigate the effect of shim on the measurement of G_{IIIC} from split cantilever beam specimens involved the compliance method, beam theory, and the area method. The computer program listed in the Appendix was used for these computations. Input values for the computer program were load, displacement, and crack length. Comparisons between G_{IIIC} values from compliance method, beam theory, and area method were made.

Further data reduction involved the computation of the amount of mode I added during the shim testing. Beam theory was used to estimate mode I stress at the crack tip. End opening was measured with feeler gauges. Figure 18a illustrates mode I end opening (1). Boundary conditions are shown in Figure 18b. Figure 18c is a freebody diagram. Summing forces and moments results in

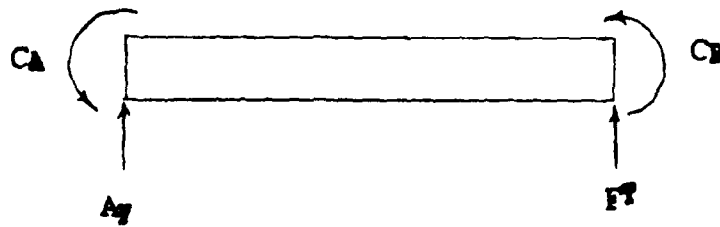


(a)

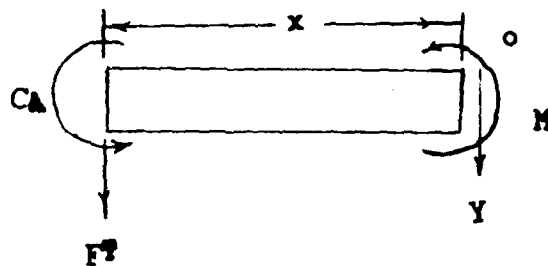


(b)

Figure 18. Mode I Diagram Donaldson (1)
 (a) End Opening (b) Boundary Conditions



(c)



(d)

Figure 18 (cont). Mode I Diagram Donaldson (1)
 (c) Beam Free Body Diagram
 (d) Beam Segment Free Body Diagram

$$A_y = -F^T \quad (57)$$

$$C_A + -F^T a + C_B = 0 \quad (58)$$

Taking one segment of the beam and summing moments about the right end of Figure 18d gives

$$M = -C_A - F^T x \quad (59)$$

Using the beam bending equation gives

$$E^f I^t (d^2 y / dx^2) = M \quad (60)$$

where

y = displacement

$E^f I^t$ = transverse flexural modulus of the beam

I^t = transverse area moment of inertia of the beam

Substitution of Equation 59 into equation 60 followed by integration of the equation twice results in

$$E^f I^t y = -F^T x^3 / 6 - C_A x^2 / 2 + C_1 x + C_2 \quad (61)$$

Figure 18b provides us with three boundary conditions

$$x = 0, \quad dy/dx = 0$$

$$x = 0, \quad y = 0$$

$$x = a, \quad dy/dx = 0$$

Solving Equation 61 for y gives

$$y = (F^T a x^2 / 4 - F^T x^3 / 6) / (E^f I^t) \quad (62)$$

At the end of the beam $x = a$. Thus

$$y(x = a) = d/2$$

$$y = F^T a^3 / (12 E^f I^t) \quad (63)$$

Now combine equations 1, 19, and 63 giving

$$GI = 3 E^f I^t h^3 d^2 / (32 a^4) \quad (64)$$

where

h = full width of the specimen

a = the crack length

d = feeler gauge measurement

E_{ft} = transverse flexural modulus of the laminate
beam combination

Equation 64 was used in the determination of mode I where end opening was increased from addition of shim (1).

Data reduction performed to investigate the effect of temperature data on the measurement of G_{IIIC} from split cantilever beam specimens involved the compliance method, beam theory, and the area method.

Reduction of the split cantilever plate data was accomplished using only the compliance method and the area method. G_{IIIC} from compliance was calculated using Equation 29 where $\partial C/\partial a$ was computed using a B^*na^{n-1} where B^* is the antilogarithm of the y intercept of the logarithm of C versus the logarithm of a , n is the slope of the plot, and a is the crack length.

The area method G_{IIIC} was computed by summing the area under the F versus v curve and applying

$$G_{IIIC} = (1/b)/(dU/da) \quad (65)$$

where dU is the change in energy computed from the area under the F versus v curve and da is the change in crack length.

VI Results and Discussion

Effect of Adherend Thickness

The results from testing the effect of aluminum adherend thickness on the critical strain energy release rate of the split cantilever beam specimen are presented in Table I. Figure 19 shows the compliance versus crack length data for three thicknesses. A first order least squares fit of the data was fitted to the data for each thickness. The slope of the specimen with $h = 8.128$ mm is the top line with slope 2.89 and y intercept -3.13. The slope of the specimen with $h = 12.7$ mm is 2.67 with a y intercept of -3.15. The slope of the bottom line corresponded to the $h = 19.05$ mm specimen and has a slope of 2.58 with a y intercept of -3.24. All slopes fall within the expected compliance versus crack length slope range of 2 to 3. Except for two specimens with $h = 8.128$ mm, which were quite similar to the $h = 8.128$ mm plot shown, all results of G_{IIIC} versus crack length are plotted in Figures 20 through 25 for the 24 ply laminate specimens. Each figure shows the values of G_{IIIC} from beam theory, compliance method, and area method values for an individual specimen. Scatter in the data primarily results from major and minor extensions of the crack as it grows. This can be attributed to the non-uniformity of the composite. Scatter in calculated G_{IIIC} also occurs as the

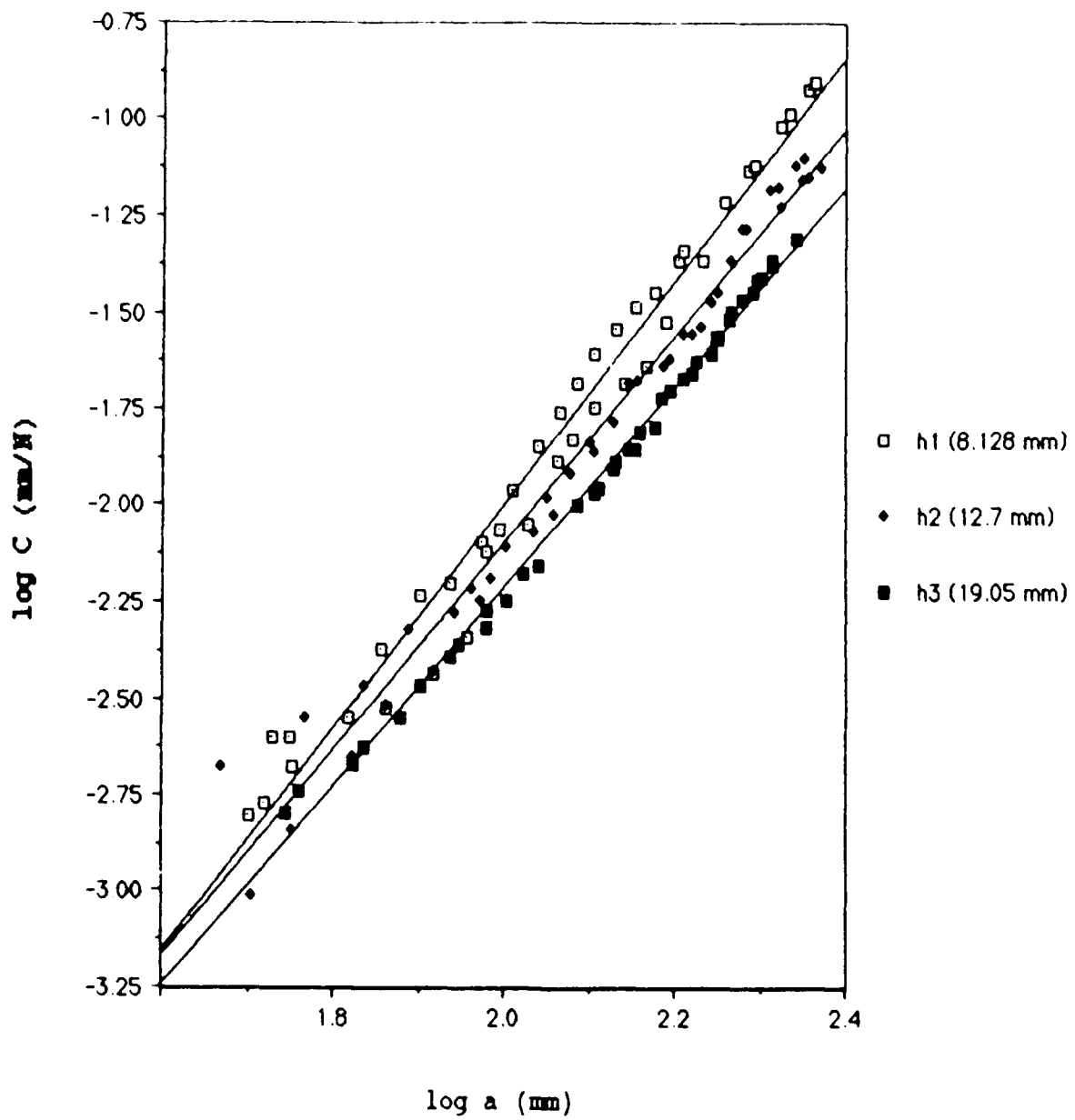


Figure 19. Compliance versus Crack Length From Thickness Testing

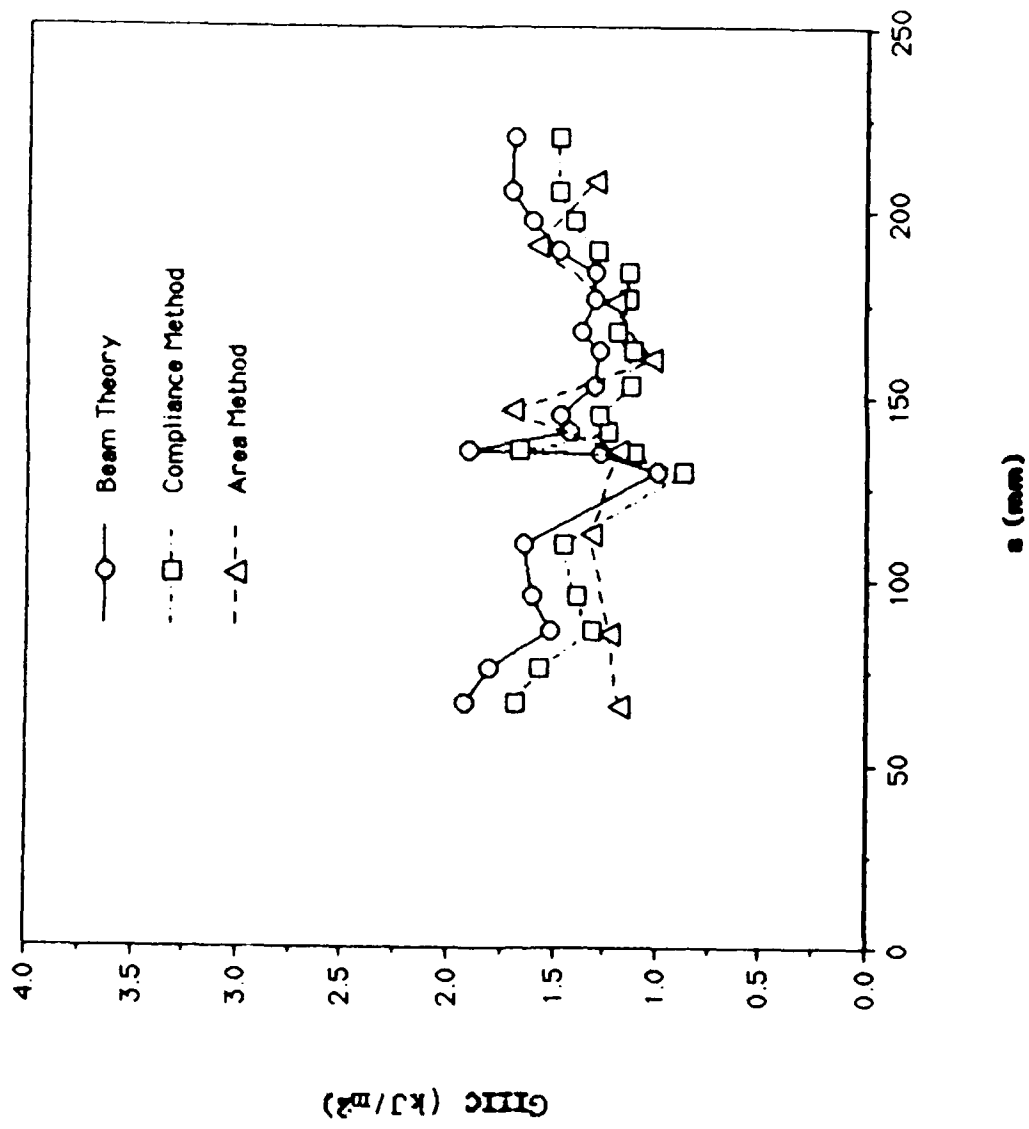


Figure 20. GIIC versus Crack Length (19.05 mm thickness - specimen #1)

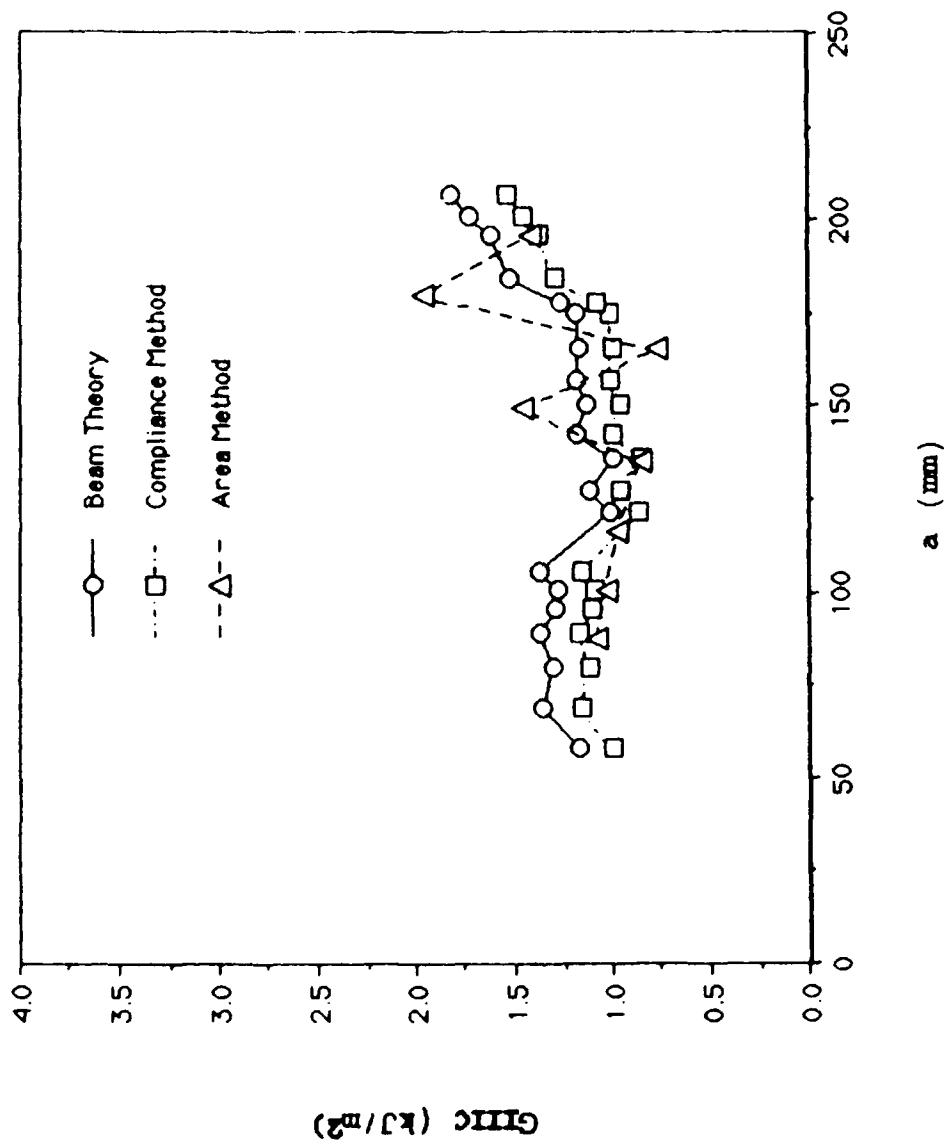


Figure 21. GIIIC versus Crack Length (19.05 mm thickness - specimen #2)

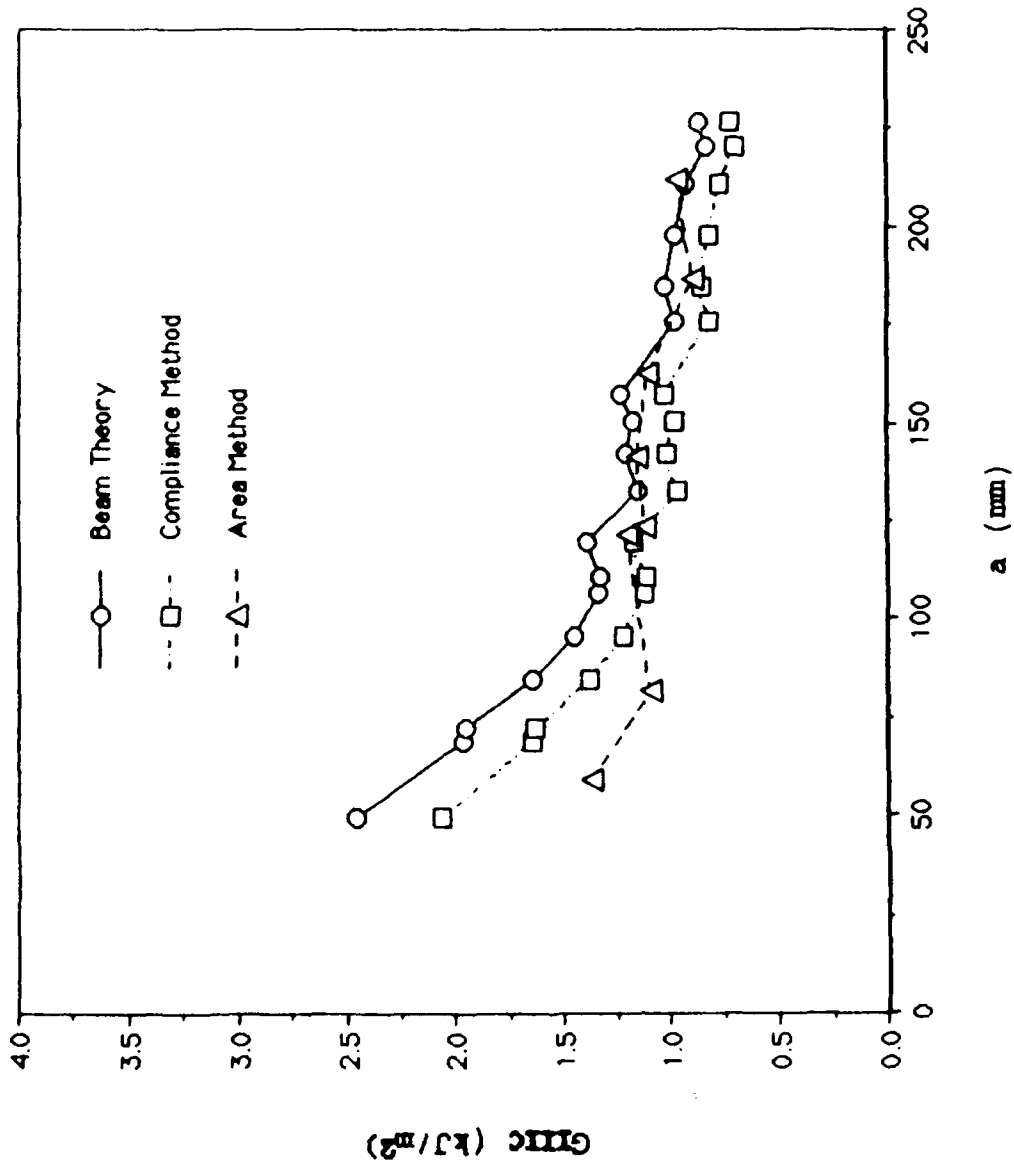


Figure 22. GIIIC versus Crack Length (12.7 mm thickness - specimen #1)

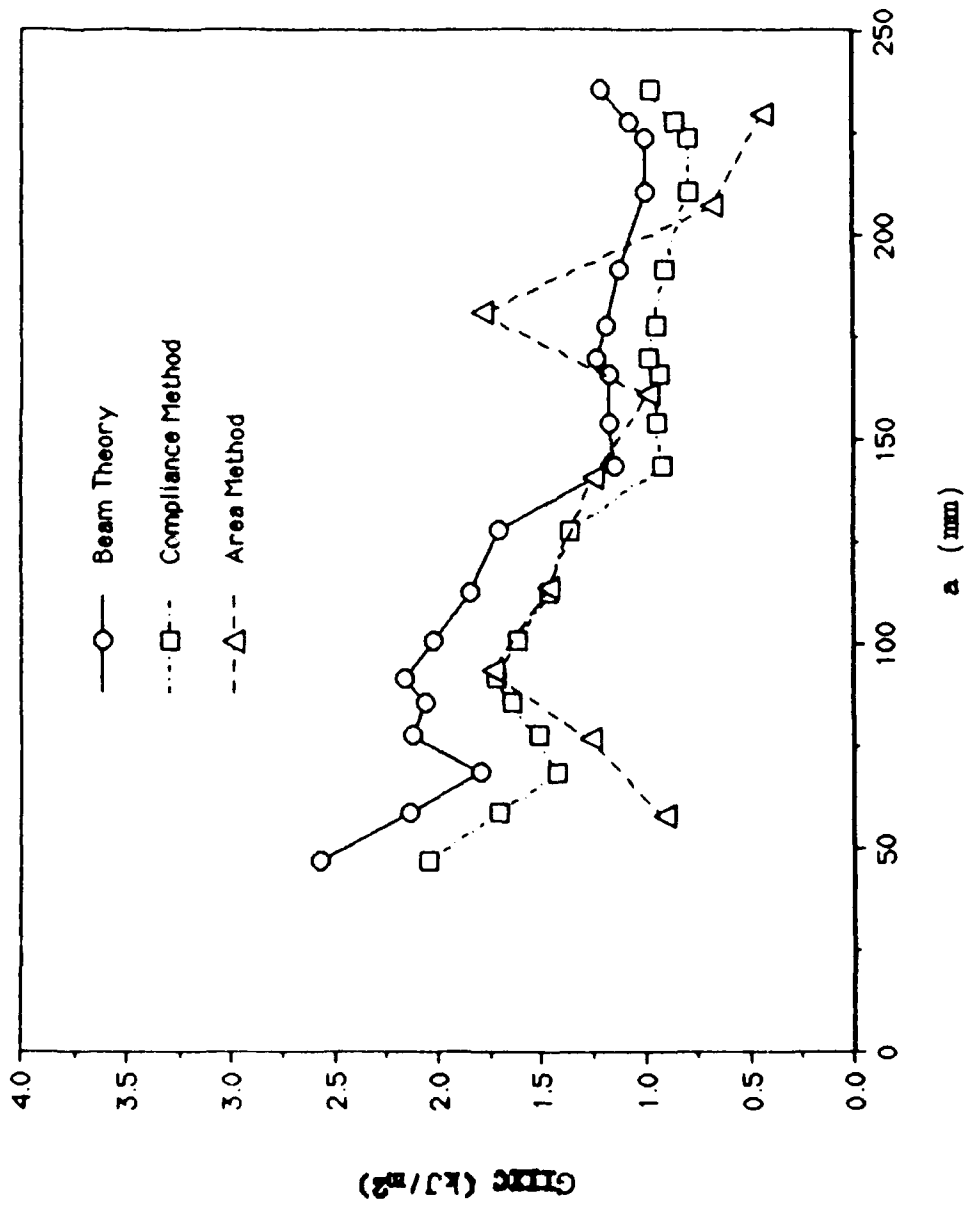


Figure 23. GIIC versus Crack Length (12.7 mm thickness - specimen #2)

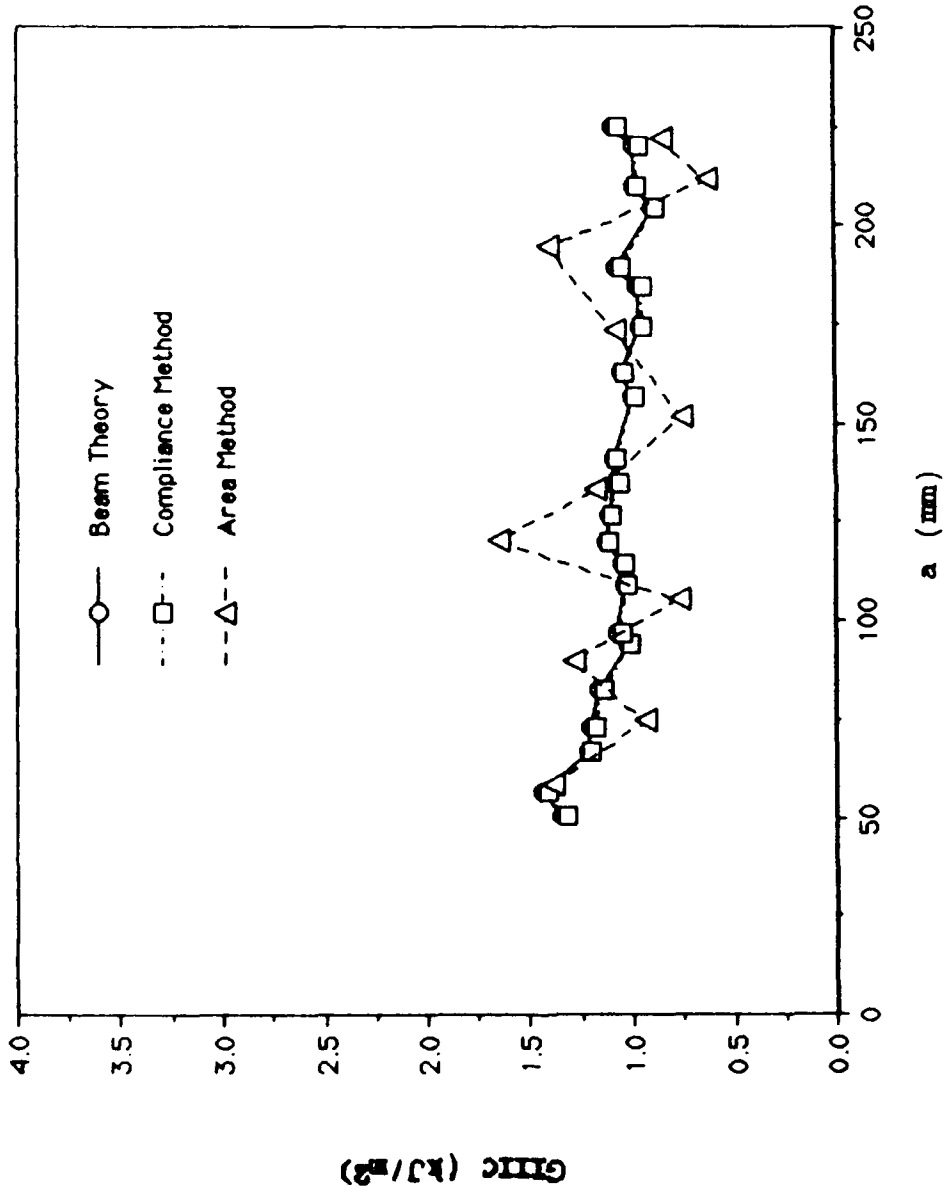


Figure 24. GIIIc versus Crack Length (12.7 mm thickness - specimen #3)

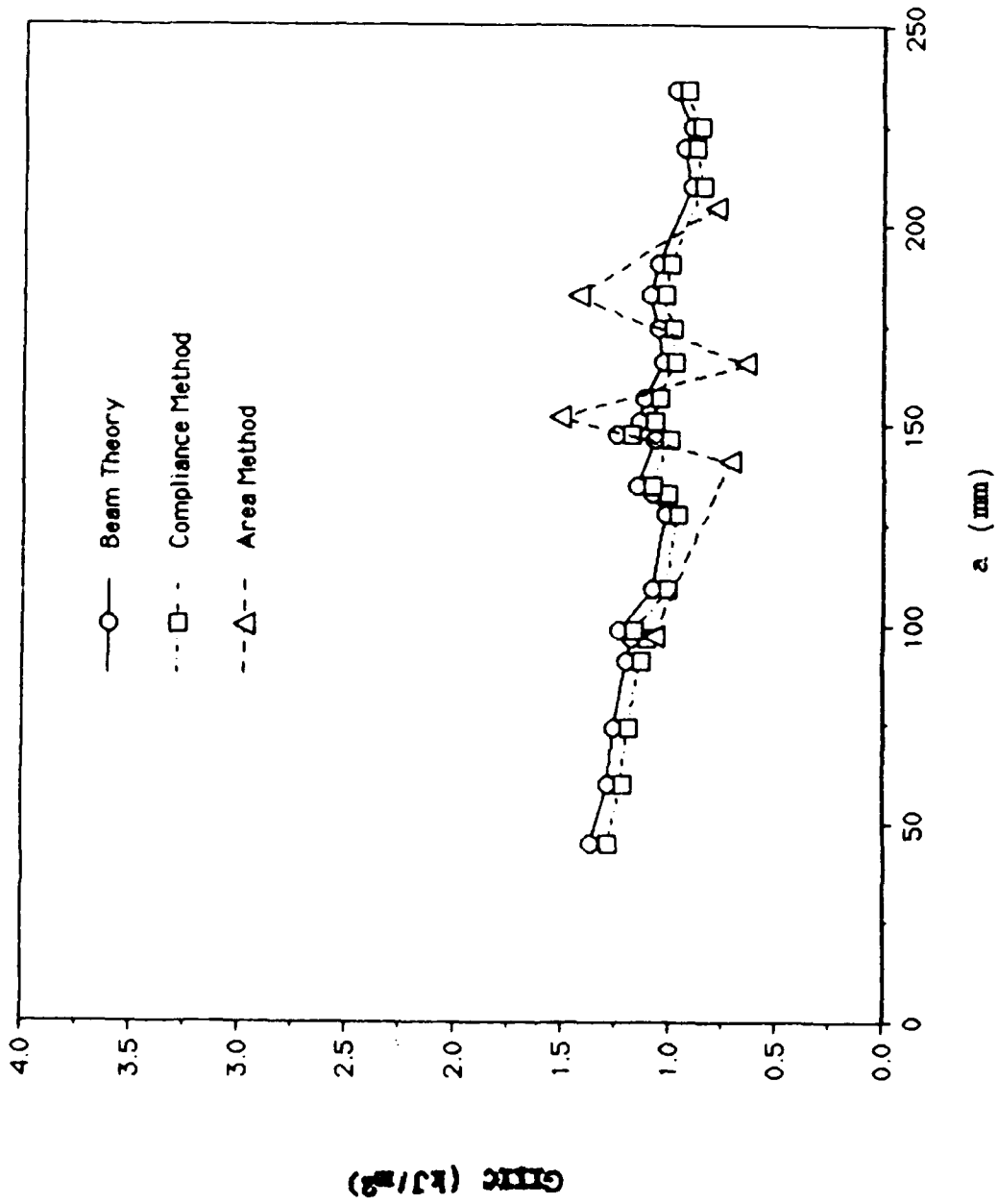


Figure 25. GIIIC versus Crack Length (8.128 mm thickness - specimen #1)

crack grows. Some of this scatter is due to errors in reading crack length. The G_{IIIC} value, however, is nearly constant when averaged throughout the specimen. Also, these figures show that area method and compliance method are in good agreement. At the shorter crack lengths, any difficulty in reading crack length results in a greater dispersion from a mean value of G_{IIIC} due to G_{IIIC} 's dependence on crack length a . This trend is seen in Figure 22 where the G_{IIIC} value tends to stabilize as the crack length increases. Thus, G_{IIIC} is more sensitive to any error in crack length reading at shorter crack lengths. Figure 26 plots all G_{IIIC} versus thickness data from Table I and also includes the data from Donaldson's 25.4 mm specimens. This comparison shows that the critical strain energy release rate does not vary with changes in adherend thickness or within each specimen. In mode I specimens, researchers have found that fiber bridging tends to increase as the crack extends and the apparent toughness increases as the crack grows. However, in this present study of mode III effect of thickness testing the fiber bridging was minimal throughout testing.

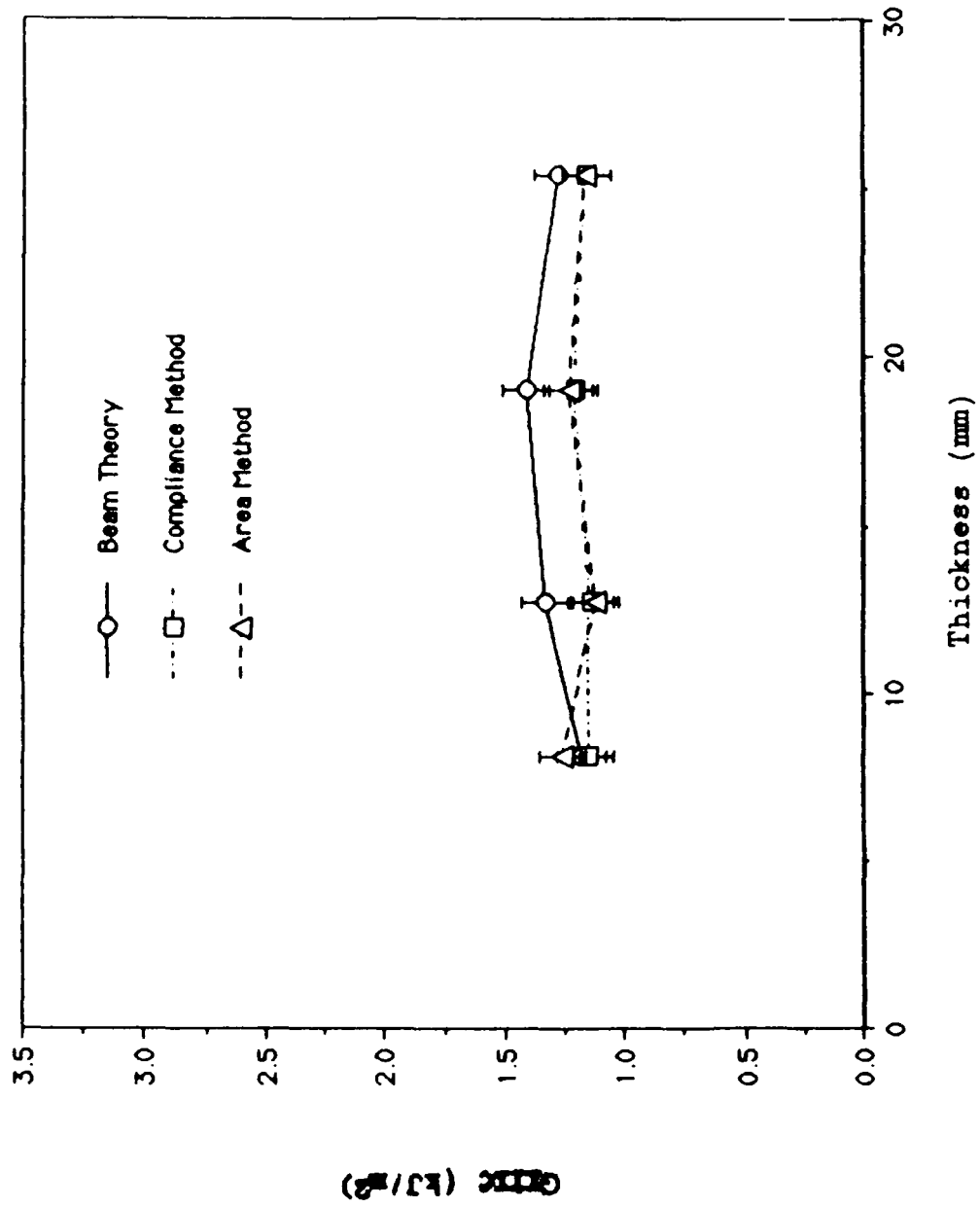


Figure 26. GIIIC versus Thickness

Table I
Effect of Adherend Thickness

Thickness h (mm)	GIIIC Beam Theory (kJ/m ²)	GIIIC Compliance Method (kJ/m ²)	GIIIC Area Method (kJ/m ²)	Number of Specimens
8.13	1.18 ± 0.09	1.15 ± 0.09	1.26 ± 0.10	3
12.70	1.33 ± 0.12	1.14 ± 0.10	1.12 ± 0.09	3
19.05	1.41 ± 0.13	1.21 ± 0.11	1.23 ± 0.11	2
25.40 ¹	1.28 ¹	1.16 ¹	1.16 ¹	3 ¹

1. Indicates data obtained from Donaldson (1).

Effect of Loading Rate

Test results from the effect of loading rate on the critical strain energy release rate of the split cantilever beam test specimen are shown in Table II. Figure 27 is a compliance versus crack length plot of all data from the effect of crosshead rate testing. The slope of the curve is 2.24 and the y intercept is -2.245. The slope falls within the predicted range of 2 to 3. The compliance was not affected by loading rate; however, the strain energy release rate was sensitive to changes in rate. Figure 28 is a plot of the GIIIC versus rate data in Table II. The figure shows a decrease in GIIIC with an increase in loading rate. This decrease is fifty percent over six decades of increase in loading rate. Smiley (23) had similar results in a mode II study. Lower crack growth rates also provided the most

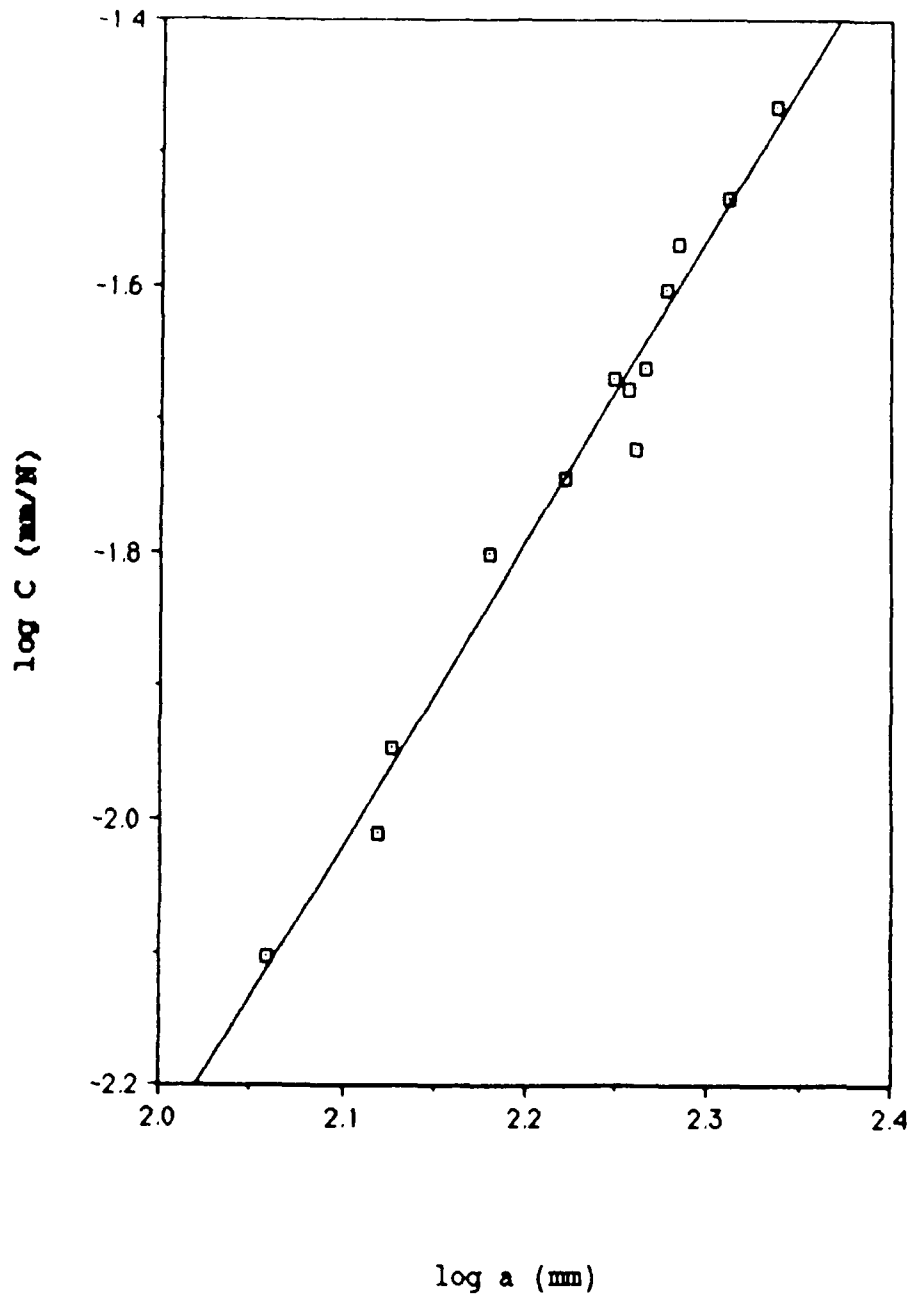


Figure 27. Compliance versus Crack Length from Crosshead Rate Testing

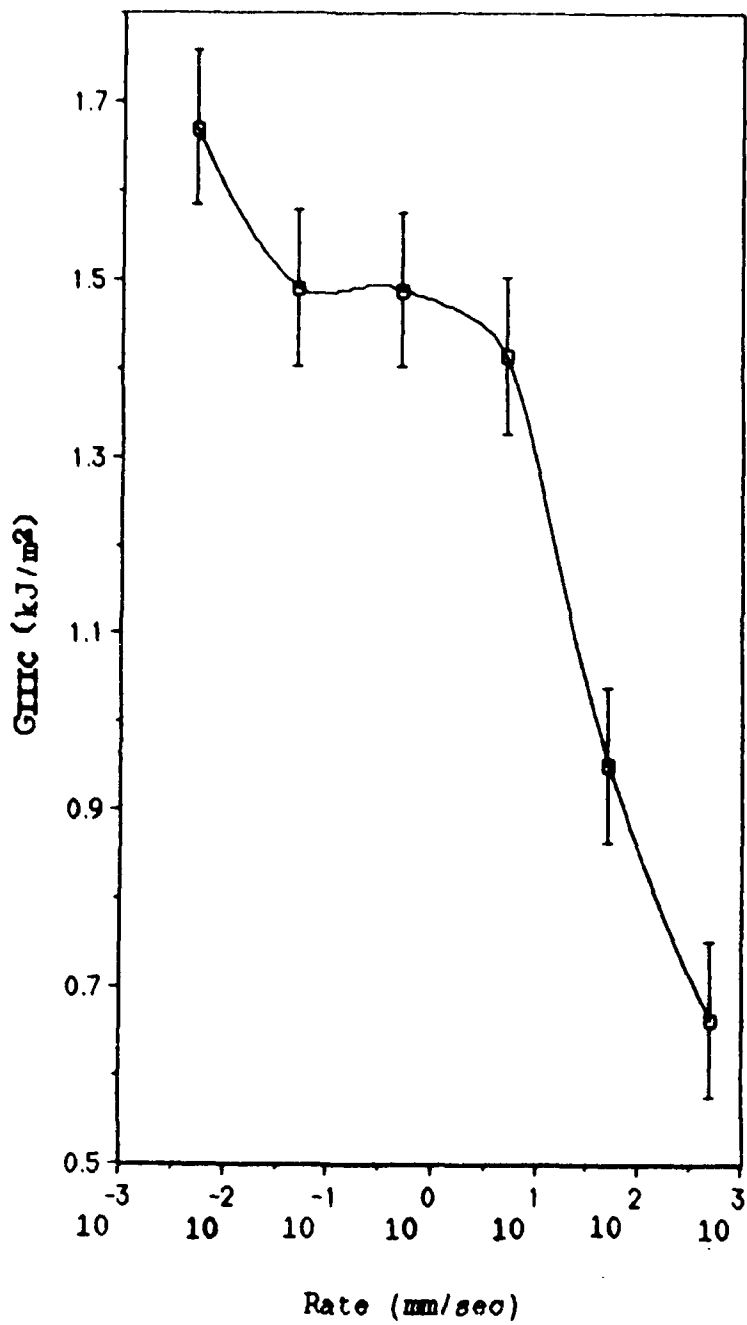


Figure 28. GIIIC versus Crosshead Rate

symmetrical crack growth as could be measured from top and bottom of the specimen.

G_{IIIC} versus crosshead speed is merely one possible way of characterizing loading rate data. Mall, Law, and Katouzian (25) state that rate dependence of fracture toughness would be most reasonably quantified in terms of some measure of crack-tip stress or strain field, but it is extremely difficult to determine this type of stress or strain field at the tip of a crack. Therefore, one alternative is to assume that the load versus displacement history measured by the MTS machine is related in a more-or-less direct way to the event at the crack tip (25). Two such parameters are nominal strain rate and inverse of fracture initiation time; these parameters are an attempt at relating occurrences at the crosshead to occurrences at the tip of the crack.

Figure 29 is a plot of G_{IIIC} versus strain rate ($\dot{\epsilon}$). At higher rates fracture toughness decreases. As shown, a best fit line through the data resulted in

$$G_{IIIC} = m_1 \log(\dot{\epsilon}) + b_1 \quad (66)$$

where

$$m_1 = -0.15297 \text{ J-s/m}^2$$

$$b_1 = 0.82461 \text{ J/m}^2$$

Figure 30 is a plot of G_{IIIC} versus the inverse of fracture initiation time. Again, G_{IIIC} decreases as the inverse of

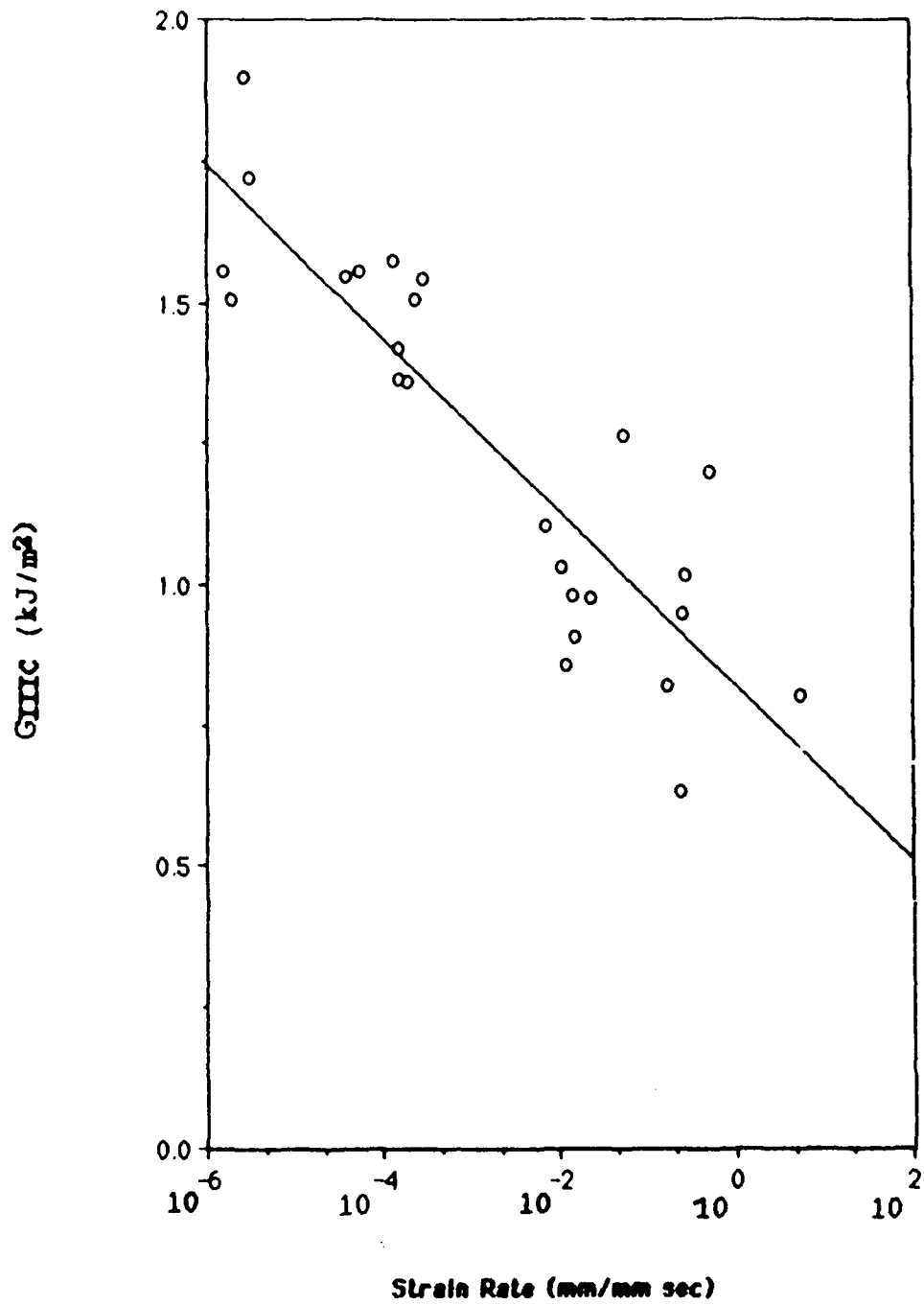


Figure 29. GIIC versus Strain Rate

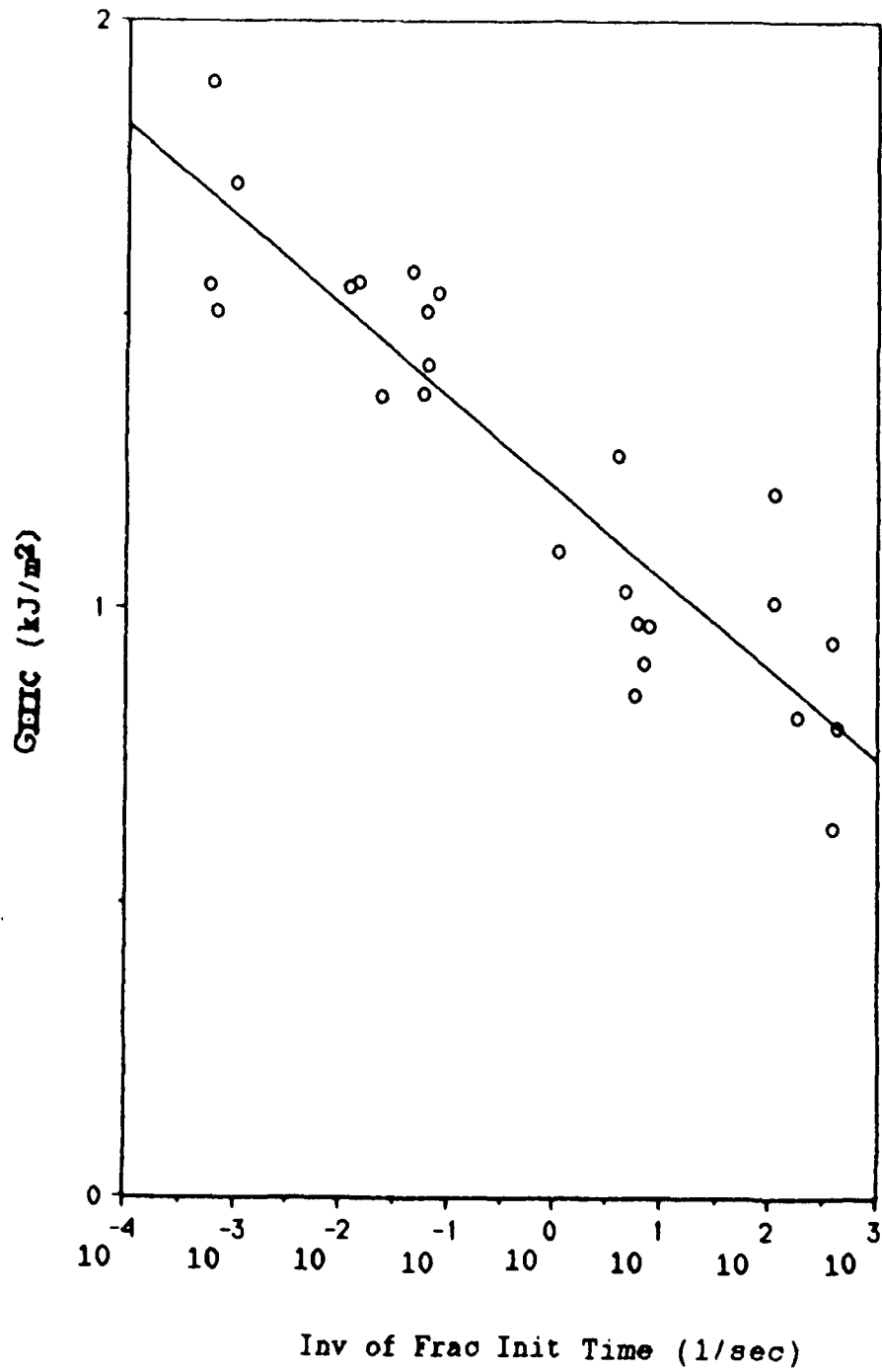


Figure 30. GIIIC versus Inverse of Fracture Initiation Time

fracture initiation time increases. As shown, a best fit line through the data resulted in

$$GIIC = m_2 \log(t_f^{-1}) + b_2 \quad (67)$$

where

$$m_2 = -0.15379 \text{ J-s/m}^2$$

$$b_2 = 1.2107 \text{ J/m}^2$$

Figures 29 and 30 show a decrease in the mode III critical strain energy release rate of AS4/3502 graphite epoxy composite laminate with increasing loading rate in spite of the scatter in the data. Similar results were found by Mall, Law, and Katouzian (25) in a mode I study of graphite/PEEK composites.

Table II

Split Cantilever Beam Effect of Crosshead Rate Results

Rate (mm/sec)	GIIC (kJ/m ²)	Number in Sample
0.00508	1.67 ± 0.13	4
0.0508	1.49 ± 0.14	3
0.508	1.48 ± 0.12	5
5.08	1.41 ± 0.11	4
50.8	0.95 ± 0.13	5
508.0	0.66 ± 0.14	22

Effect of End Opening

The test results from the effect of end opening testing on the strain energy release rate of split cantilever beam specimens composed of [024]_T AS4/3502 graphite/epoxy composite laminates are presented in Table III. Compliance versus crack length for the specimens with an added mode I component are shown in Figure 31. The top two data sets have a slope of 2.7 and the bottom has a slope of 2.9. The slope of the logarithm of compliance versus the logarithm of crack length is again within the expected range of 2 to 3. Figures 32 through 36 are the G_C versus crack length data for the specimens tested. Figure 37 shows the trend of the G_{IIIC} versus compression and end opening. Small amounts of compression increase the friction, thereby increasing the G_{IIIC} or strain energy necessary to grow the crack. Increasing the end opening a slight amount changes the strain energy required to grow the crack by only a small amount. Only at greater than a 2.54 mm end opening did the mode I component cause the G_C value to drop off noticeably. Figures 38, 39, and 40 show the effect of adding 1.729 mm, 2.416 mm, and 2.991 mm of mode I respectively. G_C and G_{IIIC} is plotted as a function of crack length in millimeters.

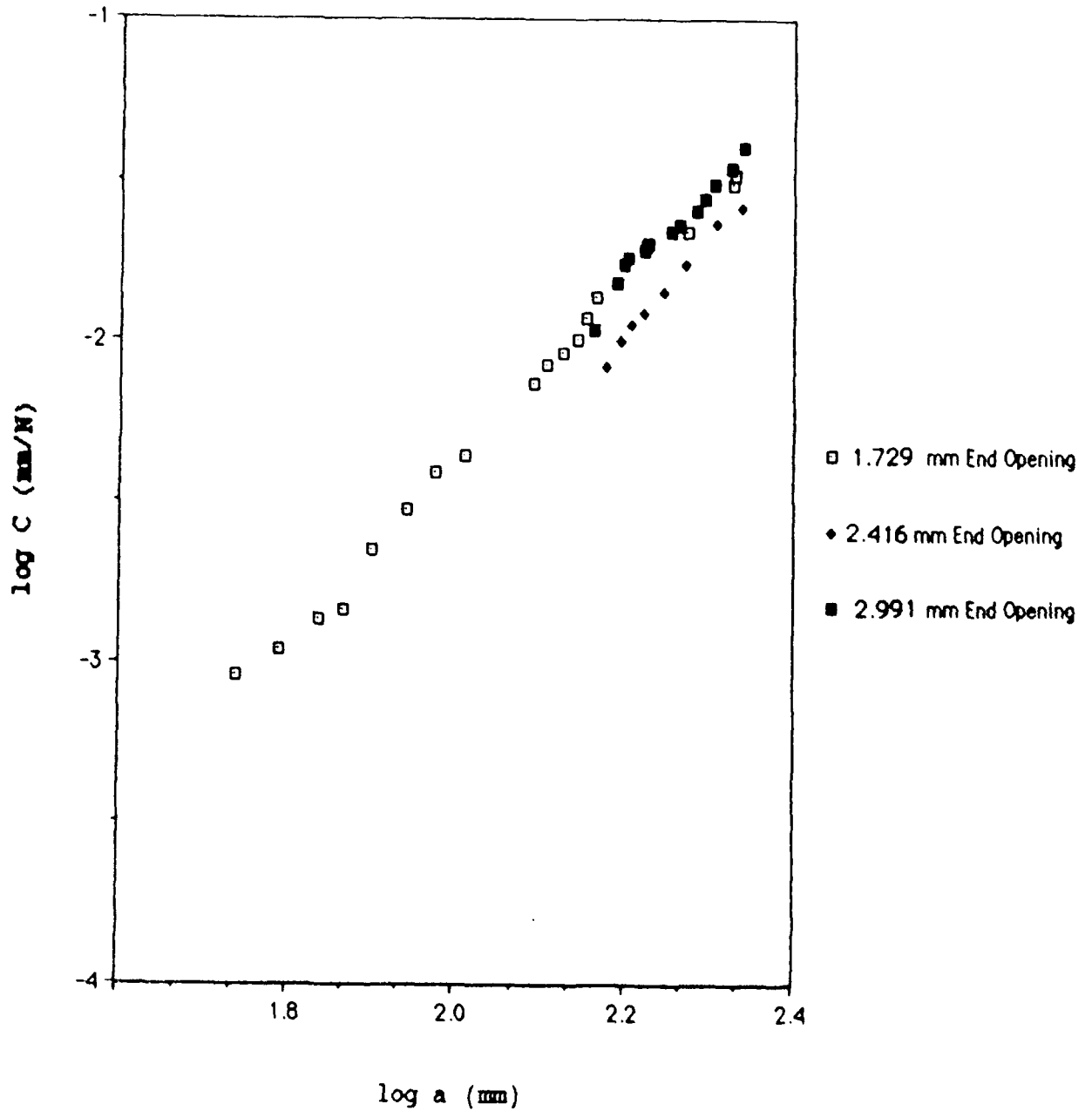


Figure 31. Compliance versus Crack Length from End Opening Testing

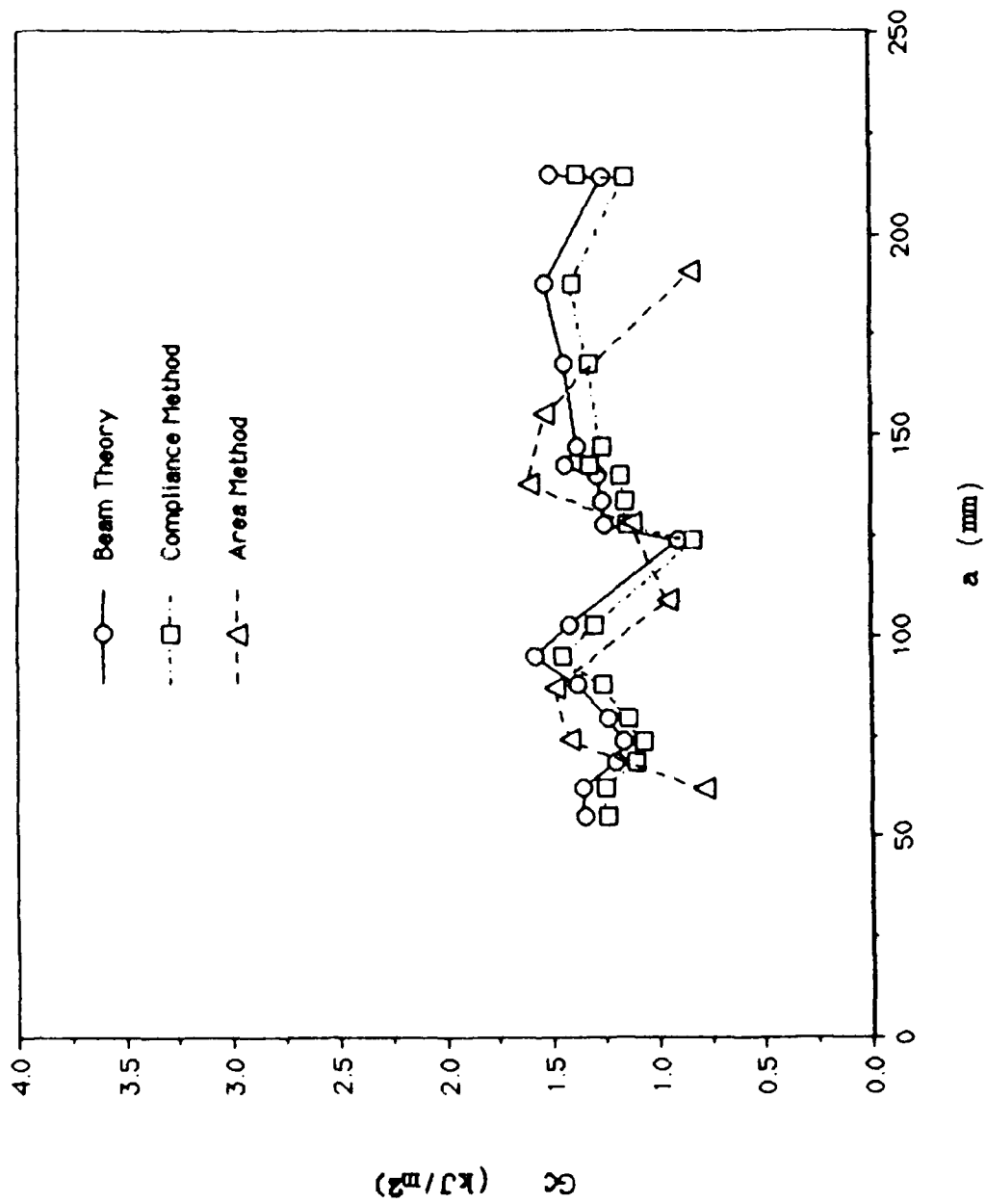


Figure 32. G_c versus Crack Length from 1.729 mm End Opening

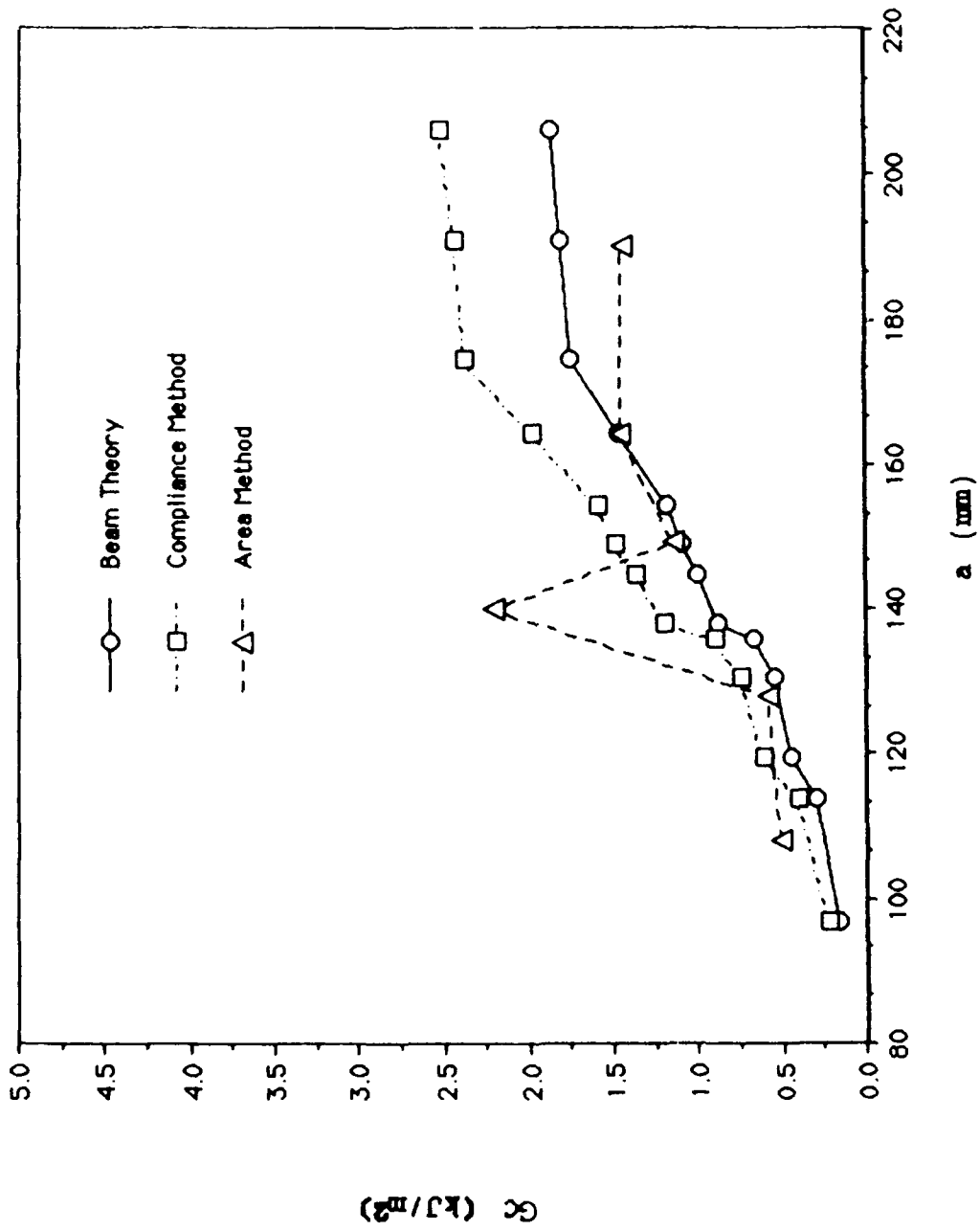


Figure 33. G_c versus Crack Length from 2.416 mm End Opening

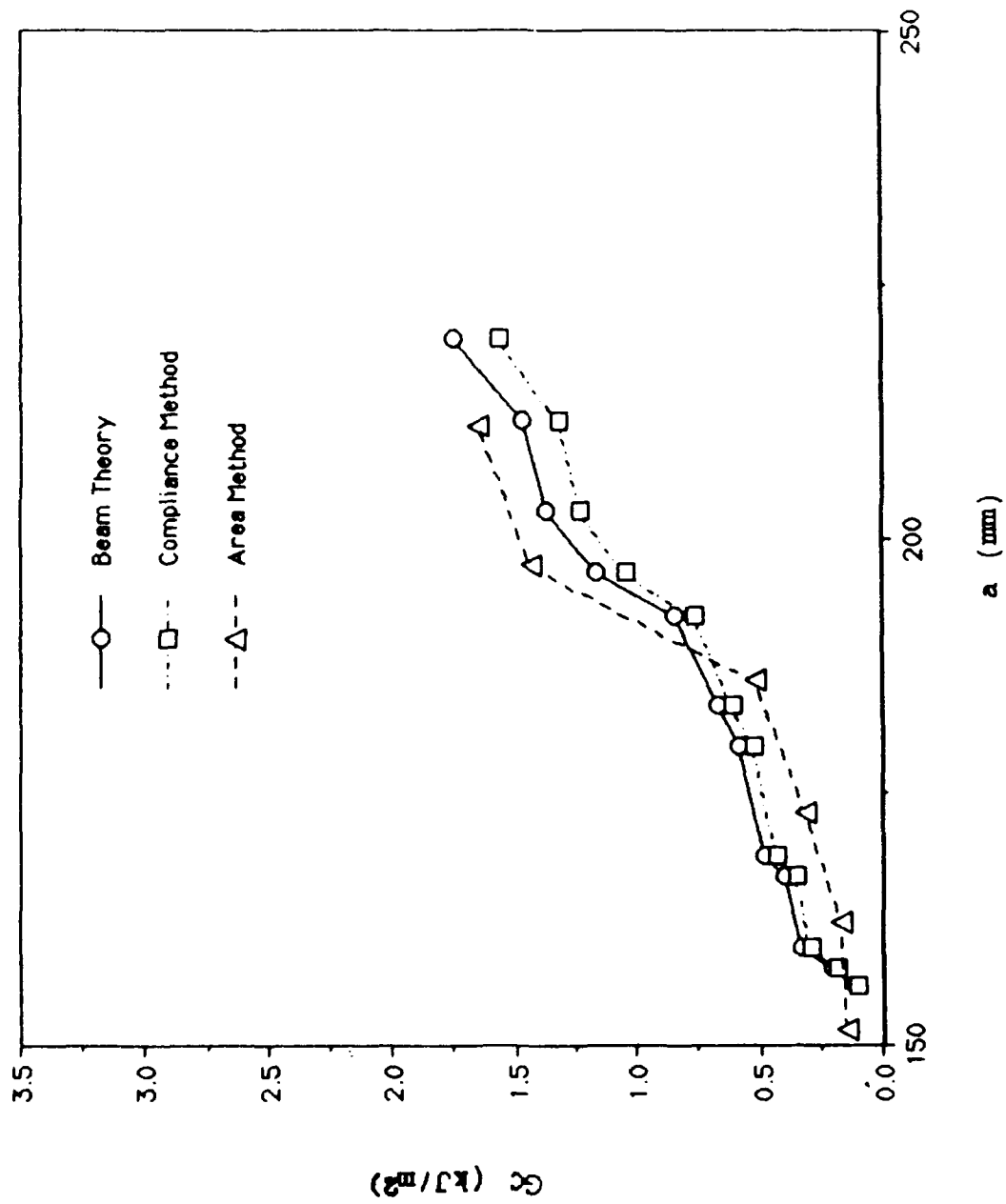


Figure 34. G_c versus Crack Length from 2.991 mm End Opening

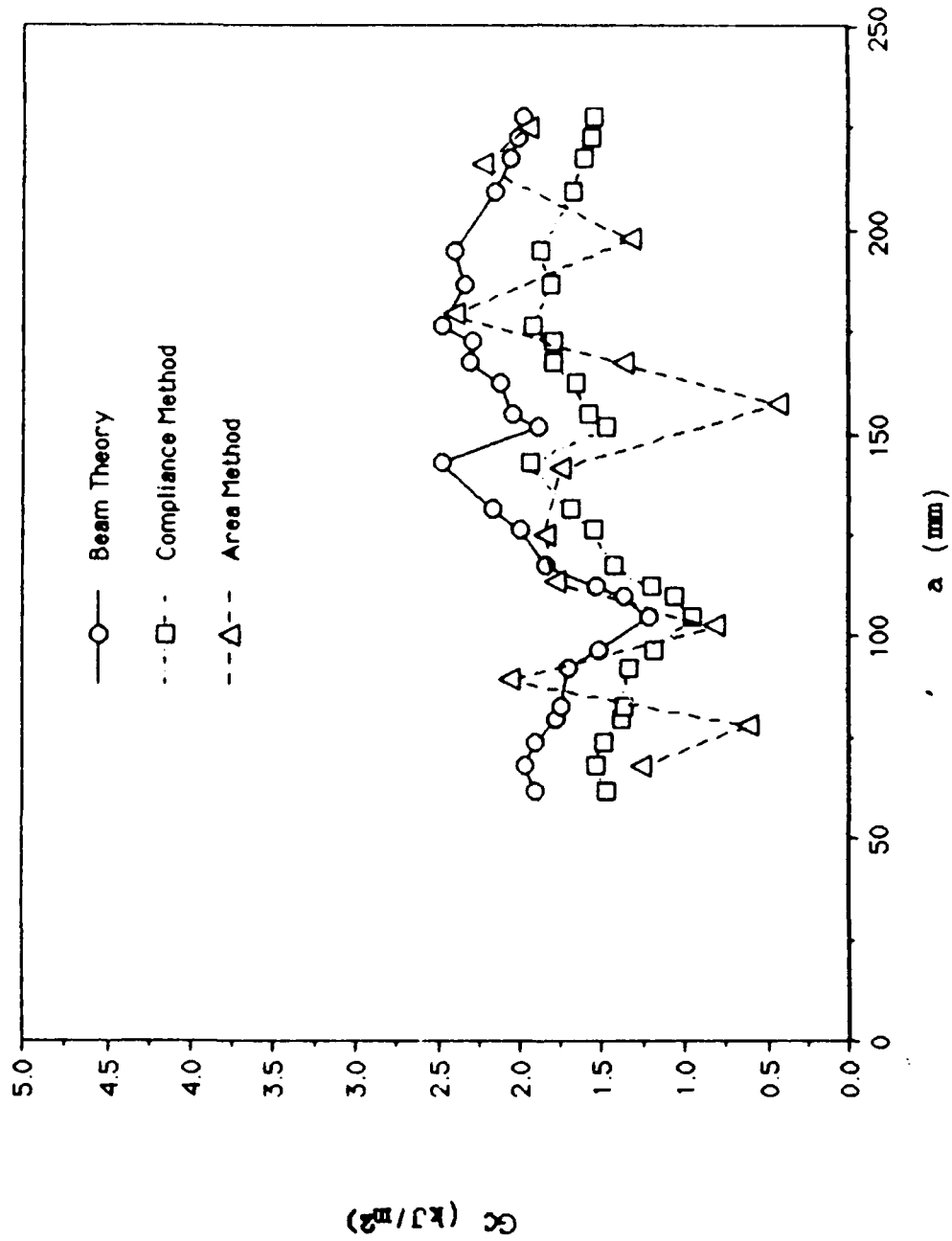


Figure 35. G_c versus Crack Length from 0.772 mm Compression

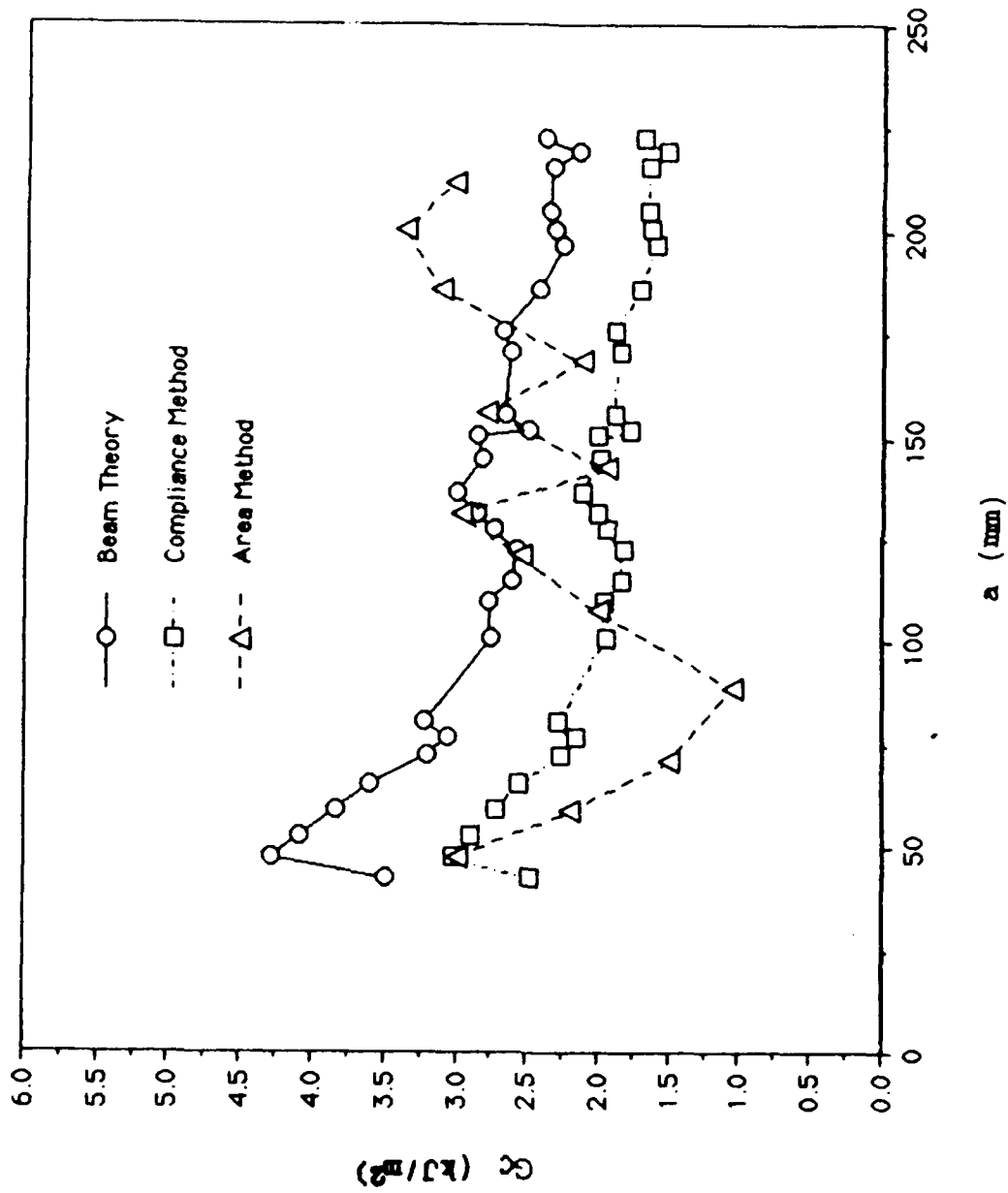


Figure 36. G_c versus Crack Length from 0.890 mm Compression

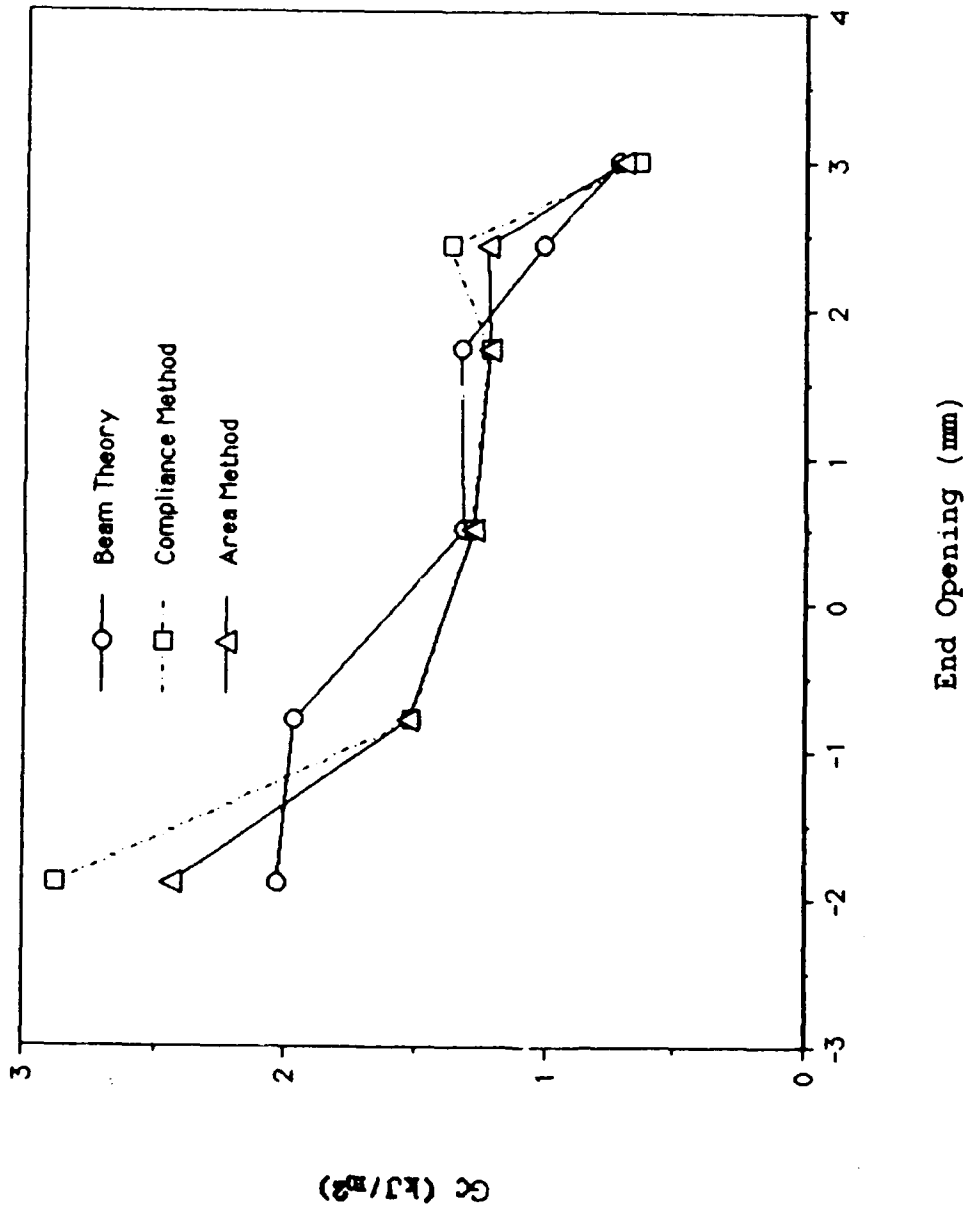


Figure 37. G_c versus End Opening

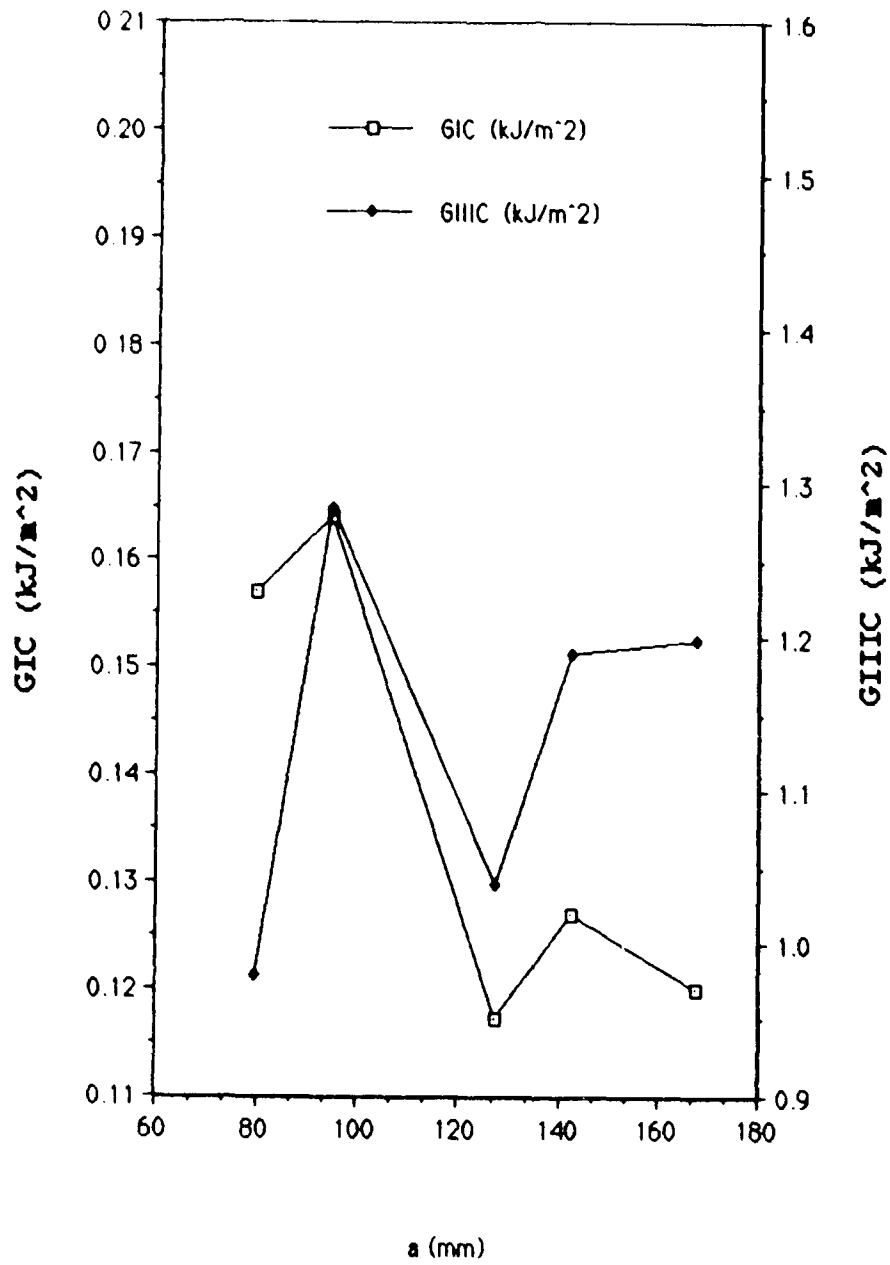


Figure 38. GIC and GIIC versus Crack Length
1.729 mm End Opening

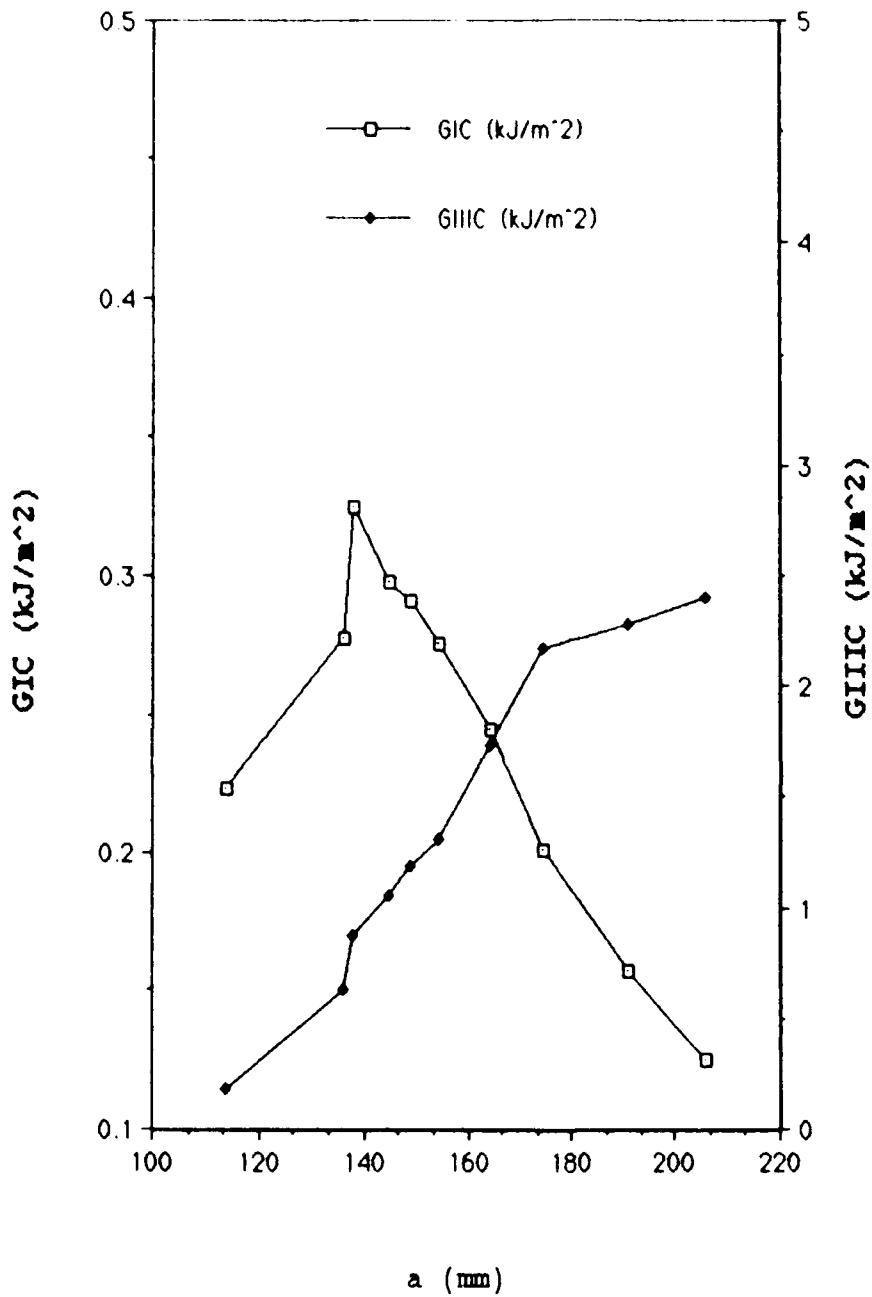


Figure 39. GIC and GIIC versus Crack Length
2.416 mm End Opening

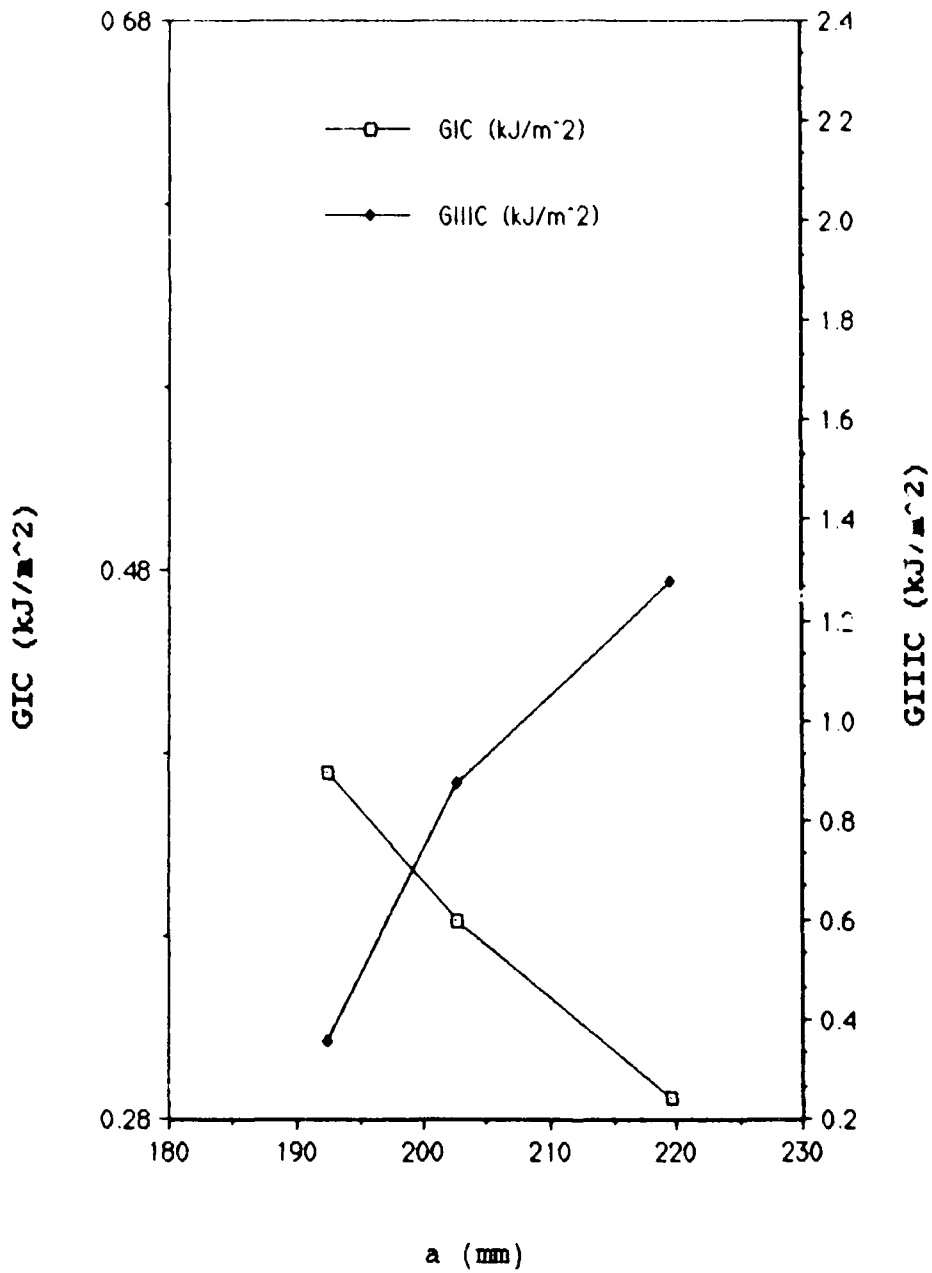


Figure 40. GIC and GIIC versus Crack Length
2.991 mm End Opening

Table III
Results From the Effect of End Opening

End Opening (mm)	G _c Beam Theory (kJ/m ²)	G _c Compliance Method (kJ/m ²)	G _c Area Method (kJ/m ²)
+0.501	1.321 ± 0.13	1.276 ± 0.10	1.278 ± 0.12
+1.729	1.330 ± 0.10	1.218 ± 0.11	1.217 ± 0.14
+2.416	1.019 ± 0.09	1.373 ± 0.12	1.226 ± 0.13
+2.991	0.726 ± 0.09	0.648 ± 0.08	0.702 ± 0.14
-0.772	1.972 ± 0.14	1.524 ± 0.13	1.527 ± 0.14
-1.890	2.036 ± 0.15	2.879 ± 0.15	2.434 ± 0.14

Effect of Temperature

The very first attempt to investigate the effect of temperature on the strain energy release rate of the split cantilever beam specimen was accomplished using a film adhesive which cured at 150.0 C, AS4/3502 [024]_T layup, and aluminum adherends. Upon removing the specimens from the oven and unclamping them, thermal residual forces cracked the specimens in a mode I delamination failure rendering them useless for any mode III testing.

The next attempt to investigate the effect of temperature on the split cantilever beam specimen was accomplished using a room temperature cured paste epoxy with an [024]_T AS4/3502 layup and aluminum adherends. Testing was

accomplished at a temperature of 65.6 C. These tests resulted in debonding from thermal expansion coefficient mismatch after the crack had grown approximately half the length of the specimen. Only a few data points at the beginning of a specimen could be used. A decision was made to test [90₁₁/0₁]_s and use steel adherends to decrease the differential between the laminate and the adherend thermal expansion coefficients.

The test results from the effect of temperature on the critical strain energy release rate of the split cantilever plate specimen are presented in Table IV. Figure 41 shows the G_{IIIIC} versus temperature data. In the [90₁₁/0₁]_s steel adherend specimens crack jumped to bondline for crack growth between 10 and 14 cm at all temperatures, crack growth beyond 14 cm was heavily fiber bridged and grew parallel to the second crack which grew along the bondline; thus, data beyond these points were not useful but has been tabulated in parentheses in Table IV. Fiber bridging was more pronounced after the crack jumped to the bondline at all temperatures. The failure of the crack to grow between the two zero degree plies most likely is due to the weakness of the 90 degree plies in the symmetric laminate used. A typical [0₂₄] specimen had normal growth until approximately 12 cm. At approximately 12 cm, a parallel crack nearer to the bondline initiated. Fiber bridging became more pronounced after the second crack started. This phenomenon appeared at

Table IV

Results from the Effect of Temperature

Temperature (C)	Laminate	Adherend	GIIC Beam Theory (kJ/m ²)	GIIC Compliance (kJ/m ²)	GIIC Area Method (kJ/m ²)	Number of Specimens
-53.8	[024]T	Aluminum	0.98 (1.20)	1.47 (1.79)	2.02 (1.23)	1
-17.8	[024]T	Aluminum	1.66 (1.94)	1.17 (1.35)	1.45 (1.88)	1
21.1	[024]T	Aluminum	1.19 (1.79)	1.16 (1.69)	1.15 (1.61)	6
21.1	[9011/01]S	Steel	1.28 (2.81)	1.28 (2.88)	1.34 (4.37)	3
65.5	[9011/01]S	Steel	0.86 (1.01)	1.11 (1.25)	1.15 (1.00)	2
65.5	[024]T	Steel	1.20 (0.57)	0.78 (0.37)	0.48 (0.76)	1
121.1	[9011/01]S	Steel	-----1	-----1	-----1	1

1Complete debonding at the metal/laminate interface.

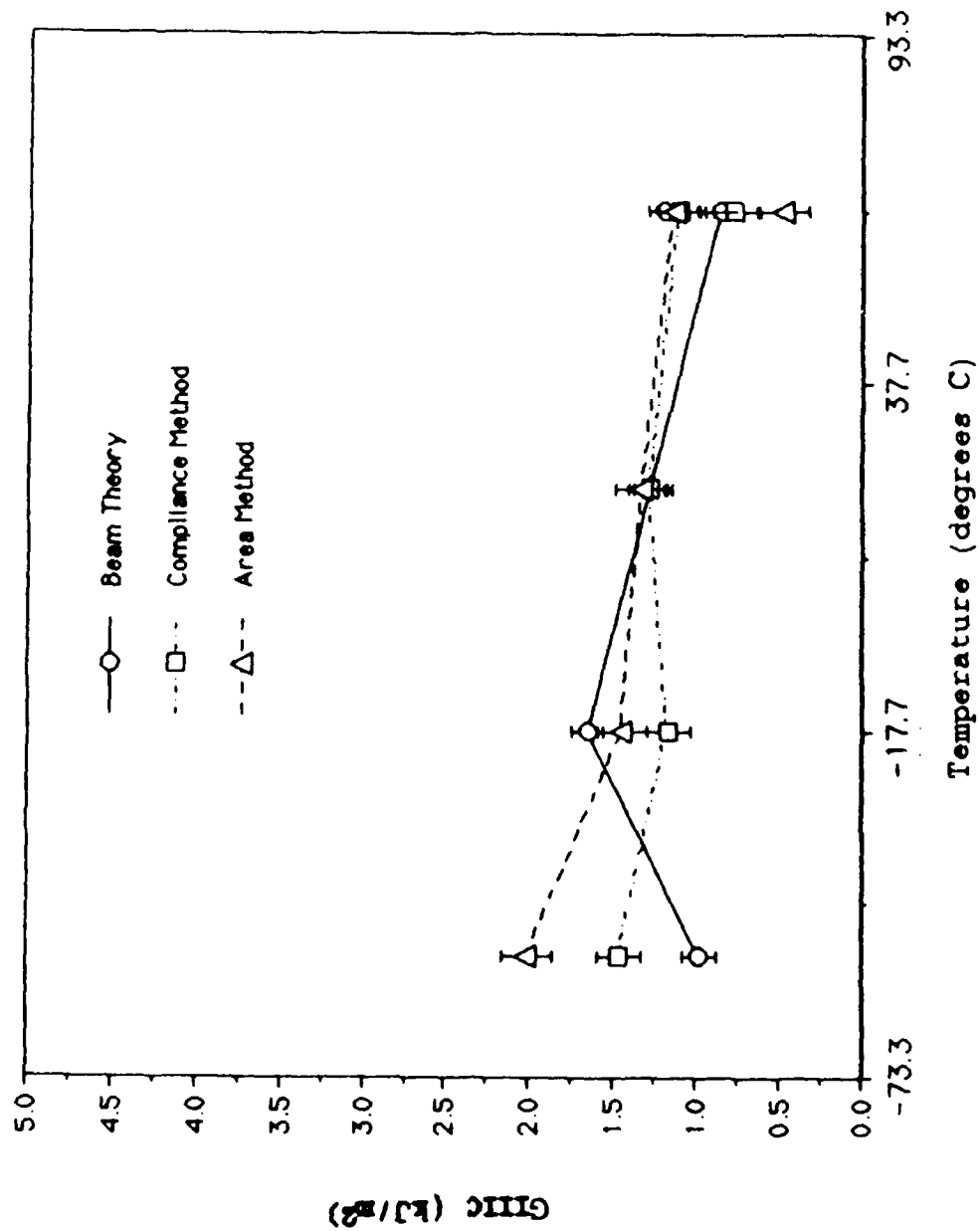


Figure 41. GIIC versus Temperature

all the temperatures tested in the chamber and was not significantly affected by adherend type. Data collected after fiber bridging is again shown in parentheses in Table IV

Mode I debonding was a problem at -53.88 C in an aluminum adherend specimen. This mode I debonding occurred opposite the loaded end. At this extremely low temperature, the mismatch of thermal contraction became a problem. The aluminum adherends with a higher thermal expansion coefficient contracted more quickly than the laminate. The aluminum thus gradually pulled itself away from the laminate at the unloaded end in a mode I type debonding. At -17.7 C mode I debonding was not a factor; however the specimen exhibited mode III secondary cracking at approximately 12 cm and debonding at the aluminum and laminate interface. Upon loading at 121 C, instantaneous debonding occurred at the steel and laminate interface precluding the collection of data.

Double Split Cantilever Plate Test

The results from testing the critical strain energy release rate of AS4/3502 [024]_T layup composite laminates without any aluminum adherend support and with the lamination plane rotated perpendicular to the split cantilever beam tests are presented in Table V. The strain energy release rates from the measured compliances ranged from 1.48 to

Table V
Double Split Cantilever Plate Specimen Results

Specimen Number	Thickness (mm)	Initial Crack Length (mm)	Measured Compliance (mm/N)	GIII	
				Area Method (kJ/m ²)	Compliance Method (kJ/m ²)
1	3.48	80.96	5.26E-2	1.31	1.48
2	3.40	39.69	9.36E-3	2.22	1.53
3	3.43	65.10	2.48E-2	1.73	1.90
4	3.56	52.38	2.40E-2	1.16	1.81
5	3.48	28.58	4.17E-3	3.65	1.82
Averages	3.48	n/a	1.57E-2	1.86	1.71

1.90 kJ/m² with a mean value of 1.71 kJ/m². This indicates that G_{IIIC} increases slightly as the lamination plane is rotated 90 degrees from the loading plane. The G_{IIIC} average is higher than the 1.1 to 1.26 kJ/m² reported by Donaldson (1) for his split cantilever beam specimens. Figure 42 shows a compliance versus crack length plot for the five specimens tested. The slope of the curve is 2.36 and therefore within the expected slope range of 2 to 3. Figure 43 is a plot of G_{IIIC} versus crack length for all specimens tested. The area method G_{IIIC} is higher for the shorter crack lengths. This scatter results from a non-uniform crack growth rate due to the anisotropic nature of the composite material. The overall mean critical strain energy release rate is higher than that of a split cantilever beam specimen. This is a direct result of the fact that the lamination plane has been rotated 90 degrees forcing the crack to grow through areas where the fibers are more likely to be crossed from manufacturing processes.

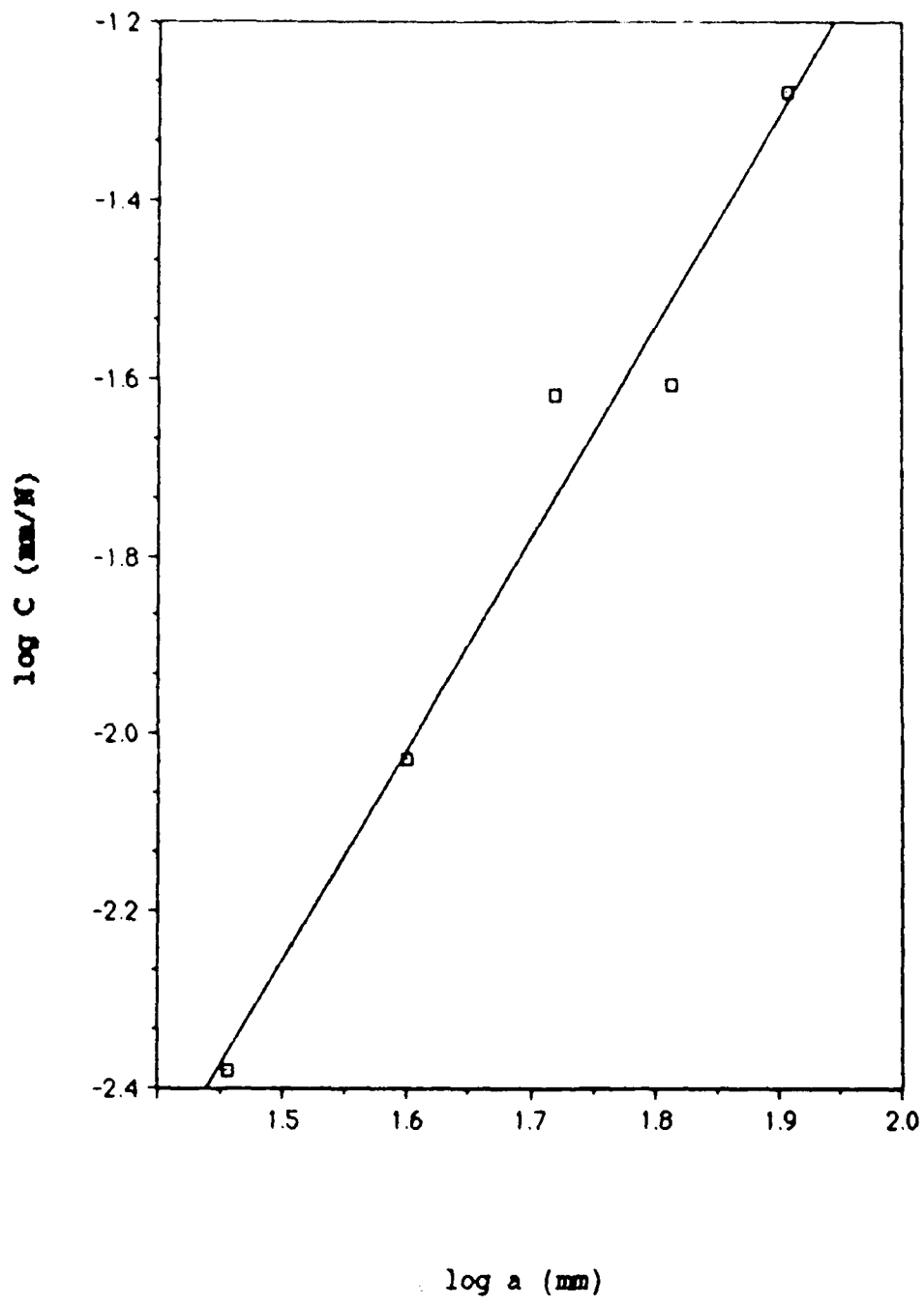


Figure 42. Double Split Cantilever Plate Compliance Calibration

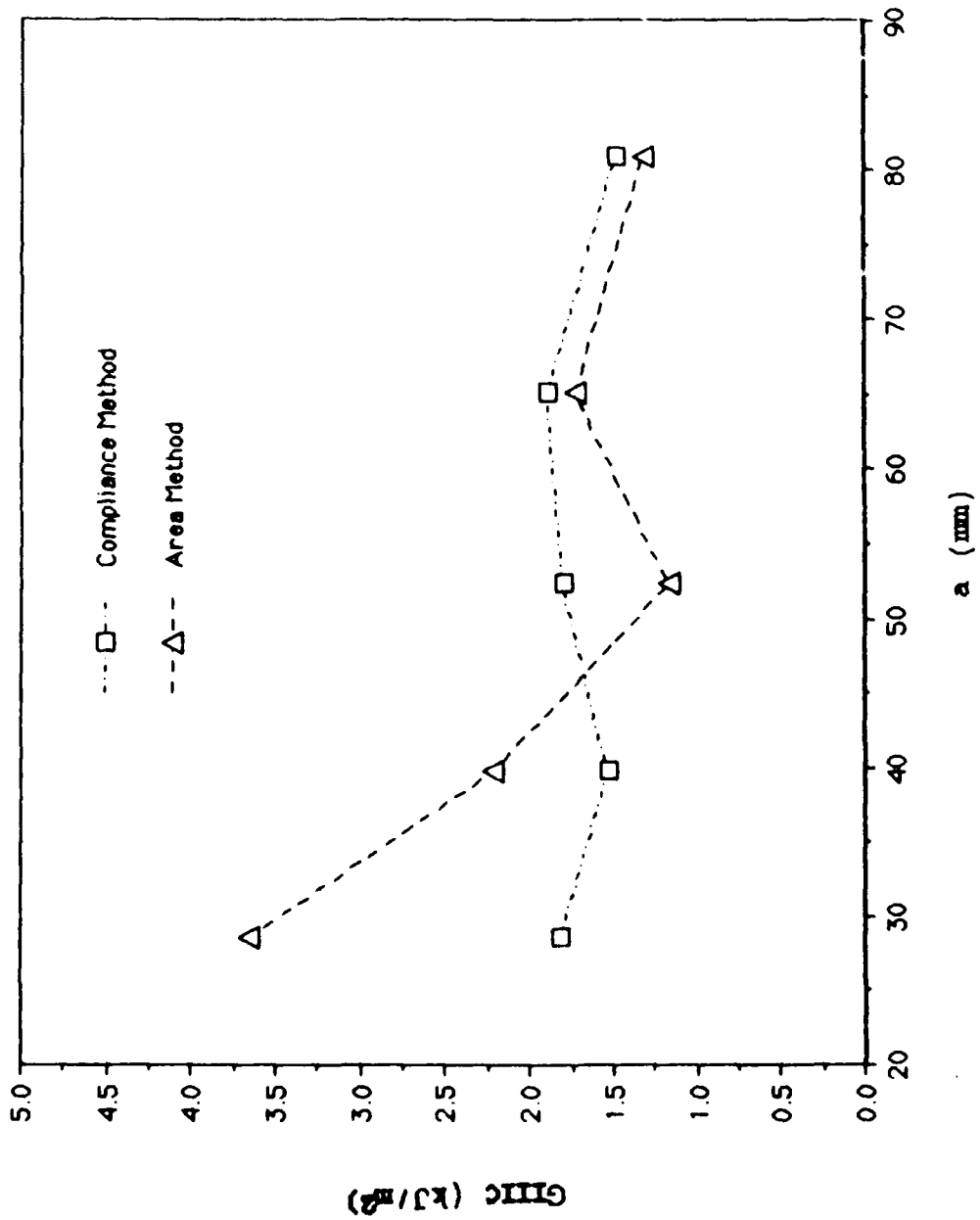


Figure 43. GIIC versus Crack Length from double split cantilever plate specimens

VII Scanning Electron Microscopy and Surface Photography

Scanning electron microscopy (SEM) was performed on three specimens. The first specimen was a shim specimen in which a large amount of mode I component was added in the mode III specimen. The second was a specimen in which mode I had been eliminated through compression. The last specimen was a rate specimen that was run entirely at a crosshead speed of 508.0 mm/sec. All specimens were coated with 10 Angstroms of palladium gold prior to viewing. The specimen was traversed in the SEM from the upper to the lower edge in a direction perpendicular to the direction of crack growth at a constant crack length. Photographs were taken at selected intervals during SEM. Magnification of 1000x was used throughout when a photo was taken of the image.

Figure 44 is a photo of the high mode I specimen taken ten percent inward from the upper edge of the specimen at a crack length of 20 cm. Most of the fibers are covered with matrix. Shear hackles are present. The large mode I component in this mode III specimen results in fewer shear hackles than in a typical mode III specimen (1).

Figure 45 is a photo taken from the lower edge of the high mode I component specimen at a crack length of 20 cm. Even fewer shear hackles appear in this photo than in Figure 44. The failure mode is predominantly mode I.

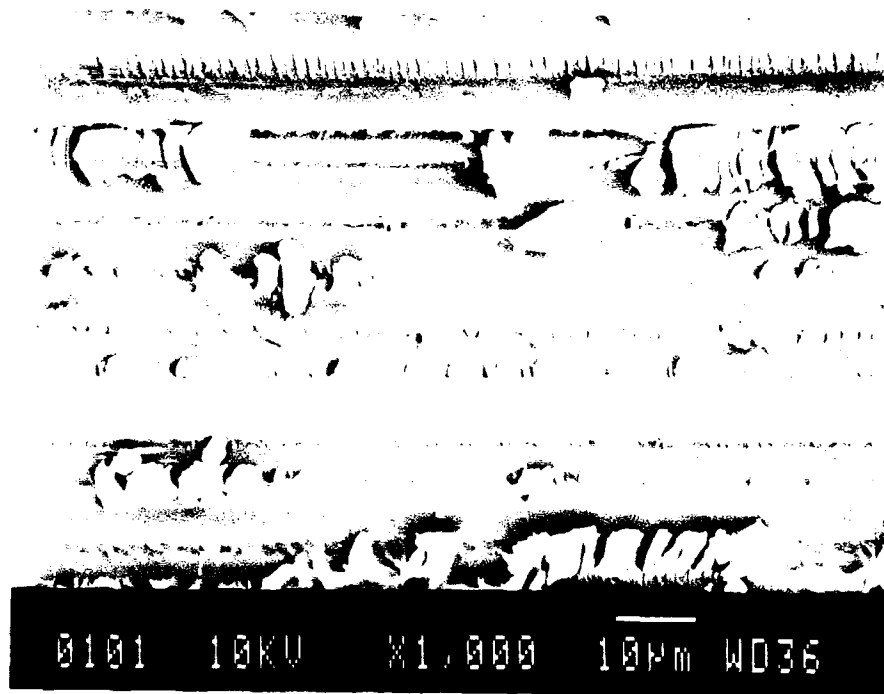


Figure 44. SEM from high mode I component specimen

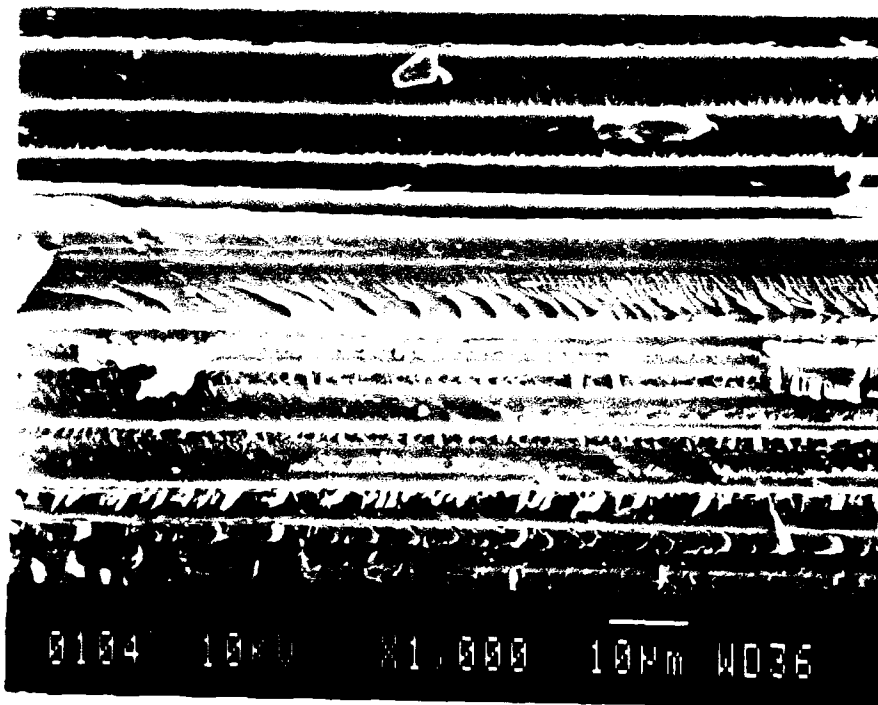


Figure 45. SEM from high mode I component specimen

Figure 46 is a view close to the upper edge of the high mode I component specimen at a crack length of 20 cm. Shear hackles are almost nonexistent. Transverse splitting is apparent in the lower portion of the photo.

Figure 47 shows a view near the top edge of a specimen in which the mode I component has been eliminated through compression at a crack length of 8.5 cm. A large number of hackles of various sizes can be seen throughout the photo. A row of large hackles can be seen near the top of the photo. The increase in the number of hackles can be correlated to the decrease in mode I from an increase in compression.

Figure 48 shows a view taken closer to the center of the high compression specimen at a crack length of 8.5 cm. The area shows the crushing effects of compression upon the fibers and matrix of the composite. Some areas of compression are recessed. The contrast between Figures 47 and 48 indicate that compression was not constant from top to bottom of the specimen. Less compression is seen near the edges of the specimen.

Figure 49 shows the SEM photo taken at the center of the high compression specimen at a crack length of 8.5 cm. Broken fibers can be seen along with chunks of crushed matrix. Centrally, greater amounts of damage due to crushing can be seen in this high amount of compression specimen.

Figure 50 is a photo taken from near the top edge of the high compression specimen at a crack length of 8.5 cm.

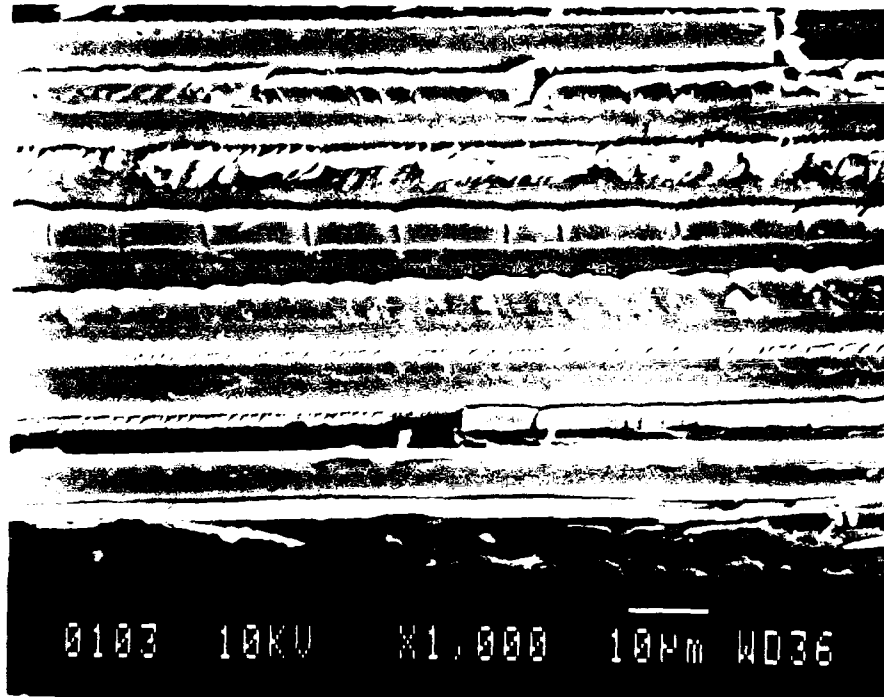


Figure 46. SEM from high mode I component specimen



Figure 47. SEM from high compression specimen

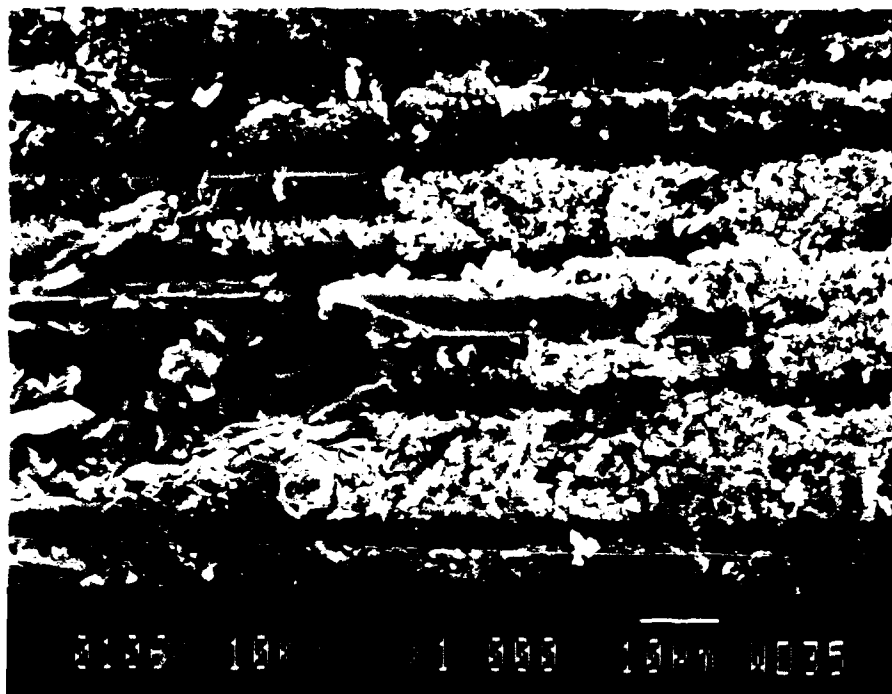


Figure 48. SEM from high compression specimen



Figure 49. SEM from high compression specimen

The amount of visible crushed matrix has decreased. A large chunk of detached matrix appears near the center of the photo. The lower right quadrant shows fiber and matrix damage. Some shear hackles are visible. Fiber splitting and crushing is evident in the lower right. A resin rich area appears between hackles.

Figure 51 is a photo of the high crosshead speed mode III specimen taken near the top edge at a crack length of 7 cm. Toughness values were lower for this specimen. No appreciable change in the fracture surface is seen from that of a mode III specimen run at a normal crosshead speed.

Figure 52 is a photo from the center of the high crosshead speed specimen at a crack length of 7 cm. Here fibers and matrix appear smooth with very few shear hackles. Longitudinal splitting of fibers can be seen in the center of the photo.

Figure 53 is an SEM photo taken from midway between the center and the lower edge of the specimen at a crack length of 7 cm. Hackles again are very closely packed. The larger hackles appear toward the bottom of the photo. These hackles are formed from local shearing stresses and indicate the presence of mode II. The hackles in this photo face the opposite direction as those near the top edge of the specimen (Figure 51). The hackle orientation has changed since the crack tip has effectively rotated when viewed from the opposite side.

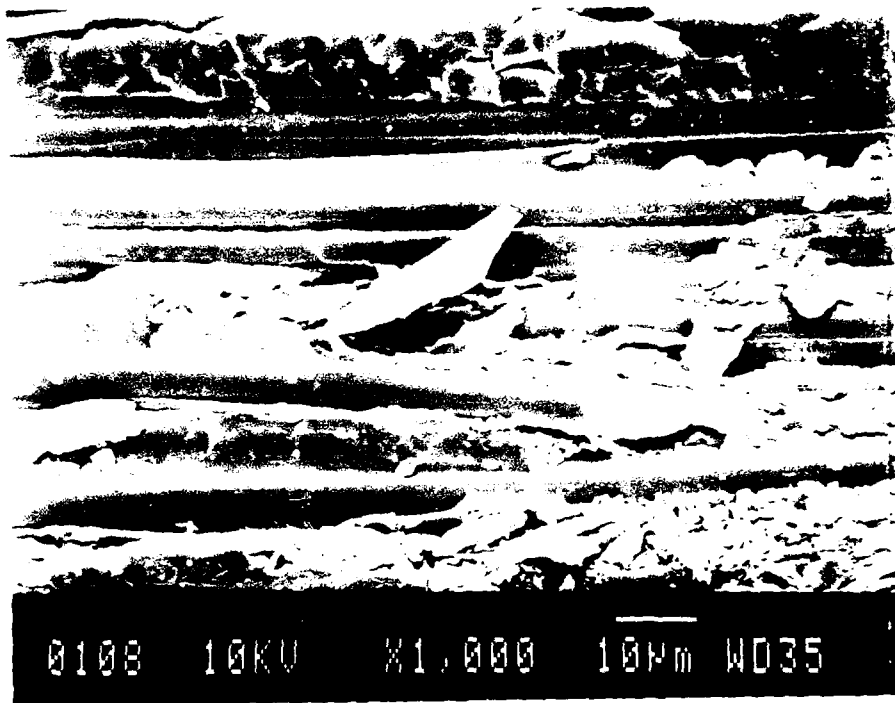


Figure 50. SEM from high compression specimen

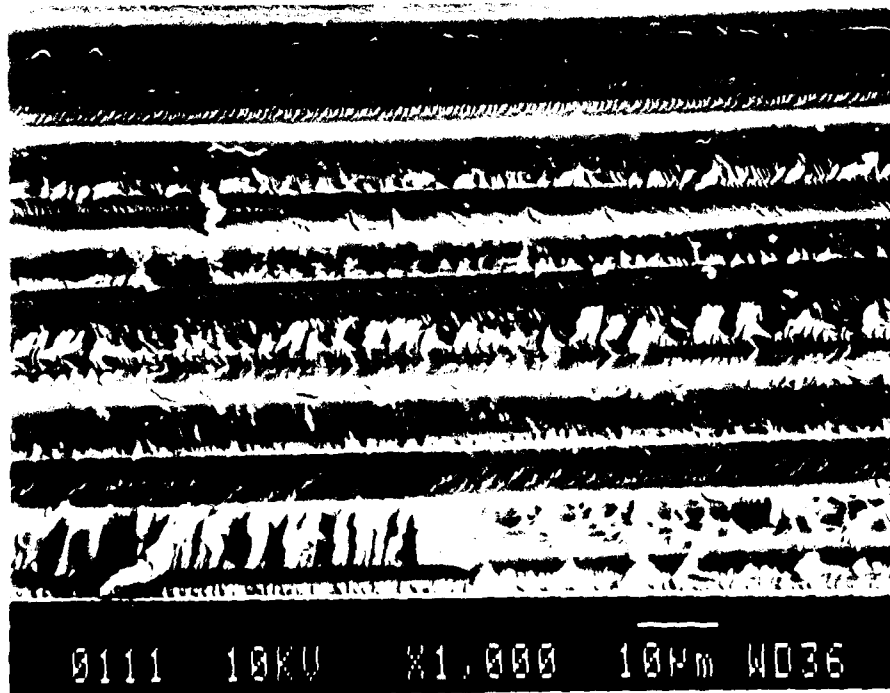


Figure 51. SEM from high crosshead rate specimen

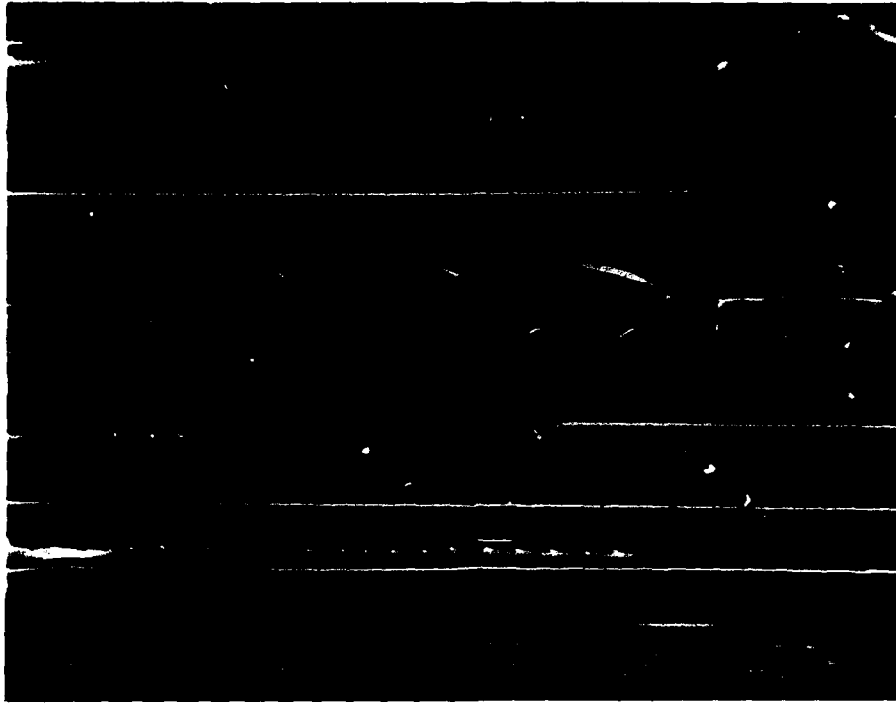


Figure 52. SEM from high crosshead rate specimen

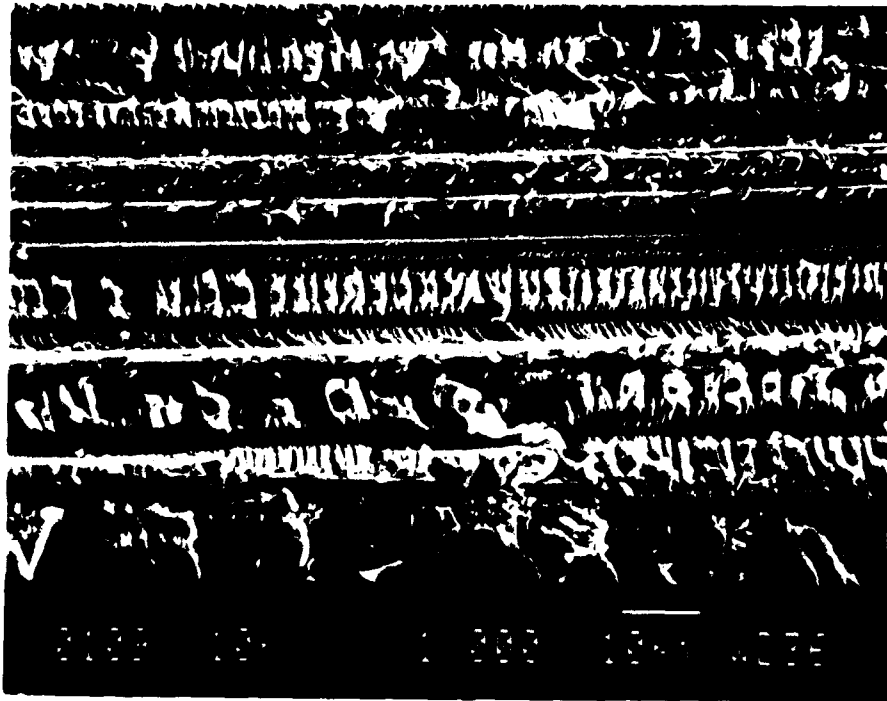


Figure 53. SEM from high crosshead rate specimen

Figure 54 is a fracture surface photograph of three specimens. The dark thin lines toward the center of each bar indicate small fiber bridging areas. The Kapton implant area is the first 50.8 mm on the left of the specimens shown. The precrack area immediately follows the Kapton implant.

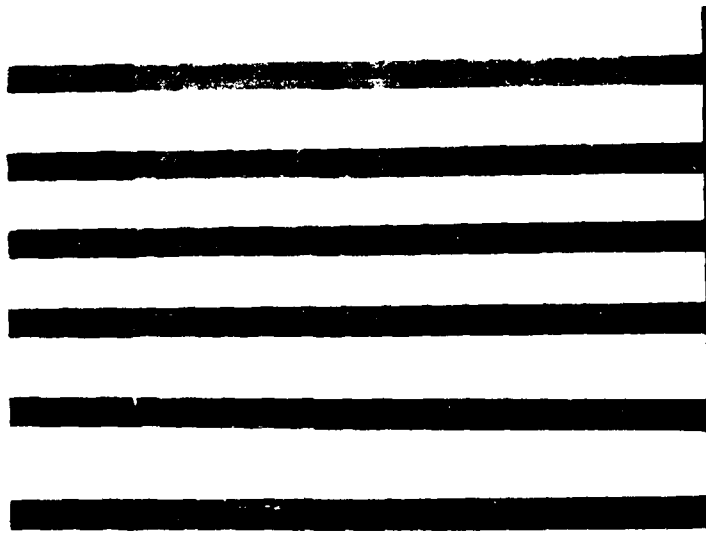


Figure 54. Split Cantilever Beam Specimen Fracture Surface

VIII Conclusions and Recommendations

Interlaminar failure will include, in general, modes I, II, and III failure. Predicting delamination in composite materials therefore necessitates having data from all three modes. While the majority of delamination data is a result of studies on the mode I and mode II phenomenon, Donaldson proposed the split cantilever beam test specimen for the analysis of mode III (1). The specimen is a composite laminate containing a Kapton implant starter crack bonded with a Hysol adhesive between two parallel aluminum bars. The present study was undertaken to provide a critical analysis of the mode III split cantilever beam test specimen. Interlaminar mode III critical strain energy release rates in a brittle graphite/epoxy composite were measured as a function of various test parameters.

The effect of changing the thickness of the two aluminum adherends on the G_{IIIc} strain energy release rate was investigated. The critical strain energy release rate of the unidirectional AS4/3502 composite material ranged from 1.07 to 1.56 kJ/m². This is nearly three times the previously reported G_{IIc} values (5) and nine times the previously reported G_{Ic} values (26). The G_{IIIc} values from testing with 19.05, 12.7, and 8.13 mm specimen thicknesses were in agreement with the 25.4 thickness specimens tested by

Donaldson Thus, changing the aluminum adherend thickness or beam support in the ranges used did not affect the GIIIC critical strain energy release rate, a measure of the material toughness.

In the testing of the effect of crosshead speed or strain rate on the critical strain energy release rate of the split cantilever beam specimen, the critical strain energy release rates were found to decrease with an increased crosshead speed. Changing the strain rate by increasing crosshead speed produced a decrease in strain energy release rate of nearly 50 percent over 6 decades. The GIIIC value at the lowest crosshead speed of 0.00508 mm/sec was 1.67 kJ/m². At a very high crosshead rate of 508.0 mm/sec, GIIIC was 0.66 kJ/m². Normal testing is conducted at 0.508 mm/min in a nearly level section of the curve and indicates that at this rate small changes in crosshead rate will not produce any significant difference in measured GIIIC.

In the testing of the effect of increasing or decreasing a mode I component on the critical strain energy release rate of the mode III split cantilever beam specimen, it was found that the addition of compression from decreasing the end opening in the split cantilever beam test increased interlaminar friction between the plies. This increase in friction resulted in a higher critical strain energy release rate required to induce crack growth. Using the area method, compliance method, and beam theory with 0.772 mm compression

the G_c value increased to 1 527, 1 524, 1 972 kJ/m² respectively. Thus, compressing the end opening led to the appearance of higher measured toughness. When the amount of compression due to shim was increased to 1.890 mm the values of G_c increased even more. The area method value from the 1.890 mm of compression testing was approximately double the lower end of the range obtained from the thickness testing. The numbers from the compliance method and beam theory were also approximately double the lower half of the thickness testing range. Thus, small amounts of compression due to the addition of mode I influence the G_c critical strain energy release rate obtained. The critical strain energy release rate increases due to the influence of interlaminar friction.

When a small mode I component was added, the effect on critical strain energy release rate was not significant; however, beyond a 2.54 mm end opening the effects of mode I began to dominate. These effects resulted in a decrease in critical strain energy release rate. The specimens used in the testing of the effects of thickness, temperature, and loading rate were in the range where influence of addition or subtraction of a mode I component on the critical strain energy release rate was not significant.

Conclusions from the effects of temperature on the split cantilever beam test specimen above room temperature

include decreasing critical strain energy release rate with increasing temperatures. G_{IIIC} showed increases at -17.77 C with the exception of the compliance method which indicated a small decrease. At -53.8 C , where one would expect the failure to be brittle, and the fracture toughness to decrease, G_{IIIC} continued to increase when using the compliance and area methods for analysis; however, beam theory indicated a decrease in G_{IIIC} .

Conclusions from the split cantilever plate testing are difficult to define. The data was widely scattered, with the compliance method G_{IIIC} ranging from 1.48 to 1.82 kJ/m^2 . Area method G_{IIIC} ranged from 1.16 to 3.65 kJ/m^2 . The difficulty with the G_{IIIC} values obtained from the measured compliance data appear to be related to the thickness of the specimen. Visual evidence of external crack growth appeared slightly after the onset of cracking noise from internal cracking. The data suggests that the split plate specimens may be sensitive to precracking technique and specimen thickness. The split plate specimens used in this study were 3.05 mm thick.

Recommendations for further testing of the G_{IIIC} split cantilever beam specimens could include further narrowing the aluminum adherend width to a total of 6.35 mm. The aluminum adherends could be further step notched down from 8.128 mm to 6.35 mm. Time did not permit investigation of this further

narrowed aluminum adherend width

The split cantilever beam specimens tested in this study were all 12.7 mm deep. While Donaldson tested some 25.4 mm deep specimens (1), nothing less than 12.7 mm has been tested. Also no depth between 12.7 and 25.4 mm has been attempted.

Recommendations associated with split plate testing would include using a unidirectional laminate of fewer than 24 plies. Tests could be accomplished using only a very short natural precrack. This would facilitate forming a set of balanced natural cracks through the thickness of the plate specimen.

Appendix

Computer Program

The following computer program was developed at the Air Force Materials Laboratory for data reduction of the split cantilever beam data. The load, crack length, and displacement data from the tests were used to calculate mode III critical strain energy release rates using the beam theory method, the area method, and the compliance method.

```

PROGRAM SCB
C
C THIS PROGRAM REDUCES THE SPLIT CANTILEVER BEAM DATA
C TO CALCULATE MODE III CRITICAL STRAIN ENERGY RELEASE
C RATE. BEAM THEORY, THE COMPLIANCE METHOD, AND THE
C AREA METHOD ARE USED.
C
LOGICAL EXST
CHARACTER *8 DF1,DF2
DIMENSION P(50),ACM(50),AIN(50),DEL(50),GBT(50),GCM(50)
DIMENSION AINP(50),ILOW(50),IUP(50)
DIMENSION AAVG(50),GAM(50)
C
C SET UP DATA FILES
C
55 WRITE (*,90)
90 FORMAT (/ ,5X, 'ENTER INPUT DATA FILE NAME: ')
READ (*,95) DF1
95 FORMAT (A8)
INQUIRE (FILE=DF1,EXIST=EXST)
IF (EXST) THEN
OPEN (7,FILE=DF1,STATUS='OLD')
CLOSE (7,STATUS='DELETE')
END IF
OPEN (7,FILE=DF1,STATUS='NEW')
C
WRITE (*,97) DF1
97 FORMAT (5X,'DF1 (INPUT FILE) = ',A8)
C
91 WRITE (*,92)
92 FORMAT (/ ,5X, 'ENTER OUTPUT DATA FILE NAME: ')
READ (*,95) DF2
INQUIRE (FILE=DF2,EXIST=EXST)
IF (EXST) THEN
OPEN (8,FILE=DF2,STATUS='OLD')
CLOSE (8,STATUS='DELETE')
END IF
OPEN (8,FILE=DF2,STATUS='NEW')
C
WRITE (*,98) DF2
98 FORMAT (5X,'DF2 (OUTPUT FILE) = ',A8)
C
C ENTER DATA FROM THE PLOT
C
WRITE (*,100)
100 FORMAT (/ ,5X, 'ENTER DATA IN THE FOLLOWING FORM: ', / ,5X,
1 'P(LB),A(CM),DEL(IN)', / ,5X, 'ENTER P .GE. 999. TO
2QUIT')
C
DO 300 J=1,100
WRITE (*,110)
110 FORMAT (5X,'P,A,DEL:')

```

```

        READ (*,*) P(J),ACM(J),DEL(J)
        IF (P(J).GE.998.) GO TO 310
300 CONTINUE
C
310 CONTINUE
    N = J - 1
    WRITE (*,120)
120 FORMAT (/ ,5X, 'ENTER DIST FROM BEAM
1END TO PIN, IN INCHES;')
    READ (*,*) OFFSET
    WRITE (*,130)
130 FORMAT (/ ,5X, 'ENTER THE BEAM WIDTH (IN):')
    READ (*,*) B
C
C    WRITE INPUT DATA TO THE INPUT DATA FILE
C
    WRITE (7,850) N
850 FORMAT (I2)
    DO 810 J=1,N
    WRITE (7,800) P(J),ACM(J),DEL(J)
800 FORMAT (3E12.5)
810 CONTINUE
    WRITE (7,820) OFFSET, B
820 FORMAT (2F12.4)
C
C    ENTER THE LOWER AND UPPER NUMBER OF DATA TO HAVE
C    AREA CALCULATED
C
    WRITE (*,132)
132 FORMAT (/ ,5X, 'ENTER THE AREA METHOD PARAMETERS' , / ,5X,
1 'ENTER I .GE. 99 TO QUIT')
C
    DO 315 J=1,100
    WRITE (*,135) J
135 FORMAT (5X, 'SELECT I LIMITS FOR DELTA-', I2, / ,
1 ' ILOWER, IUPPER:')
    READ (*,*) ILOW(J),IUP(J)
    IF (ILOW(J).GE.98) GO TO 317
315 CONTINUE
317 CONTINUE
    NDEL = J - 1
C
C    WRITE HEADINGS
C
    WRITE (*,140) B,OFFSET
140 FORMAT (/// ,5X, 'SPECIMEN ID:', 20X, 'B =
1', F6.3, 5X, 'OFFSET =', F6.2)
    WRITE (*,150)
150 FORMAT (/// ,2X, 'I', 5X, 'P', 5X, 'A,SPEC', 2X, 'A,OFFS', 4X,
1 'DEL', 5X, 'GBT', 6X, 'GCM')
    WRITE (*,160)
160 FORMAT (7X, '(LB)', 4X, '(CM)', 4X, '(IN)', 5X, '(IN)', 4X,

```

```

1 (US) , 5X, (US) , / )
C
C   CALCULATE THE ACTUAL OFFSET CRACK LENGTHS IN INCHES
C
DO 680 J=1,N
    AIN(J) = ACM(J)/2.54
    AINP(J) = AIN(J) - OFFSET
680 CONTINUE
C
C   CALCULATE THE SLOPE USED IN THE COMPLIANCE METHOD USING
C   THE LEAST SQUARES METHOD
C
SX = 0.0
SY = 0.0
SXY = 0.0
SX2 = 0.0
C
ISKIP = 1
DO 630 J=1,N
    DDP = DEL(J)/P(J)
    DPLOG = LOG10(DDP)
    AALOG = LOG10(AINP(J))
    SX = SX + AALOG
    SY = SY + DPLOG
    SXY = SXY + AALOG * DPLOG
    SX2 = SX2 + AALOG**2
    IF (ISKIP.NE 2) GO TO 765
    WRITE (*,991) DPLOG, AALOG, SX, SY, SXY, SX2
991 FORMAT (2X,6E12.4)
765 CONTINUE
630 CONTINUE
C
C   SLOPE = (SX*SY-FLOAT(N)*SXY) / (SX**2-FLOAT(N)*SX2)
C
SGBT = 0.0
SGCM = 0.0
C
DO 320 J=1,N
C
C   CALCULATE GC USING BEAM THEORY
C
GBT(J) = 1.5*P(J)*DEL(J) / (B*AINP(J))
SGBT = SGBT + GBT(J)
C
C   CALCULATE GC USING THE COMPLIANCE METHOD
C
GCM(J) = SLOPE/2.0 * P(J)*DEL(J) / (B*AINP(J))
SGCM = SGCM + GCM(J)
C
WRITE (*,170)
1J,P(J),ACM(J),AINP(J),DEL(J),GBT(J),GCM(J)

```

```

170 FORMAT (1X,I2,3X,F5.1,4X,F4.1,4X,F5.2,3X,F6.4,3X,
1F5.2,3X,F5.2)
320 CONTINUE
C
WRITE (*,180) SGBT/FLOAT(N), SGCM/FLOAT(N)
180 FORMAT (29X,'AVERAGES = ',F5.2,3X,F5.2)
WRITE (*,181) SLOPE
181 FORMAT (29X,'COMPLIANCE METHOD EXP = ',F6.3)
C
WRITE HEADINGS
C
WRITE (*,190)
190 FORMAT (//,2X,'J',3X,'IUP',2X,'ILOW',2X,
1'A,AVG',6X,'AREA',6X,'GAM')
C
CALCULATE USING THE AREA METHOD
C
SGAM = 0.0
C
DO 330 J=1,NDEL
AAVG(J) = (AINP(IUP(J)) + AINP(ILOW(J)))/2.0
DA = AINP(IUP(J)) - AINP(ILOW(J))
NTRI = IUP(J) - ILOW(J)
AREA = 0.0
ILOWH = ILOW(J)
IUPH = ILOW(J) + 1
C
DO 644 I=1,NTRI
DP = P(ILOWH) - P(IUPH)
DDEL = DEL(IUPH) - DEL(ILOWH)
AREA = AREA + P(ILOWH) * DDEL + DEL(ILOWH) * DP
ILOWH = ILOWH + 1
IUPH = IUPH + 1
644 CONTINUE
C
GAM(J) = 1.0 / (2.0*B*DA) * AREA
SGAM = SGAM + GAM(J)
WRITE (*,500) J,ILOW(J),IUP(J),AAVG(J),AREA,GAM(J)
500 FORMAT (1X,I2,3X,I2,3X,I2,5X,F4.2,5X,F5.2,5X,F5.2)
C
330 CONTINUE
C
WRITE (*,620) SGAM/NDEL
620 FORMAT (27X,'AVERAGE = ',F5.2)
C
WRITE TO DATA FILE
C
XEIGHT = 888.
XNINE = 999.
DO 340 J=1,N
WRITE (8,700) AINP(J),GBT(J)
700 FORMAT (5X,2E12.4)

```

```
340 CONTINUE
C
  WRITE (8,710) XNINE,XNINE
710 FORMAT (5X,2F10.2)
  DO 345 J=1,N
  WRITE (8,700) AINP(J),GCM(J)
345 CONTINUE
  WRITE (8,710) XNINE,XNINE
  DO 350 J=1,NDEL
  WRITE (8,700) AAVG(J),GAM(J)
350 CONTINUE
  WRITE (8,700) XNINE,XNINE
  WRITE (8,700) XEIGHT, XEIGHT
C
  CLOSE (7)
  CLOSE (8)
C
  PAUSE
  STOP
  END
```

Bibliography

1. Donaldson, Steven L. Mode III Interlaminar Fracture Characterization of Composite Materials. MS thesis University of Dayton, Dayton OH, April 1987.
2. Armanios, E. A. Rehfield, L. W., "Interlaminar Analysis of Laminated Composites Using a Sublaminar Approach," 27th AIAA/ASME/ASCE/AHS Structures, Structural Dynamics, and Materials Conference, Part I: 442-452, (May 1986).
3. Broek, D. Elementary Engineering Fracture Mechanics. Dordrecht, The Netherlands Martinus Nijhoff Publishers, 1986.
4. Chai, H., "The Characterization of Mode I Delamination Failure in Non-Woven, Multi-directional Laminates," Composites, Vol 15 No 4: 277-290 (1984).
5. Carlsson, L., Gillespie, J. W., and Tretheway, B. R., "Mode II Interlaminar Fracture of Graphite/Epoxy and Graphite/PEEK," Journal of Reinforced Plastics and Composites, Vol 5 No 3: 170-187 (1986).
6. Giare, G. S., "Fracture Toughness of Unidirectional Fiber Reinforced Composites in Mode II," Engineering Fracture Mechanics, Vol 20 No 1: Vol 20 No 1: 11-21 (1984).
7. Donaldson, S. L., "Fracture Toughness Testing of Graphite/Epoxy and Graphite/PEEK Composites," Composites Vol 16 No 2: 103-112 (1985).
8. Wang, S. S., "Fracture Mechanics for Delamination Problems in Composite Materials," Journal of Composite Materials, 17: 210-223 (1983).
9. Kim, K. S. and C. S. Hong "Delamination Growth in Angle Ply Laminated Composites," Journal of Composite Materials, 20: 423-438 (1986).
10. Blikstad, M., Fracture Toughness of Graphite Composites. Dissertation No 126 Linkoping Studies in Science and Technology. Linkoping University, Sweden.
11. Anderson, G. P., Bennett, S. J., and DeVries, K. L. Analysis and Testing of Adhesive Bonds. New York: Academic Press, 1977.

12. Chatterjee, S. N., Dick, W. A. and Pipes, R. B. "Mixed-mode Delamination Fracture in Laminated Composites," Composites Science and Technology, 25: 49-67 (1986).
13. Agarwal, B. D. and G. S. Giare "Fracture Toughness of Short Fiber Composites in Modes II and III," Engineering Fracture Mechanics, Vol 15 No 1-2: 219-230 (1981).
14. Sidey, G. R. and F. J. Bradshaw "Some Investigations on Carbon Fiber Reinforced Plastics under Impact Loading, and Measurements of Fracture Energies," International Conference on Carbon Fibres, their Composites and Applications, The Plastics Institute, London (1971).
15. Ripling, E. J., Santer, J. S., and Crosley, P. B., "Fracture Toughness of Composite Adherend Adhesive Joints under Mixed Mode I and III Loading," Journal of Materials Science, 18: 2274-2282 (1983).
16. DeBaise, G. R., Mechanics and Morphology of Wood Shear Fracture. PhD thesis, 71-7755, State University College of Forestry at Syracuse University. University Microfilms International, Ann Arbor MI, 1970.
17. Smiley A. J. and R. B. Pipes "Rate Effects on Mode I Interlaminar Fracture Toughness in Composite Materials," Journal of Composite Materials, 21: 671-684 (July 1987).
18. Miller, A. G. et al. "Toughness Testing of Composite Materials," Sampe Quarterly: 36-42 (January 1981).
19. Aliyu A. A. and I. M. Daniel "Effects of Strain Rate on Delamination Fracture Toughness of Graphite/Epoxy," ASTM STP 876, 336-348 (1985).
20. Smiley, A. J. Rate Sensitivity of Interlaminar Fracture Toughness in Composite Materials. MS thesis, University of Delaware, Newark DE, December 1985.
21. Hunston, D. L. and W. D. Bascom. "Effects of Layup, Temperature, and Loading Rate in Double Cantilever Beam Tests of Interlaminar Crack Growth," Composites Technology Review, 5: 118-119 (1983).

22. Gillespie, J. W. et al. "Rate-Dependent Mode I Interlaminar Crack Growth Mechanisms in Graphite/Epoxy and Graphite/PeeK," Composites Science and Technology, 28: 1-15.
23. Smiley A. J. and R. B. Pipes. "Rate Sensitivity of Mode II Interlaminar Fracture Toughness in Graphite/Epoxy and Graphite/PEEK Composite Materials," Composites Science and Technology, 29: 1-13.
24. Berry, J. P., "Determination of Fracture Surface Energies by the Cleavage Technique," Journal of Applied Physics, 34: 62 (1963).
25. Mall, S., Law, G.E., and Katouzian, M. "Loading Rate Effect on Interlaminar Fracture Toughness of a Thermoplastic Composite," Journal of Composite Materials, 21: 569-579 (1987).
26. Whitney, J. M., Browning, C. E., and Hoogsteden, W., "A Double Cantilever Beam Test for Characterizing Mode I Delamination of Composite Materials," Journal of Reinforced Plastics and Composites, 1: 297-313 (1982).

VITA

Captain Cynthia L. Lingg [REDACTED]

[REDACTED] [REDACTED]
[REDACTED] in 1974 and attended Villanova University and the University of Delaware prior to entering active duty in 1977. In 1983 she received the degree of Bachelor of Science in Mechanical Engineering from the University of Arizona through the AECP program. Upon graduation, she received her commission from OTS. She then served as a project engineer in the 544 IES, Offutt AFB, Nebraska until entering the Air Force Institute of Technology in May 1987.

REPORT DOCUMENTATION PAGE

Form Approved
OMB No. 0704-0188

REPORT SECURITY CLASSIFICATION UNCLASSIFIED		1b RESTRICTIVE MARKINGS	
2a SECURITY CLASSIFICATION AUTHORITY		3 DISTRIBUTION/AVAILABILITY OF REPORT Approved for public release; distribution unlimited.	
2b DECLASSIFICATION/DOWNGRADING SCHEDULE		4 PERFORMING ORGANIZATION REPORT NUMBER(S) AFIT/GAE/AA/88D-21	
4 PERFORMING ORGANIZATION REPORT NUMBER(S) AFIT/GAE/AA/88D-21		5 MONITORING ORGANIZATION REPORT NUMBER(S)	
6a NAME OF PERFORMING ORGANIZATION School of Engineering	6b OFFICE SYMBOL (If applicable) AFIT/ENY	7a NAME OF MONITORING ORGANIZATION	
6c ADDRESS (City, State, and ZIP Code) Air Force Institute of Technology Wright Patterson AFB, OH 45433-6583		7b ADDRESS (City, State, and ZIP Code)	
8a NAME OF FUNDING SPONSORING ORGANIZATION Materials Lab, Non Metallic Division	8b OFFICE SYMBOL (If applicable) AFNAL/MLBM	9 PROCUREMENT INSTRUMENT IDENTIFICATION NUMBER	
8c ADDRESS (City, State, and ZIP Code) AFNAL/MLBM Wright-Patterson AFB, OH 45433-6583		10 SOURCE OF FUNDING NUMBERS	
		PROGRAM ELEMENT NO	PROJECT NO
		TASK NO	WORK UNIT ACCESSION NO
11 TITLE (Include Security Classification) CHARACTERIZATION OF DELAMINATION IN ADVANCED COMPOSITE MATERIALS UNDER MODE III LOADING CONDITIONS			
PERSONAL AUTHOR(S) CYNTHIA L. LINGG, Capt, USAF			
13a TYPE OF REPORT MS THESIS	13b TIME COVERED FROM _____ TO _____	14 DATE OF REPORT (Year, Month, Day) 1988 December	15 PAGE COUNT 127
16 SUPPLEMENTARY NOTATION			
17 COSATI CODES		18 SUBJECT TERMS (Continue on reverse if necessary and identify by block number)	
FIELD	GROUP	SUB-GROUP	
	04		
		Critical Strain Energy Release Rate, Split Cantilever Beam Specimen, Double Split Cantilever Plate Specimen, Mode III	
19 ABSTRACT (Continue on reverse if necessary and identify by block number)			
Thesis Chairman: Dr. S. Mall Professor of Aeronautics and Astronautics			
20 DISTRIBUTION/AVAILABILITY OF ABSTRACT <input type="checkbox"/> UNCLASSIFIED/UNLIMITED <input checked="" type="checkbox"/> SAME AS RPT <input type="checkbox"/> DTIC USERS		21 ABSTRACT SECURITY CLASSIFICATION UNCLASSIFIED	
22a NAME OF RESPONSIBLE INDIVIDUAL Dr. S. Mall		22b TELEPHONE (Include Area Code) (513) 255-3517	22c OFFICE SYMBOL AFIT/ENY

Approved for release by
ACM 1, 1989
12 Jan 1989

UNCLASSIFIED

Abstract

Delamination is the weakest and major failure mode in laminated fiber reinforced composite materials. Delamination is also a fundamental issue in the evaluation of laminated composite structures for durability and damage tolerance. This study involved the characterization of mode III delamination primarily using the mode III split cantilever beam specimen. The effects of altering four test parameters on the critical strain energy release rate of the split cantilever beam test specimen were studied, resulting in a critical evaluation of this mode III test specimen. This evaluation involved the investigation of altering aluminum adherend thickness on the mode III critical strain energy release value, investigation of altering crosshead rate on the mode III critical strain energy release rate, the effect of temperature on the mode III critical strain energy release rate, and the addition and subtraction of a mode I component on the critical strain energy release rate. For comparison, a few double split cantilever plate specimens were also tested.

Results obtained from the compliance method, area method, and beam theory showed that altering adherend thickness produced no effect on mode III critical strain energy release rate. Results obtained from the compliance method showed that higher crosshead rates produced lower mode III critical strain energy release rates. Results obtained from compliance method and area method showed that increasing end opening decreased critical strain energy release rate. Above room temperature GIIIC decreased with increasing temperature.

UNCLASSIFIED